https://doi.org/10.15388/vu.thesis.35

VILNIUS UNIVERSITY

Nadežda
DREIŽĖ

Elucidation of the complexity of molecular mechanisms of cancer cell drug resistance to enhance treatment efficiency

DOCTORAL DISSERTATION

Natural sciences,
Biochemistry N004

VILNIUS 2020

This dissertation was written between 2015 and 2019 at Proteomics Center, Institute of Biochemistry, Life Sciences Center, Vilnius University.
The research was supported by the Research Council of Lithuania (doctoral studies were financed from the EU structural funds).

Academic supervisor:

Dr. Mindaugas Valius (Vilnius University, natural sciences, biochemistry N004).

https://doi.org/10.15388/vu.thesis.35

VILNIAUS UNIVERSITETAS

Nadežda
DREIŽĖ

Navikinių ląstelių atsparumo vaistams molekulinių mechanizmų kompleksiškumo tyrimas terapijos veiksmingumo gerinimui

DAKTARO DISERTACIJA

Gamtos mokslai,
Biochemija N004

VILNIUS 2020

Disertacija rengta 2015–2019 metais Vilniaus universiteto Gyvybės mokslų centro Biochemijos instituto Proteomikos centre.
Mokslinius tyrimus rėmė Lietuvos mokslo taryba (doktorantūra buvo finansuojama ES struktūrinių fondų lėšomis).

Mokslinis vadovas:

Dr. Mindaugas Valius (Vilniaus universitetas, gamtos mokslai, biochemija N004).

TABLE OF CONTENT

LIST OF ABBREVIATIONS 7
INTRODUCTION 8
SCIENTIFIC NOVELTY AND PRACTICAL VALUE 10
STATEMENTS TO DEFEND 11
1. LITERATURE OVERVIEW 12
1.1. Models of cancer cell resistance 12
1.1.1. Cancer stem cells 13
1.2. General principles of drug resistance 14
1.2.1. Drug influx and efflux 14
1.2.2. Drug inactivation or lack of activation 16
1.2.3. Alterations in drug targets 17
1.3. Adaptive responses to DNA damage 18
1.3.1. Cell cycle arrest in response to DNA damage 18
1.3.2. Changes in p53 protein function 20
1.3.3. Alterations of DNA damage repair 21
1.4. Downstream resistance mechanisms 22
1.4.1. The prosurvival signaling via receptor tyrosine kinases 22
1.4.2. Promotion of cancer cell stemness through receptor stimulation 24
1.4.3. Oncogenic bypass through PI3K-AKT-mTOR pathway 24
1.4.4. Inhibition of stress-activated MAP kinases 25
1.4.5. Dysfunctional apoptotic signaling 26
1.5. Tumor cell heterogeneity and plasticity 28
1.5.1. Genomic instability and clonal evolution 28
2. MATERIALS AND METHODS 32
2.1. Cell culture, drug treatment and establishment of resistant cell lines 32
2.2. Drugs and inhibitors 32
2.3. Assessment of cell viability and cell death 33
2.4. Cell cycle analysis and other flow cytometric assays 34
2.5. Western blot analysis 34
2.6. Oligoprecipitation assay 35
2.7. Confocal microscopy 36
2.8. Sphere-forming assay 36
2.9. Wound-healing assay 37
2.10. Generation of stable expression cell lines using lentiviral vectors 37
2.11. Genome engineering using the CRISPR/Cas9 system 38
2.12. Real-time qPCR for evaluation of the mRNA expression 39
2.13. RNA isolation, miRNA sequencing, and data processing 40

2.14. miRNA target analysis 41
2.15. Sample preparation for mass spectrometry analysis 41
2.16. Multiplexed inhibitor bead affinity extraction 42
2.17. Phosphoproteome 42
2.18. Computational functional analysis of proteomic data 43
3. RESULTS AND DISCUSSION 44
3.1. Generation of resistant cell lines 44
3.2. Characterization of RH1-resistant breast cancer cell line 45
3.2.1. Combined kinome and phosphoproteome analysis 46
3.2.2. Assessment of cell cycle changes 53
3.2.3. Evaluation of cancer stem cell population 55
3.2.3.1. Analysis of ABC transporters 57
3.2.3.2. Role of stem cell factor receptor c-KIT 59
3.3. Characterization of 5-fluorouracil-resistant colorectal cancer cell line 61
3.3.1. Assessment of 5-fluorouracil caused DNA damage 63
3.4. Characterization of oxaliplatin-resistant colorectal cancer cell line .. 66
3.4.1. Analysis of miRNA expression profile 69
3.4.1.1. Identification of miR-23b targets and their functional bioinformatics analysis 72
3.4.1.2. Evaluation of epithelial-mesenchymal transition 76
3.4.1.3. Manipulation of EMT-inducing transcription factor SNAI2 79
3.4.2. Differential proteomic analysis 81
3.4.2.1. Transcriptional target and mutational analysis of p53 84
3.4.2.2. Evaluation of p53 knockdown cells resistance 88
3.4.2.3. Inducible wild-type and mutant p53 expression 90
3.4.2.4. P53 knockout using CRISPR/Cas9 system 93
3.4.2.5. Elucidation of unconventional cytotoxicity mechanism of oxaliplatin 96
FINAL REMARKS 102
CONCLUSIONS 105
PUBLICATIONS AND SCIENTIFIC PARTICIPATION 106
REFERENCES 108
ACKNOWLEDGEMENTS 119

LIST OF ABBREVIATIONS

5-FU	5-fluorouracil
ABC	ATP-binding cassette
CDK	cyclin-dependent kinase
CisPt	cisplatin
CRC	colorectal cancer
CSC	cancer stem cell
DAPI	4′,6-diamidino-2-phenylindole
EMT	epithelial-mesenchymal transition
FASP	filter-aided sample preparation
FBS	fetal bovine serum
IC50	the half-maximal inhibitory concentration
MAPK	mitogen-activated protein kinase
MIB	multiplexed kinase inhibitor bead
MMR	mismatch repair
MOMP	mitochondrial outer membrane permeabilization
NER	nucleotide excision repair
OxaPt	oxaliplatin
PBS	phosphate-buffered saline
RH1	2,5-diaziridinyl-3-(hydroxymethyl)-6-methyl-1,4-benzoquinone
ROS	reactive oxygen species
RTK	receptor tyrosine kinase
RT-qPCR	real-time quantitative polymerase chain reaction
TNBC	triple-negative breast cancer
WT	wild-type

INTRODUCTION

Tumor resistance to chemotherapy drugs limits the efficiency of cancer treatment and remains a major problem in recurrent cancer therapy. Cancer cell resistance can be innate rendering cancer treatment ineffective due to preexisting changes in resistance-associated factors. Otherwise, cancer cell resistance can be acquired during previous rounds of treatment due to various therapy-induced adaptive responses or intrinsic tumor cell heterogeneity. In both cases, elucidation of biological processes and pathways that are crucial for the development of drug resistance provides the potential for establishing the course of the most efficient therapy. Moreover, it allows the selection of molecular targets for successful targeted individualized combinatorial treatment.

Recent data from various studies of chemoresistant cancers show the growing complexity of the emergence of resistant cells in tumor environment involving cancer stem cells, tumor cell heterogeneity and plasticity. All these processes are frequently linked with changes in response to genotoxic damage, prosurvival and proapoptotic signaling and dysfunctional cell death regulating mechanisms that arise due to mutational, protein activity and expression changes. In clinical cases often only mutational profiles of most prominent oncogenes and tumor suppressors are explored giving not enough credit to changes in protein expression, signaling and pathway regulation.

High-throughoutput analysis of global proteome, active kinases or protein phosphorylation can give more insights into molecular mechanisms and biological processes inducing tumor cell changes leading to resistance and inefficient cancer treatment. Targeting those mechanisms or using drugs that bypass altered damage-response processes will allow us to eradicate drug-resistant cells and increase the efficacy of anticancer therapy. Moreover, incorporation of confocal microscopy analysis to visualize a specific fraction of cells can lead to the identification of the drug-tolerant cell population otherwise hindered by the dominating population. This can help to eradicate the subset of cells that have increased plasticity and tumor-initiating properties and, thus, can give rise to recurrent or metastatic tumors.

This research was focused on two different cancers that are most common, aggressive and resistance-prone: triple-negative breast cancer and colorectal cancer using MDA-MB-231 and HCT116 cell lines, respectively, as a model for cell resistance.

This study was aimed to elucidate molecular mechanisms and biological processes leading to cancer cell resistance using high-throughoutput analysis of global proteome, active kinases or protein phosphorylation. Additionally, validate these findings using protein visualization and genetic manipulation techniques.

The following **tasks were raised** to attain this aim:

- To perform combined differential high-throughoutput active kinase and protein phosphorylation analysis of parental and drug-resistant MDA-MB-231 cells and validate results by other methods.
- To investigate the importance of c-KIT-AKT-mTOR axis activation for the development of the RH1-resistant cell population.
- To identify protein changes in 5-fluorouracil-resistant HCT116 cell line via differential global proteomic analysis and evaluate the extent of DNA damage after drug treatment.
- To combine miRNomic and proteomic data for elucidation of basis for acquired resistance to oxaliplatin and investigate the role of partial epithelial-mesenchymal phenotype for the emergence of drug-resistance.
- To determine the significance of tumor suppressor protein p53 mutations for oxaliplatin resistance and use CRISPR/Cas9-modified p53-deficient cells for the elucidation of the mechanism of oxaliplatin-exerted cytotoxicity.

SCIENTIFIC NOVELTY AND PRACTICAL VALUE

In this thesis, the resistance mechanisms of two different cancer tumor types and different types of drugs were investigated. In the first case, we demonstrated that experimental cancer drugs can have alternative cytotoxic mechanisms of action that could be not limited to cancer cells and, thus, responsible for side effects. But, more importantly, we showed the importance of cancer stem cell potential to give rise to the drug-resistant population using the combination of active kinase and phosphoproteomic analyses. Using this new approach that gave us detailed insights into alterations of signaling pathways, we suggested the combination therapy that eradicates these cells and prevents the development of a drug-resistant phenotype that is a newly emerging strategy in cancer therapy.

In the second case, we showed the potential of the combination of miRNA and global proteome analyses to elucidate phenotypical changes of resistant cell population and, therefore, giving some clues to how resistance develops. The results of this approach pointed out the partial epithelial-mesenchymal phenotype of the resistant cells that is linked to cancer cell plasticity according to the newest research. Cancer cell plasticity is one of the most important factors for early stages of the emergence of drug-tolerant cells consequently leading to genomic instability and mutational changes in tumor suppressor genes or oncogenes leading to permanent drug-resistance. This concept of resistance development is a prospect for future research and can shed some light on the new cancer combinatorial treatment therapies involving compounds used to prevent cell plasticity.

STATEMENTS TO DEFEND

1. The expansion of stem cell-like cancer cells caused by autocrine stimulation of the c-KIT-AKT-mTOR axis in the RH1-resistant cell line caused resistance to the RH1 and this process can be avoided by combination treatment with stem cell receptor c-KIT inhibition.

2. The differences in 5-fluorouracil metabolism-related proteins revealed by differential proteomic analysis of the resistant cell line can be a prognostic marker for a 5-fluorouracil-specific resistance mechanism.

3. The resistance to oxaliplatin can manifest in partial epithelial-mesenchymal transition phenotype which is regulated by EMT-associated miRNA miR-23b and EMT-inducing transcription factor SNAI2.

4. Mutational status of p53 protein is an important indicator of oxaliplatin treatment efficacy, as transcriptional activity of p53 protein is crucial for the response to drug treatment and inactivating mutations of this protein can make the treatment ineffective.

1. LITERATURE OVERVIEW

1.1. Models of cancer cell resistance

Cancer cell resistance to chemotherapy drugs is a complex process that can't be explained by one determined model. Generally, drug resistance is divided into two broad categories: intrinsic and acquired. Intrinsic resistance means that resistance-mediating factors are pre-existing before treatment in a vast majority of tumor cells and, therefore, drug therapy will be ineffective. In the cases of acquired cancer cell resistance, the initial tumor is sensitive to the drug, but certain changes are happening during treatment that makes cells resistant to further treatment. These changes involve mutations arising during treatment and other adaptive responses such as increased expression of the therapeutic target and activation of alternative compensatory signaling pathways [1].

There are two models of acquired cancer cell resistance: (I) the conventional model that states that due to genetic instability of cancer cells genetic alterations causing resistance can happen and (II) the cancer stem cell (CSC) model that states that resistance is mediated by cells exhibiting stem cell-like properties (Figure 1). In the case of a conventional model, the population of cells that gains mutations promoting the drug resistance survive therapy and proliferate to form a recurrent tumor composed of mutated drug-resistant cells. In the CSC model, the tumor contains a small population of cancer cells that confers higher differentiating and tumor-initiating capacities. Due to their innate properties, this population survives therapy and repopulate tumor, resulting in a heterogeneous population of CSC and variably differentiated descendant cells [2].

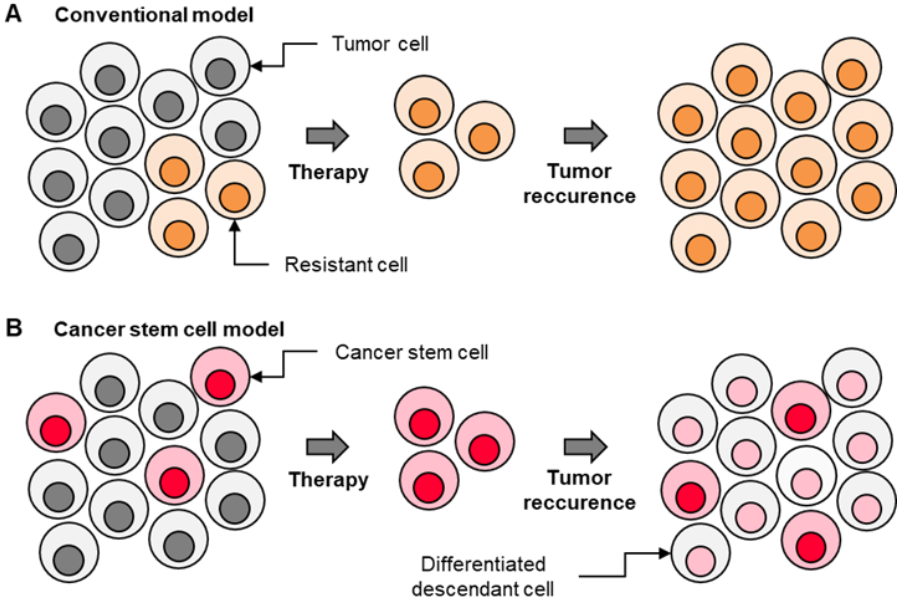

Figure 1. Schematic representation of conventional and cancer stem cell tumor resistance models. [2]

1.1.1. Cancer stem cells

Cancer stem cell is the term used to indicate a subset of tumor cells that are capable of initiating tumor and giving rise to heterogeneous progeny that is similar to the tissue it was originally isolated from [3]. Cells with stem cell-like properties were first identified in hematopoietic malignancies and then this concept was adapted to some solid tumors. CSCs make only a small fraction of malignant tumor cells but are a major problem in chemotherapy treatment as only one cell can give rise to a colony and passes the capability to regenerate all tumor [2].

CSCs share many properties of tissue-specific stem cells that provide for a long lifespan and relative quiescence, an active DNA-repair capacity, and resistance to apoptosis [4]. These cells express stem cell-specific markers such as CD44, CD133, or LGR5, that are originally used for stem cell detection in normal tissues. Moreover, CSCs can be characterized as more resistant to drugs and toxins through the expression of several ATP-binding cassette (ABC) transporters that are responsible for the efflux of certain substances from the cell [2].

Some CSCs adapt signaling pathways that regulate normal stem cell functions to regulate tumor maintenance and progression. One of the best-characterized examples of this process is the WNT-β-catenin pathway. This

pathway is frequently mutated in several different types of cancer and is required to sustain tumor growth and progression. Furthermore, activation of this pathway is consistent with the reprogramming of tumor cells into an embryonic-like fate in breast cancer subtypes as well as with transcriptional signature that resembles stem and progenitor cells in glioblastoma [5].

1.2. General principles of drug resistance

Drug resistance can be predetermined by pharmacokinetic or pharmacodynamic factors (Figure 2). The pharmacokinetic factors such as drug absorption, distribution, metabolism, and elimination affect the amount of drug that reaches the tumor and causes intracellular effects. When the drug reaches a tumor environment, the pharmacodynamic properties of cells play a major role such as limited drug influx or excessive efflux, drug inactivation, or lack of proper activation or alterations in drug target. Some adaptive responses to cellular damage as well as activation of pro-survival signals and dysfunctional apoptosis can lead to resistance to anticancer therapy [1].

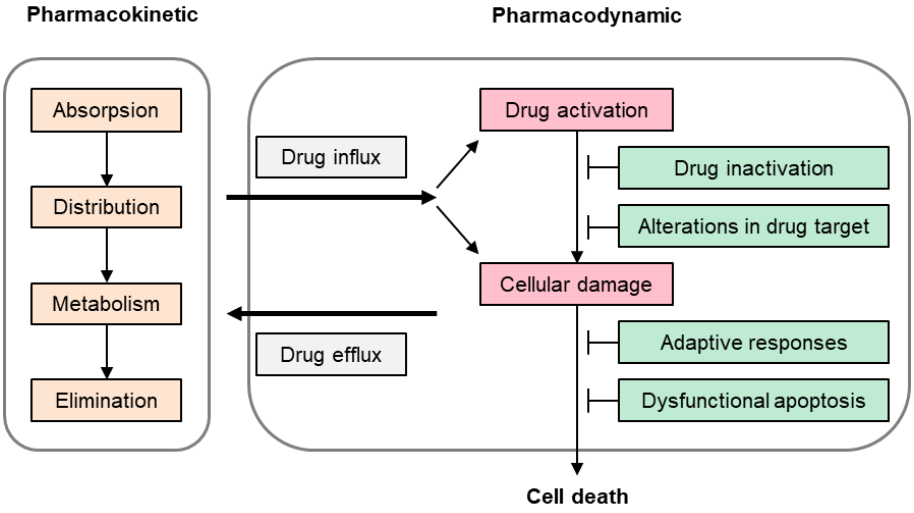

Figure 2. Pharmacokinetic and pharmacodynamic factors of drug resistance. [1]

1.2.1. Drug influx and efflux

ATP-binding cassette (ABC) transporter family of transmembrane proteins regulate the flux across the plasma membrane of multiple structurally and mechanistically unrelated chemotherapeutic agents. This

protein family has many members which are important for various cellular functions, but only three members are extensively studied concerning multidrug resistance (Table 1). These are multi-drug resistance protein 1 (MDR1; also known as P-glycoprotein and ABCB1), MDR-associated protein 1 (MRP1; also known as ABCC1), and breast cancer resistance protein (BCRP; also known as ABCG2). All three have broad, overlapping substrate specificity and promote the elimination of various hydrophobic compounds, including major cancer chemotherapeutics such as taxanes, topoisomerase inhibitors, and antimetabolites [6].

Table 1. ABC transporters involved in drug resistance. The most extensively studied ABC transporters are highlighted in grey. [2]

Gene	Protein	Chemotherapeutic drugs effluxed by the transporter	Other drugs and substrates
ABCA2	ABCA2	Estramustine	–
ABCB1	PGP/ MDR1	Colchicine, doxorubicin, etoposide, vinblastine, paclitaxel	Digoxin saquinavir
ABCC1	MRP1	Doxorubicin, daunorubicin, vincristine, etoposide, colchicine, camptothecins, methotrexate	Rhodamine
ABCC2	MRP2	Vinblastine, cisplatin, doxorubicin, methotrexate	Sulfinpyrazone
ABCC3	MRP3	Methotrexate, etoposide	–
ABCC4	MRP4	6-mercaptopurine, 6-thioguanine and metabolites, methotrexate	PMEA, cAMP, cGMP
ABCC5	MRP5	6-mercaptopurine, 6-thioguanine and metabolites	PMEA, cAMP, cGMP
ABCC6	MRP6	Etoposide	–
ABCC11	MRP8	5-fluorouracil	PMEA, cAMP, cGMP
ABCG2	MXR/ BCRP	Mitoxantrone, topotecan, doxorubicin, daunorubicin, irinotecan, imatinib, methotrexate	Pheophorbide A, Hoechst 33342, rhodamine

Interestingly, these transporters also have important roles in normal physiology in the transport of drugs across the placenta and the intestine and are important components of the blood-brain and blood-testis barriers. Moreover, the expression of ABC transporters is a known marker of CSCs used in isolation and analysis of these cells as the majority of cells accumulate the fluorescent dyes Hoechst33342 and rhodamine123, but these compounds are effluxed by ABCG2 and ABCB1 in stem cells. [2]

Another example of drug transport-mediated resistance could be the changes in platinum compound trafficking trough cellular membrane resulting in tumor resistance to cisplatin and carboplatin due to inadequate

levels of platinum reaching the target DNA. Platinum compounds can get into cells via copper influx transporters CTR1 and CTR2 and are transported from the cells via copper efflux transporters ATP7A and ATP7B. In each case, there is strong evidence from loss- and gain-of-function experiments that these transporters can modulate the level of drug in cell and, therefore, mediate cell resistance (Figure 3) [7].

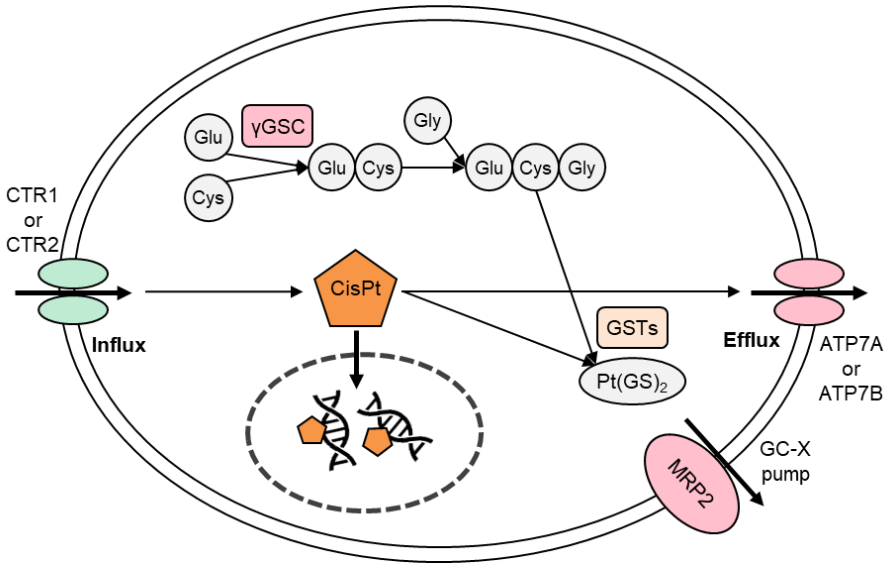

Figure 3. Tumour resistance to cisplatin and carboplatin mediated by inadequate levels of platinum reaching target DNA due to changes in transport and drug inactivation. Expression of proteins in red is usually increased in resistant cells and expression of the proteins in green is usually decreased. [7]

1.2.2. Drug inactivation or lack of activation

Most of the drugs are inactivated in cells as a result of normal metabolic processes, but for the desired efficiency of treatment, the drug should be metabolized only after exerting its desired effect. In some cases, the drug gets inactivated even before reaching its target in the cell, therefore, compromising the significance of all therapy. An example of this mechanism of resistance could be the increased amount of glutathione in cisplatin-resistant cells as a consequence of increased expression of γ-glutamylcysteine synthetase and γ-glutamyl transpeptidase synthetic enzymes (Figure 3). When platinum compound, such as cisplatin or carboplatin, is chelated by glutathione, it becomes ineffective and is effluxed out from the cell by export pumps for glutathione S-conjugates (GS-X) [7].

Some of the drugs reach cells in an inactive form that gets converted to the active form by enzymes in the cell cytoplasm. One of the examples is the fluoropyrimidine 5-fluorouracil (5-FU), an antimetabolite drug that is converted to three main active metabolites: fluorodeoxyuridine monophosphate, fluorodeoxyuridine triphosphate, and fluorouridine triphosphate. The main mechanism of 5-FU activation is conversion to fluorouridine monophosphate by thymidine phosphorylase which expression is deregulated in many 5-FU-resistant cancers. Although the data on the role of thymidine phosphorylase in modulating 5-FU responsiveness is contradictory, the overexpression of thymidine phosphorylase had been shown to increase sensitivity to the drug [8].

Another strategy for effective cancer treatment is to exploit metabolic and signaling aberrations in cancer cells to an effective conversion of pre-drug to its active form. For instance, cancer cells are less sensitive to oxidative stress due to elevated expression of enzymes with antioxidant functions, such as haem oxygenase (HMOX1), NAD(P)H:quinone oxidoreductase 1 (NQO1) or glutathione S-transferases (GSTs). Even though cancer cells have strong antioxidant mechanisms, they maintain higher levels of reactive oxygen species (ROS) levels than normal cells and might be more sensitive to agents that cause further accumulation of ROS [9].

1.2.3. Alterations in drug targets

Drug response and resistance can be affected by alterations to the drug target, such as mutations or changes in expression level. For example, one of the ways 5-FU exerts its anticancer effect is through the inhibition of thymidylate synthase, and most of the preclinical studies have demonstrated that thymidylate synthase expression is a key determinant of 5-FU sensitivity. Therefore, gene amplification of thymidylate synthase or changes in thymidylate synthase promoter activity resulting in higher thymidylate synthase expression levels is a contraindication for 5-FU-based treatment [8].

Cancers are often highly dependent on specific oncogenic mutations that occur in kinases, thus, inhibition of those kinases is a promising strategy for cancer therapy. Unfortunately, the long term efficacy of these drugs is hindered by the development of drug resistance due to mutation of the targeted protein. In the case of inhibiting receptor tyrosine kinases BCR/ABL and EGFR that are found to be driver oncogenes in chronic myeloid leukemia and non-small cell lung cancer, respectively, resistance

emerges as a result of mutations occurring at the gatekeeper residues of the kinase domain which disables drug binding [10].

1.3. Adaptive responses to DNA damage

Many chemotherapeutic drugs induce DNA damage either directly by interacting with DNA sequence or indirectly targeting DNA replication-associated proteins. Depending on the severity of DNA damage cells either repair existing damage and continue to proliferate or induce cell death-associated mechanisms. Thus, the effectiveness of these chemotherapy drugs highly depends on the DNA damage repair capacity of cancer cells [1].

1.3.1. Cell cycle arrest in response to DNA damage

Normally, tight regulation of cell cycle progression assures repair of DNA damage at G1/S, intra-S, and G2/M phase checkpoints, whereas, cancer cells have often acquired traits to bypass these control mechanisms. Most of the drugs causing DNA damage via DNA modification or double-strand breaks induce activation of the PI3K-like kinase ataxia- telangiectasia mutated (ATM) and drugs causing replication fork stalling induced activation of ataxia-telangiectasia and Rad3-related (ATR). These kinases phosphorylate the checkpoint effector kinase CHK2 and CHK1, respectively, which activate p53 and p21 proteins responsible for G1/S checkpoint arrest (Figure 4). Alternatively, CHK2 and CHK1 inhibit various cell division-associated proteins to cause cell cycle arrest at the intra-S or G2/M checkpoints. During cell cycle arrest normal cells attempt to repair existing DNA damage and in the case of failure go into senescence or apoptosis, whereas, genomically unstable cancer cells continue to proliferate acquiring even more mutations [11].

The cell cycle is driven by a family of cyclin-dependent kinases (CDKs) which are positively regulated by cyclins and negatively regulated by CDK inhibitors. The pattern of cyclin expression varies with the progression of a cell through the cell cycle. As the position of the cells in the cell cycle and various cell cycle aberrations can affect sensitivity to the chemotherapy drug treatment, the cell cycle-mediated resistance is emerging concept that may be evaded by the usage of a novel class of cell cycle-specific modulators or by appropriate sequencing and scheduling of agents in combination chemotherapy [12]. Cell cycle based agents have been categorized as CDK inhibitors, Cdc25 inhibitors, checkpoint inhibitors, and mitotic inhibitors. Although the efficacy of these inhibitors in the clinic has been modest, it has

been suggested that cell cycle agents could play a better role as a partner with chemotherapy drugs [13].

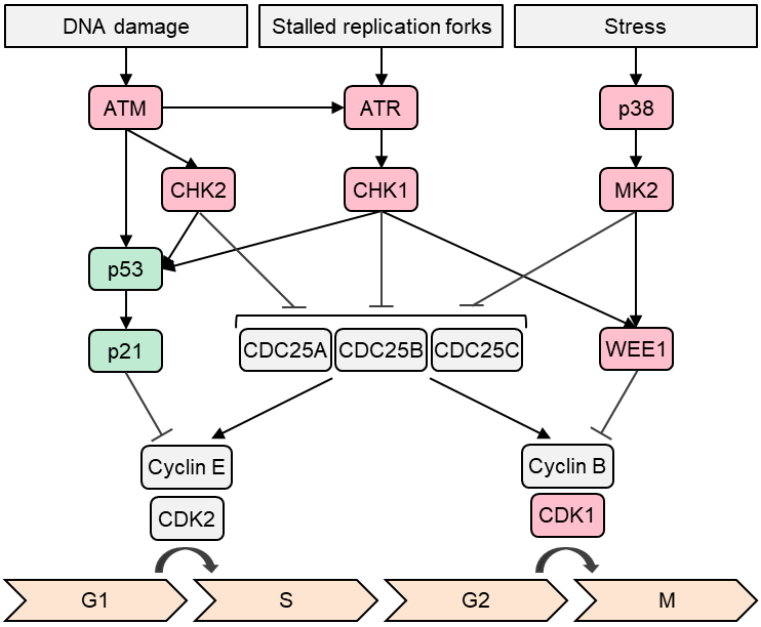

Figure 4. DNA damage-induced cell cycle checkpoints. Expression of proteins in red is usually increased in resistant cells and expression of the proteins in green is usually decreased. [11]

There are two strategies to overcome the lack of cell cycle control mechanisms in cancer cells: (I) one of them is to override cell cycle checkpoints by the inhibition of DNA damage-sensing kinases in anticipation of extensive DNA damage leading to mitotic catastrophe and cell death or (II) reactivating proteins involved in DNA damage-mediated cell cycle checkpoint activation [11]. As p53 protein, also called 'the guardian of the genome', is a substrate for both the ATM and ATR kinases, as well as for CHK1 and CHK2, reactivation of p53 function is a useful therapeutic strategy. Most of DNA damage-sensing kinases phosphorylate N-terminus of p53 protein to promote its stabilization by disrupting its interaction with negative regulators MDM2 and MDM4. Moreover, phosphorylation allows the interaction of p53 with transcriptional cofactors and DNA, which is ultimately important for the activation of target genes and responses such as cell cycle arrest, DNA repair, apoptosis, and senescence [14].

1.3.2. Changes in p53 protein function

Cancer genome sequencing has shown that nearly 50% of cases across 12 different tumor types carry mutations in the *TP53* gene encoding p53 protein. Most of these mutations are missense mutations located in the core DNA-binding domain and impair the normal function of p53 protein by disrupting DNA binding or destabilizing its structure. DNA-contact mutants have substitutions in amino acid residues that make direct contact with DNA and do not have a profound effect on protein structure. On the other hand, structural p53 mutants carry amino acid substitutions that disrupt the folding of the core domain and often are located in the tightly packed hydrophobic β-sheet [15].

Wild type p53 promotes basic cellular functions of cell cycle arrest, senescence, and apoptosis primarily through the activation of specific genes. In the earliest models, p53 tumor suppressor activity was based on the cell cycle arrest in response to DNA-damage signals allowing cells to repair their genomes and thereby limiting the propagation of potentially oncogenic mutations. Newer models show the involvement of p53 in various DNA repair mechanisms by activating numerous target genes that are implicated in different DNA repair programs. This data shows the complexity of p53 function in the active maintenance of genomic integrity [14]. Moreover, p53 controls additional non-canonical cellular programs and can modulate autophagy, alter metabolism, repress pluripotency and cellular plasticity, and facilitate an iron-dependent form of cell death known as ferroptosis [16].

In contrast, mutant p53 proteins can gain tumor-promoting functions resulting in increased metastasis and genomic instability. Mutant p53 protein can exert its oncogenic function via a variety of mechanisms, such as (I) alterations in DNA-binding ability, (II) changes in the interaction with other proteins including other transcription factors or (III) proteins not directly related to the regulation of gene expression [17]. Despite causing genomic instability by losing its normal functions due to DNA-binding alterations, mutations in p53 protein can have other biological manifestations. One distinctive feature of many p53 mutants is the ability to promote an elevated resistance to a variety of proapoptotic signals. Furthermore, p53 mutant cells harbor higher metastatic potential due to increased cell migration and invasion potential [18]. In addition, recent data suggest that mutant p53 can alternate many cellular functions through chromatin remodeling, rendering portions of the genome accessible or inaccessible to available transcription

factors and resulting in broad, genome-wide changes in gene expression [19].

Making matters even more complex, p53 protein can be involved in contradictory responses independently from its mutational status. If some activities of p53 that normally contribute to tumor suppression are not properly regulated, they might help promote cancer development, for example, the prosurvival functions of p53, which protect cells undergoing repair following mild stress, could be extremely counterproductive if maintained in irreparably damaged cells [20]. All these p53-mediated processes are tightly regulated by the oscillatory dynamics in single cells affecting DNA damage response and, therefore, resistance to the chemotherapeutic drug of individual cells [21], [22].

1.3.3. Alterations of DNA damage repair

DNA damage repair-deficiency can be exploited for more effective cancer cell treatment. For example, platinum compounds cause DNA inter-strand and intra-strand crosslinks that are recognized and repaired by nucleotide excision repair (NER) or homologous recombination. Therefore, these agents are effective in patients with ovarian cancer because these tumors commonly harbor defects in homologous recombination and patients with ERCC1-negative non-small-cell lung cancers as ERCC1–ERCC4 complex is essential for NER pathway [7], [23].

On the other hand, other alterations in DNA damage repair systems could have the opposite effect and reduce the efficacy of chemotherapy drug treatment. For instance, increased tolerance to platinum-induced DNA damage can occur through loss of function of the mismatch repair (MMR) pathway. Interestingly, cisplatin-induced DNA adducts are recognized by the MMR proteins MSH2, MSH3, and MSH6 and, after a few unsuccessful repair cycles, MMR proteins trigger an apoptotic response. Loss of MMR function due to mutations or decreased expression of MMR proteins results in reduced apoptosis induction and, consequently, drug resistance [7].

Fortunately, loss of function of DNA repair genes can cripple the affected pathway to the extent that tumor cells become highly sensitive to certain types of DNA damage and remaining repair pathways may become essential for survival. This phenomenon had given rise to the concept of synthetic lethality which states that two genes are said to be ‘synthetic lethal’ if mutation of either gene alone is compatible with viability but simultaneous mutation of both genes causes death [24]. An example of synthetic lethality

could be the inhibition of PARP proteins in cells with defects in either the BRCA1 or BRCA2 genes. PARP inhibition allows the persistence of spontaneously occurring single-stranded breaks which in normal cells are successfully repaired by homologous recombination. Since homologous recombination relies on functioning BRCA1 or BRCA2 proteins, alterations of these genes cause accumulation of DNA breaks and consequential cell death [25].

1.4. Downstream resistance mechanisms

After a sufficient amount of active drug has accumulated and inhibited its cellular target or induced genotoxic response, the outcome of treatment is dependent on how the cancer cell responds. Ideally, drug-induced damage should be tightly coupled to the induction of cell death, however, numerous intrinsic adaptive responses that usually involve changes in cell signaling leading to apoptosis induction occur and promote cancer cell survival [1].

1.4.1. The prosurvival signaling via receptor tyrosine kinases

The activation of receptor tyrosine kinases (RTK) often promotes cell proliferation, survival, invasion, and metastasis, thus, mutations in RTKs or their downstream targets resulting in uncontrollable activation are quite frequent. As such, RTKs are the subject of major ongoing efforts to develop targeted cancer therapies. Several strategies are used to develop RTK-based cancer therapies, such as monoclonal antibodies blocking either receptor or its ligand, and small-molecule inhibitors (Figure 5). However, tumor cells frequently develop secondary RTK mutations or alternative activation pathways emerge [26].

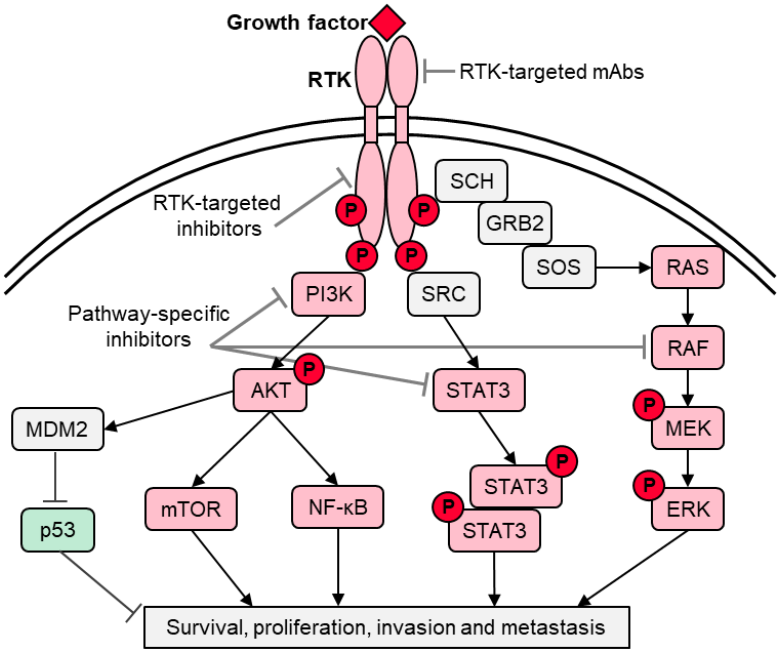

Figure 5. Resistance-promoting activation of prosurvival signaling via receptor tyrosine kinases. Expression of proteins in red is usually increased in resistant cells and expression of the proteins in green is usually decreased. [1]

Furthermore, activation of prosurvival signals can lead to decreased sensitivity to conventional chemotherapy drug rendering treatment less effective. Exploiting tumor cell addiction to a specific signaling pathway activation can contribute to the efficiency of treatment. Therefore, the molecularly targeted agents that are used to block these pathways are themselves subject to various adaptive resistance mechanisms and well as targeted combination therapy [1]. For example, sequential administration of EGFR inhibitors sensitizes cancer cells to subsequent genotoxic chemotherapy confirming the interconnection between DNA damage response and prosurvival signaling networks [27].

The strength of signal transduction can be altered not only by mutation of RTK or its downstream targets but with RTK surface abundance and distribution. Locally high surface levels of an individual RTK may promote homodimerization or clustering, and a high surface abundance of two or more RTKs may also increase heterodimer pairing [28]. Moreover, an increase in RTK ligand levels, through autocrine production or paracrine contribution from the tumor microenvironment could confer persistent activation of the signaling pathway and resistance [1].

1.4.2. Promotion of cancer cell stemness through receptor stimulation

Certain signaling pathways activation is essential for promoting and maintaining stem cell-like characteristics such as self-renewal and differentiation potential. CSCs display many characteristics of embryonic or tissue stem cells and activate developmental signaling pathways through WNT, Hedgehog, and Notch receptors. Therefore, activation of these pathways may play an important role in the expansion of CSCs and hence the resistance to therapy [4].

In particular, WNT activating mutations are essential for the initiation and maintenance of several tumor types including colorectal, breast, and ovarian cancer. Increased WNT signaling activity, WNT pathway activating gene mutations or amplifications as well as autocrine production of various WNT ligands cause an increase in β-catenin stability leading to the chemoresistant, aggressive tumor phenotype and poor treatment outcome [29].

Another example of stemness promoting signaling pathways is c-KIT pathway activation via its sole ligand SCF. C-KIT is used as one of the markers of CSC and circulating tumor cells, not to mention, c-KIT-expressing cells have the higher metastatic and tumor-initiating capacity. Furthermore, c-KIT has been implicated in several tumor types, including small cell lung carcinoma, malignant melanomas, colorectal cancer, and in more than 80% of cases of gastrointestinal stromal tumors [30]. C-KIT can be used as an effective marker for predicting cancer metastasis and response to chemotherapy. Complementing the role of c-KIT, SCF may also play a role in cancer progression, as well as the SCF gradient may be one driver of bone metastasis [31].

1.4.3. Oncogenic bypass through PI3K-AKT-mTOR pathway

Although inhibiting prosurvival signals through RTK activation can increase sensitivity to chemotherapy drugs and exploit tumor addiction to certain signals, numerous cases suggest the development of various adaptive resistance mechanisms. One of the examples could be activation of PI3K-AKT-mTOR pathway through oncogenic bypass then primary drug target RTK remains unaltered and continues to be inhibited, but an alternative kinase becomes activated owing either to an adaptive feedback loop or a genetic mutation [1]. Approximately 20% of patients with oncogenic-EGFR-driven lung cancer develop amplification of other RTK, named c-MET,

which activates PI3K via an alternative pathway after administration of EGFR inhibitors [32].

As activation of PI3K kinase initiates a signal transduction cascade through the PI3K-AKT-mTOR signaling axis that promotes cancer cell growth, survival, and metabolism, PI3K pathway inhibitors are involved in early-phase clinical trials and promising designs of combination therapies [33]. Overall, investigations involving therapeutic targeting of the PI3K-AKT-mTOR pathway have resulted in the development of several distinct classes of drugs, including PI3K and AKT inhibitors, as well as allosteric mTOR and catalytic mTOR kinase inhibitors [34]. However, PI3K pathway inhibitors show limited efficacy due to the presence of signaling feedback loops resulting in alleviation of the repression of other prosurvival and growth pathways. For example, mTORC1 inhibition leads to the activation of PI3K signaling through a feedback loop [35].

Limited single-agent activity, problematic levels of toxicity, and a lack of predictive biomarkers for treatment selection have all been major barriers for effective clinical application of agents targeting components of the PI3K-AKT-mTOR pathway [34]. Even though, preclinical data suggest that PI3K-AKT pathway inhibitors might be effective in overcoming acquired resistance to therapies that target receptor tyrosine kinases and can be used in combination with other targeted therapies [33].

1.4.4. Inhibition of stress-activated MAP kinases

Mitogen-activated protein kinases (MAPKs) are signaling components downstream of RTKs that are important in converting extracellular stimuli into a wide range of cellular responses. Two major stress-activated MAPK pathways, the Jun N-terminal kinase (JNK) and p38 MAPK are activated by environmental and genotoxic stresses and have key roles in controlling cell proliferation, differentiation, survival, and migration of specific cell types. Altered expression of JNK and p38 MAPK proteins in human tumors and cancer cell lines is often observed [36].

The JNK pathway is involved in stimulating apoptotic signaling by the JNK translocation to the nucleus and the transactivation of c-Jun transcription factor. Moreover, an alternative pathway contributing to JNK-mediated apoptosis involves the phosphorylation of p53 protein by JNK, induction of caspase-8-dependent cleavage of Bid, and modulation of the activities of other pro-apoptotic BH3-only subgroups of Bcl2 family of proteins [37].

The p38 MAPK pathway controls cell cycle at G0, G1/S andG2/M transition in response to various environmental and genotoxic insults. Depending on the cell type, p38 MAPK can either induce progression or inhibition at G1/S transition by differential regulation of specific cyclin levels as well as by phosphorylation of RB protein, which is a hallmark of G1/S progression and by phosphorylation of the p53 tumor suppressor on two activating sites in the N-terminal region. On the other hand, activation of p38 MAPK initiates G2/M checkpoint and G1 arrest following UV-induced DNA damage [38].

In summary, drug-induced activation of JNK and p38 MAPKs could be a strategy worth exploring for sensitizing cancer cells to apoptotic death. However, given the many tumorigenesis-related functions that stress-activated MAPKs can control, both in the cancer cell and in the tumor microenvironment, inhibition of these pathways for therapeutic purposes should be strictly dependent on cell context, tumor cell type, and tumor stage [36].

1.4.5. Dysfunctional apoptotic signaling

Although resistance to apoptosis is a hallmark of cancer, cancer cells rarely rely on anti-apoptotic proteins for their survival and apoptosis-targeted therapy is not widely used. On the other hand, evading apoptosis is a useful strategy for developing resistance chemotherapeutic agents that don't target apoptosis-inducing proteins directly [1].

One of the most extensively studied pathways involved in the apoptotic response to chemotherapy is the activation of Bcl-2 family members (Figure 6). Various Bcl-2 family proteins have roles in regulating chemotherapy-induced apoptosis, including the anti-apoptotic Bcl-2 family members, pro-apoptotic family members (BAX, BAD, and BAK) and BH3-only proteins that can antagonize the anti-apoptotic BCL-2 family members. The interplay between members of this family is critical in determining cell fate by either inhibiting or facilitating MOMP induction. Moreover, the ratio of anti-apoptotic and pro-apoptotic Bcl-2 proteins rather than the expression levels of one particular protein of the Bcl-2 family regulate apoptosis sensitivity [39]. Recently, substantial progress has been made in generating pharmacological inhibitors of anti-apoptotic Bcl-2 family members for cancer treatment, however, resistance mechanisms limit the effectiveness of these agents [1].

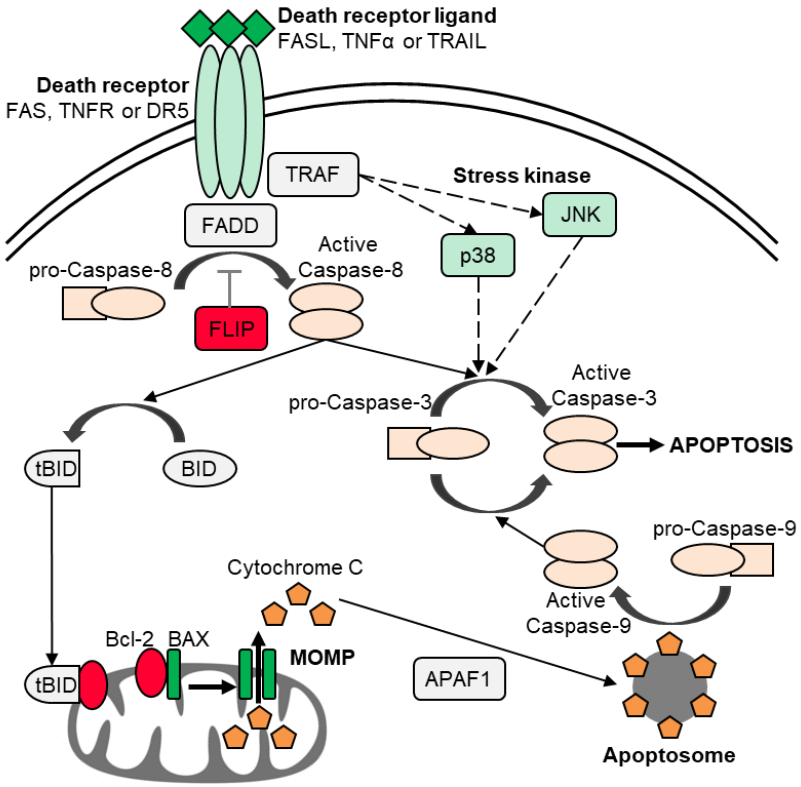

Figure 6. Apoptosis signaling via death receptors resulting in mitochondrial outer membrane permeabilization and executive caspase-3 activation. Expression of proteins in red is usually increased in resistant cells and expression of the proteins in green is usually decreased. [1]

The second apoptosis-inducing pathway altered in chemotherapy-resistant tumors is the death receptor pathway activated by TNF receptor superfamily members such as FAS, TNF receptor 1 and TRAIL. Death receptor signaling can be impaired in cancers in several ways: (I) downregulated or even absent surface expression preventing the transmission of the death signal from the cell surface to intracellular signaling cascades, (II) abnormal transport to the cell surface or (III) functional impairment due to mutation. Furthermore, pro-apoptotic signaling of death receptors can be hindered by downstream proteins, for example by increased expression of the caspase-8 inhibitor FLIP making inhibition of FLIP a promising therapeutic strategy [39].

1.5. Tumor cell heterogeneity and plasticity

Most of the resistance-promoting adaptive responses happen due to innate tumor cell heterogeneity and plasticity. As a result of heterogeneity, the bulk tumor might include a diverse collection of cells harboring distinct molecular signatures with differential levels of sensitivity to treatment [40]. On the other hand, cell plasticity drives their transformation towards a phenotypic state that no longer depends on the drug- targeted pathway, thus, acquiring permanent resistance to therapy [41]. (Figure 7)

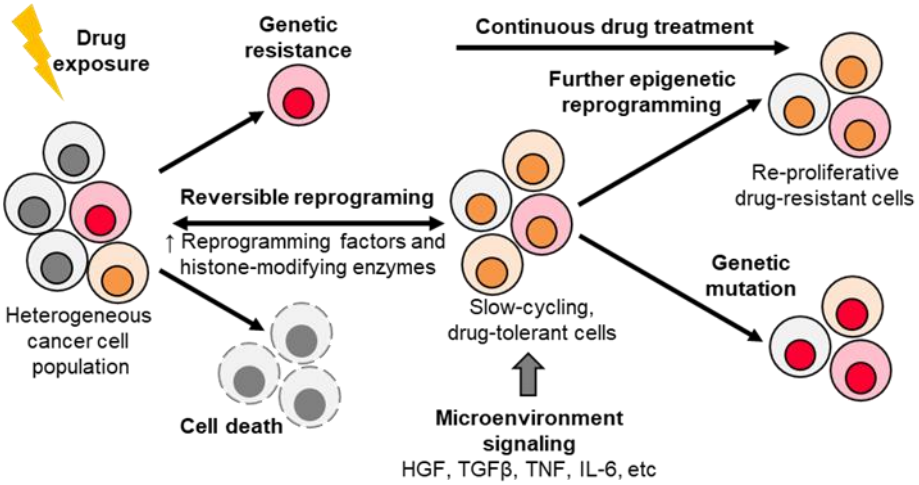

Figure 7. Role of heterogeneity and plasticity in the development of resistance-promoting adaptive responses. [41]

1.5.1. Genomic instability and clonal evolution

As tumors accumulate somatic aberrations through an evolutionary process, the majority of these events are likely to be passenger mutations that do not provide any selective benefit to the cancer cell, a small subset will represent cancer driver mutations, conferring a selective advantage [42]. Genomic instability promotes genetic diversity by providing the raw material for the generation of tumor heterogeneity, thus, is critical to the development and progression of many cancers. For example, microsatellite instability (MSI), due to deficiencies in DNA mismatch repair (MMR), drives neoplastic transformation and increases the rate of somatic mutations of the subset of colorectal cancers (CRCs) [43]. Moreover, DNA damage-based chemotherapy treatment might also increase genomic instability and promote

genetic diversity by changing the balance between the activation of oncogenes and tumor suppressors [40].

Additionally, under therapeutic selective pressure, resistance to treatment can emerge as a result of the expansion of pre-existing subclonal populations or the evolution of drug-tolerant cells. Therefore, clinical assessment of tumor heterogeneity might lead to combinatorial approaches that pair therapies targeting the predominant, drug-sensitive population in addition to the various subsets of drug-resistant and drug-tolerant cells [40]. Furthermore, an understanding of a tumor's evolutionary history and tumor development can shed light on the complexity of cancer development helping the advancement of precision medicine and screening approaches to detect disease early [42].

1.5.2. Epigenetic drivers of drug resistance

The adaptation chemotherapic treatment arises not only due to irreversible mutational changes but also due to reversible epigenetic changes. In contrast to gene mutations, which can affect gene expression in one functional step, epigenetic changes in cancer have been proposed to originate from chromatin states of multiple genes that can modulate the expression of several pathways [44]. The activation or repression of sets of genes determining the fate of the cell during development and differentiation is thought to be maintained by bivalent chromatin in embryonic stem cells. Interestingly, some of these genes are frequently DNA hypermethylated in cancer enhancing the likelihood of tumor initiation and progression from cell transformation as it renders a transient transcription-ready state of key tumor suppressors to one of heritable, permanent gene silencing [45].

There is evidence that pharmacological reversion of repressive DNA and histone epigenetic marks can lead to the resensitization of tumors to chemotherapy and some such drugs have entered clinical trials as resistance modulators showing conflicting results. Epigenetic events, such as gene promoter DNA hypermethylation, cause changes in gene expression leading to tolerance to drug treatment and these changes can be prevented or reversed by inhibition of DNA- and histone-modifying enzymes [44].

Histone deacetylase (HDAC) inhibitors and DNA methyltransferase (DNMT) inhibitors produce additive effects on gene expression inhibiting the emergence of drug-resistant clones. For instance, tolerant non-small-cell lung cancer cells that survive exposure to EGF tyrosine kinase inhibitors can be abolished by HDAC preventing stress-induced mutagenesis and selection

of new resistance-conferring mutations [46]. On the other hand, there is a potential of these inhibitors to activate unwanted genes, including drug resistance genes and genes that accelerate tumor progression, which is a major concern for wider application of this type of targeted therapy [44].

1.5.3. Epithelial-mesenchymal transition

Activation of the epithelial-mesenchymal transition (EMT) program induces profound changes in various aspects of cell morphology and physiology, most notably in cell-cell junctions, cytoskeletal composition, cellular interactions with the extracellular matrix (ECM), and cell polarity. Nonetheless, EMT can contribute to the pathogenesis of human carcinomas and is associated with metastasis and a poor prognosis. As EMT is a dynamic process, tumor cells can occupy intermediate EMT states characterized by a mix of epithelial and mesenchymal features (partial EMT) and can revert to a more epithelial phenotype through the process of mesenchymal-epithelial transition (MET) [47].

Recently, the scope of biological processes driven by the EMT program has been expanded beyond the carcinoma-cell invasion. Experimental activation of EMT, via either the overexpression EMT-inducing transcription factors or treatment with most prominent EMT inducer TGFβ, confers many of the properties of CSCs on epithelial carcinoma cells. These include CSC-specific cell-surface marker expression, an increased ability to form spheres in suspension culture, and an enhanced ability to initiate tumors in mice. Interestingly, the tumor-initiating ability of carcinoma cells is also affected by the level of EMT-program activation, peaking at an intermediate level of EMT, therefore, an extensive EMT activation is usually detrimental to tumor-initiating ability [48]. Cells in an intermediate stage of EMT with the desired combination of epithelial and mesenchymal traits that maintain their epithelial-mesenchymal plasticity, harbor different combinations of EMT-inducing transcription factors. Retention of such plasticity appears to be important, since the constitutive expression of strong EMT-inducers, blocks epithelial-mesenchymal plasticity, thereby reducing the ability of cancer cells to establish new tumors or metastatic colonies [49].

Furthermore, EMT status can be associated with cancer cell resistance as monitoring the levels of EMT-inducing transcription factors expression has been demonstrated to be of prognostic value in a variety of cancers. EMT-related transcription factors can directly influence the expression of drug-inactivating enzymes or transporters, as well as regulate other resistance-

associated traits such as reduced proliferation, upregulation of prosurvival pathways, and ALDH activity that are often attributed as characteristics of cancer stem cells [50].

2. MATERIALS AND METHODS

2.1. Cell culture, drug treatment and establishment of resistant cell lines

Human breast adenocarcinoma MDA-MB-231 (obtained from ECACC) and human colorectal carcinoma HCT116 (obtained from ATCC) cells were maintained in Dulbecco's modified Eagle's medium (DMEM) (Life Technologies) supplemented with 10% fetal bovine serum (FBS) (Life Technologies) and penicillin-streptomycin antibiotics (Life Technologies).

The treatment scheme of drug treatment was adjusted according to various parameters. (I) In the case of RH1 treatment, cells were always treated with RH1 for 2 h considering rapid RH1 clearance from the blood during the chemotherapy [51]. Then media with RH1 was removed, cells washed with PBS and left to recover in fresh growth media. The time of the treatment is counted since the input of RH1. (II) In the case of 5-fluorouracil and oxaliplatin, cells were treated with drugs for 48 h according to the duration of one standard chemotherapy cycle in the FOLFOX regimen [52]. Then media with the drug was removed, cells washed with PBS and left to recover in fresh growth media. The time of the treatment is counted since the input the drug, regular treatment performed for 48 h except for methods where the shorter time treatment was sufficient for the expected result.

The RH1-resistant cell line was established by treating MDA-MB-231 cells with RH1 pulses for 2 h followed by cell recovery stage. This development period was carried out for 6 months and included 15 treatment cycles. The 5-fluorouracil- and oxaliplatin-resistant cell lines were established using continuous repopulation of cells in medium supplemented with low doses of the drug. This development period was carried out for about 9 months by the Department of Biochemistry and Molecular Biology (Life Sciences Center, Vilnius University).

2.2. Drugs and inhibitors

RH1 was provided by N. Cenas' lab (Life Sciences Center, Vilnius University). 5-fluorouracil, oxaliplatin, and cisplatin were purchased from Teva Baltics.

JNK inhibitor SP600125, c-KIT inhibitor masitinib (AB1010), MET inhibitor PHA-665752, RTK inhibitor cabozantinib (XL184), mTOR inhibitor INK128, pan-caspase inhibitor Z-VAD-FMK, caspase-3/7 inhibitor

Z-DEVD-FMK, caspase-8 inhibitor Z-IETD-FMK, necroptosis inhibitor Necrostatin-1, BH3 mimetic ABT-737, p38 inhibitor PH-797804, and MDM2-p53 interaction inhibitor Nutlin-3a were purchased from Selleckchem. AKT inhibitor VIII, PI3K inhibitor LY294002, mTOR inhibitor rapamycin, ABCC4 inhibitor Ceefourin-1, and caspase-1 inhibitor Ac-YVAD-FMK were purchased from Sigma-Aldrich. The concentration used for each application is designated in the description of each application.

2.3. Assessment of cell viability and cell death

The resistance to RH1, conventional chemotherapy drugs or inhibitors was evaluated using MTT assay. The day before treatment cells were seeded in 96-well flat-bottomed plates (3000 cells/well). Cells were treated with various agent concentrations for the indicated time. After treatment, fresh growth media was applied and the MTT test was performed 96 hours after the beginning of the treatment. Media with 0.5 mg/mL MTT was added to each well and incubated for 0.5-1 h at 37 °C. The formazan product was dissolved by adding 100 µL dimethylsulfoxide to each well, and the plates were read at 550 nm with Varioskan Flash Multimode Reader (Thermo Scientific). Results were normalized according to untreated control and changes were evaluated. All measurements were performed in quadruplicate and each experiment was repeated at least three times.

Differences in drug-induced cell death were evaluated using ethidium bromide (Roth), propidium iodide (Roth), active caspase-3/7 dye or Guava Nexin (Merck Millipore) assay. For ethidium bromide or propidium iodide assay cells were seeded in 24-well flat-bottomed plates (5×10^4 cells/well). The next day the cells were treated with the drug at various concentrations. 48 h after treatment cells were stained with 5 µg/mL ethidium bromide of propidium iodide for 10 min, then detached with trypsin and subjected for the analysis. For active caspase-3/7 assay cells were seeded in 24-well flat-bottomed plates (5×10^4 cells/well) and treated with 2 µM CellEvent™ Caspase-3/7 Green Detection Reagent (Invitrogen) for 30 min, then detached with trypsin and subjected for the analysis. The apoptotic changes were measured by flow cytometry (Guava easyCyte 8HT Flow Cytometer, Merck-Millipore) and the results analyzed using Flowing Software (Turku Centre for Biotechnology). Each experiment was repeated at least three times.

For Guava Nexin assay cells were seeded in 22 cm^2 dishes. The next day cells were treated with 50 nM RH1 for 2 h. 48 h after treatment cells were detached with trypsin and stained with Guava Nexin reagent according to

manufacturer protocol. The apoptotic changes were measured by flow cytometry (BD FACSCanto II, BD Biosciences). Each experiment was repeated at least three times.

2.4. Cell cycle analysis and other flow cytometric assays

For cell cycle analysis, cells untreated or treated with various agent concentrations for the indicated time were harvested with trypsin. Cells were washed and resuspended in ice-cold PBS and fixed by adding 100 µL of the cell suspension to 900 µL of 96% ethanol dropwise. Cells were stored at -20°C at least overnight, treated with 100 µg/mL RNAse A for 5 min and 50 µg/mL stained with propidium iodide solution in PBS for 10 min. Cell cycle analysis was performed using Guava easyCyte 8HT Flow Cytometer (Merck-Millipore) and analyzed using Flowing Software (Turku Centre for Biotechnology). Pulse processing was used to exclude cell doublets from the analysis.

For immunofluorescent flow cytometry experiments, 1×10^5 cells were detached with Accutase (Thermo Fisher Scientific), washed with PBS containing 1% bovine serum albumin (BSA) (Roth) and stained with FITC-conjugated CD44 monoclonal antibody (Thermo Fisher Scientific) or FITC-conjugated mouse IgG2b for isotype control (Thermo Fisher Scientific) for 30 min. After staining, cells were placed in PBS containing 1% BSA and analyzed with a BD FACSCanto II flow cytometer (BD Biosciences) with a 488-nm blue laser and standard FITC 530/30nm bandpass filter. Each experiment was repeated at least three times.

For rhodamine efflux analysis, cells were seeded in 24-well flat-bottomed plates (5×10^4 cells/well) and treated with 1 µg/mL Rhodamine123 (Sigma-Aldrich) for 30 min. Then cells were detached with trypsin, washed with PBS containing 1% bovine serum albumin (BSA), subjected for the analysis by flow cytometry (Guava easyCyte 8HT Flow Cytometer, Merck-Millipore). Each experiment was repeated at least three times.

2.5. Western blot analysis

For western blot analysis, cells were seeded in 22 cm^2 dishes (1×10^6 cells/well) and treated with various agent concentrations for the indicated time. Cells were washed with PBS and lysed with EB++ buffer with protease and phosphatase inhibitors (10 mM Tris-HCl (pH 7.4), 50 mM NaCl, 5 mM EDTA, 50 mM NaF, 1% Triton X-100, 1 mM PMSF, 20 nM aprotinin, 2 mM Na_3VO_4) and centrifuged. Post-nuclear lysates were resolved using

SDS-PAGE, the proteins were transferred to polyvinylidene difluoride membrane (PVDF) (Bio-Rad) and blocked in blocking buffer (0.9% NaCl, 8 mM TRIS-HCl, 2 mM TRIS, 1% skimmed milk, 0.025% Tween-20, 0.05% NaN_3). The membranes were incubated for 2 h with the primary antibody. CD44 (8E2), JNK, phospho-JNK, AKT and phospho-AKT (Ser473) antibodies were purchased from Cell Signaling Technology, β-actin (BA3R), phospho-AKT (Thr308), p53 (DO-1) antibodies were purchased from Thermo Fisher Scientific, α-tubulin was purchased from Merk Millipore, and anti-FLAG (M2) was purchased from Sigma Aldrich.

After primary antibody treatment, (I) membranes were incubated for 1 h with the alkaline phosphatase-conjugated secondary mouse or rabbit antibody (Merk Millipore). Blots were developed using nitro-blue tetrazolium and 5-bromo-4-chloro-3-indolyl phosphate tolidium salt. Or (II) membranes were incubated for 1 h with IRDye® 800CW mouse (LiCOR) or IRDye® 680RD rabbit (LiCOR) secondary antibodies and then scanned with Odyssey® imaging system (LiCOR).

2.6. Oligoprecipitation assay

For the oligoprecipitation assay, cells were seeded in 22 cm^2 dishes (1×10^6 cells/well) and treated with 10 μM oxaliplatin for 24 h. Cell plasma membrane was lysed using cytoplasmic lysis buffer (20 mM TRIS-HCl (pH 7.5), 0.2 mM EDTA, 1 mM DTT, 0,1% Triton X-100, 20% glycerol, 1.5 mM $MgCl_2$, 10 mM NaCl, 1 mM PMSF, 2 mM Na_3VO_4) for 10 min on ice and then centrifuged at 800 g for 5 min. Then the nuclear fraction was collected and lysed with nuclear lysis buffer (20 mM TRIS-HCl (pH 7.5), 0.2 mM EDTA, 1 mM DTT, 0,1% Triton X-100, 20% glycerol, 1.5 mM $MgCl_2$, 0.5 mM NaCl, 1 mM PMSF, 2 mM Na_3VO_4) for 30 min at 4 °C rocking. Nuclear lysates were cleared by centrifugation at 20000 g for 15 min and 100 μL of supernatant was added to 400 μL DNA binding buffer (128 mM TRIS-HCl, 1 mM EDTA, 5 mM DTT, 4% glycerol, 1 mM PMSF, 2 mM Na_3VO_4) containing 1 μg poly-dIdC and 5 nmol of biotinylated oligonucleotide and incubated for 15 min at 4 °C rocking. Then 10 μL of Streptavidin-conjugated agarose (Thermo Scientific) was added to the mix and incubated for 45 min at 4 °C rocking. Agarose-oligonucleotide-protein complexes were washed 5 times with DNA binding buffer, resolved using SDS-PAGE and analyzed by western blot.

Oligonucleotides used as a bait were p53-specific p21 promoter sequence (FW: 5'-biotin-ATCATGAACATGTCCCAACATGTTGAGCTC-3', RV:

5’-GAGCTCAACATGTTGGGACATGTTCATGAT-3’) and p53-unspecific scrambled control WRNC (FW: 5’-biotin-ATCATGAAAGGTGGATTTAGGTGGAAGCTC-3’, RV: 5’-GAGCTTCCACCTAAATCCACCTTTCATGAT-3’).

2.7. Confocal microscopy

Immunofluorescence experiments were performed on cells grown in 24-well plates on glass coverslips (5×10^4 cells/well). Cells were fixed with 4% paraformaldehyde (Roth) in PBS (pH 7.4), permeabilized with 0.2% Triton X-100 (Roth) and stained with primary antibody followed by secondary antibody. Cell nuclei were stained with 300 nM DAPI dye (ThermoFisher Scientific). Specimens were analyzed with a laser scanning spectral confocal microscope (Eclipse TE2000-S, C1 plus, Nikon) with Apo TIRF 60 × N/A 1.4 objective (Nikon).

Primary antibodies used for immunofluorescence analysis were anti-vimentin clone RV202 (BD Pharmingen), anti-CD44 clone 8E2 (Cell Signaling Technology), anti-phospho-Histone H2A.X (Ser139) (Cell Signaling Technology), anti-p53 clone DO-1 (Thermo Scientific), anti-phospho-p53(Ser15) clone 14H61L24 (Thermo Scientific), anti-Ki-67 clone MIB-1 (DAKO), anti-p21 clone F-5 (Santa Cruz Biotechnology), anti-Histone-H3(S10) clone ab47297 (Abcam), anti-pATM(S1981)-PE conjugate (Merk Milipore), and anti-FLAG clone M2 (Sigma Aldrich). Secondary antibodies were Alexa Fluor™ 488-conjugated anti-mouse IgG or Alexa Fluor™ 594-conjugated anti-rabbit IgG (Thermo Fisher Scientific).

DNA synthesizing cells were visualized using Click-iT™ EdU Alexa Fluor™ 488 Imaging Kit (Thermo Scientific) according to the manufacturer’s instructions. Briefly, cells were treated with 10 μM EdU for 2 hours before fixation, then were fixed with 4% paraformaldehyde in PBS (pH 7.4), permeabilized with 0.2% Triton X-100 and stained with Click-iT™ reaction cocktail for 30 minutes. Specimens were analyzed with a laser scanning spectral confocal microscope (Eclipse TE2000-S, C1 plus, Nikon) with Apo TIRF 60x N/A 1.4 objective (Nikon).

2.8. Sphere-forming assay

For the sphere-forming assay, a 24-well plate was coated with 1% agarose in PBS to limit cell attachment to the surface. Then suspended cells were embedded in 0.3% agarose matrix in DMEM medium with 0.1% FBS and Insulin-Transferrin-Selenium (ITS) (Life Technologies) to prevent cell

clumping and seeded 500 cells per well. The plate was kept at room temperature for 30 minutes allowing agarose matrix to solidify and then cells were treated with DMEM medium with 0.1% FBS and ITS containing inhibitors or growth factors.

Cells were grown for two weeks, cell feeding was performed every five days by adding DMEM medium with 0.1% FBS and ITS. Formed spheres were dyed using MTT dye and visualized using ImageJ software. The experiment was performed in duplicates and repeated three times.

2.9. Wound-healing assay

For the wound-healing assay, cells were seeded at 90-100 % confluence in 6-well plate and allowed to attach overnight. Confluent cultures were scratched with a 200 µl pipette tip and washed to remove detached cells and cell debris. Scratch area was photographed immediately after scratch and every 24 h to measure wound healing. Phase-contrast images were analyzed using the MRI Wound Healing Tool for ImageJ. Migration was quantified as the percent of gap closure compared with gap size at the start. The experiment was performed in duplicates and repeated three times.

2.10. Generation of stable expression cell lines using lentiviral vectors

The HEK293T cell line was manipulated for lentivirus production using the 3rd generation lentiviral system which uses three different plasmids for generating stable cell lines: packaging plasmid pCMV-dR8.2 (Addgene plasmid # 8455), envelope plasmid pCMV-VSV-G (Addgene plasmid # 8454) and transfer plasmid containing shRNA or protein of interest. HEK293T cells were seeded in a 6-well plate (5×10^4 cells/well) and transfected with all three plasmids using Lipofectamine 3000 reagent (Thermo Scientific) according to manufacturer's instructions. After 24 h transfection media was removed and cells were left to recover and produce virus in fresh growth media supplemented with 20% FBS for another 24 h. The virus was collected sterile glass pipette, transferred to the glass tube and 8 µg/mL polybrene (Sigma Aldrich) was added to the aspirated media. Then media was filtered through a 0.22 µm syringe filter (Merk Milipore) and transferred onto target cells.

After 24 h with virus-containing media, target cells were washed and fresh growth media with selection antibiotic was added. HCT116 cells were

treated with 2 μg/mL puromycin (Thermo Scientific) for 3 days or with 1 mg/mL hygromycin (Thermo Scientific) for 7 days.

For RNA interference, transfer plasmids containing p53-targeted simple hairpin shRNAs in the pLKO.1 lentiviral vector were used designed by The RNAi Consortium (TRC): TRCN0000003753, TRCN0000003754, TRCN0000003755, TRCN0000003756, TRCN0000010814 (Dharmacon). pLKO.1-scrambled vector (Addgene plasmid # 136035) was used as a negative control.

For inducible protein expression, transfer plasmid pCW57-MCS1-2A-MCS2 (Addgene plasmid # 71782) was used with cloned wild-type, mutated p53 or SLUG protein-encoding cDNA sequence. Protein expression was induced via supplementing growth media with 1 μg/mL doxycycline.

2.11. Genome engineering using the CRISPR/Cas9 system

To generate a protein knockout cell line, the CRISPR/Cas9 system was utilized. The target cell lines were transfected with pSpCas9(BB)-2A-Puro (PX459) V2.0 plasmid (Addgene plasmid # 62988) with inserted p53-targeting gRNA sequence using Lipofectamine 3000 reagent (Thermo Scientific) according to manufacturer's instructions. 24 h after transfection, the transfection media was removed and cells were briefly treated with 2 μg/ml puromycin (Thermo Scientific) for 48 h. Only cells successfully transfected with Cas9-carrying plasmid were able to withstand this short-time selection.

After the selection, cells were left to recover for 24 h and cloned into 96 flat-bottomed well plate 1 cell/well using serial dilution method. Cell quantity per well was evaluated after 24 h and only wells containing one cell were selected for further analysis.

Single-cell colonies were grown for 2-3 weeks, cell feeding with fresh media was performed every 5 days. Expanded colonies were tested for the presence of target protein using western blot analysis. 15 clones were pooled to create the knockout cell line.

TP53 gene was targeted by gRNA at 2nd and 3rd exons using these oligonucleotide sequences ligated into Cas9-carrying vector: Ex2 FW: 5'-CACCGTCGACGCTAGGATCTGACTG-3', Ex2 RV: 5'-AAACCAGTCAGATCCTAGCGTCGAC-3', Ex3 FW: 5'-CACCGACTTCCTGAAAACAACGTCC-3', Ex3 RV: 5'-AAACGAACGTTGTTTTCAGGAAGTC-3'.

2.12. Real-time qPCR for evaluation of the mRNA expression

Total RNA was isolated from approximately 1×10^6 cells using the GeneJET RNA Purification Kit (Thermo FisherThermoFisher Scientific) according to the manufacturer's instructions. To validate differential gene expression changes, RevertAid RT Kit (Thermo FisherThermoFisher Scientific) was used for complementary DNA synthesis according to the manufacturer's instructions. Briefly, 1 µg of total RNA was added to 20 µL reverse transcription (RT) reaction volume containing 5 µM random hexamer primers, 1 µM of dNTP mix, 20 U RNase inhibitor, and 20 U reverse transcriptase. Then the mixture was incubated at 25 °C for 5 min followed by synthesis at 42 °C for 60 min. and terminated by heating at 70 °C for 5 min. RT-qPCR was performed on the MasterCycler RealPlex4 RT-PCR system (Eppendorf) using 2x KAPA SYBR FAST qPCR Master Mix (KAPA Biosystems) according to manufacturer's instructions. All reactions were performed in a 10 µL reaction volume containing 5 µL 2× KAPA SYBR FAST qPCR Master Mix, 1 µL 5-fold diluted cDNA, 0.2 µL of 10 µM forward and reverse primer mixture and 3.8 µL of nuclease-free water. The reaction conditions were as follows: pre-denaturation at 95 °C for 3 min followed by amplification of 40 cycles. The relative changes in gene expression were evaluated by the ΔΔCt method as described previously [53]. For the normalization of the expression data, HPRT1 and TBP were used as reference genes. Primer sequences used in amplification are shown in Table 2.

Table 2. List of primer sequences used in RT-qPCR.

Gene	Forward sequence	Reverse sequence
DPP4	AGTGGCACGGCAACACATT	AGAGCTTCTATCCCGATGACTT
CD44	CTGCCGCTTTGCAGGTGTA	CATTGTGGGCAAGGTGCTATT
MSI	TAAAGTGCTGGCGCAATCG	TCTTCTTCGTTCGAGTCACCA
ALCAM	ACTTGACGTACCTCAGAATCTC	CATCGTCGTACTGCACACTTT
PROM1	TTCTTGACCGACTGAGACCCA	TCATGTTCTCCAACGCCTCTT
ITGB1	CAAGAGAGCTGAAGACTATCC	TGAAGTCCGAAGTAATCCTCCT
CD24	CTCCTACCCACGCAGATTTATT	AGAGTGAGACCACGAAGAGAC
KIT	ACTTGAGGTTTATTCCTGACCC	GCAGACAGAGCCGATGGTAG
KITLG	AATCCTCTCGTCAAAACTGAAG	CCATCTCGCTTATCCAACAATG
VIM	CCTTGAACGCAAAGTGGAATC	CCTTGAACGCAAAGTGGAATC
SNAI2	CGAACTGGACACACATACAGT	CTGAGGATCTCTGGTTGTGGT
CDH1	ATTTTTCCCTCGACACCCGAT	TCCCAGGCGTAGACCAAGA
CDH2	CCATCAAGCCTGTGGGAATC	GCAGATCGGACCGGATACTG
SNAI1	ACTGCAACAAGGAATACCTCA	GCACTGGTACTTCTTGACATCT
CDKN1A	TACCCTTGTGCCTCGCTCAG	GGCGGATTAGGGCTTCCTCT

GADD45A	GATGCCCTGGAGGAAGTGCT	GAGCCACATCTCTGTCGTCGT
BAX	CAAACTGGTGCTCAAGGCCC	GGGCGTCCCAAAGTAGGAGA
BBC3	GAGCGGCGGAGACAAGAG	TAAGGGCAGGAGTCCCATGA
PMAIP1	CCACGCTGCCATCGACTAC	GCCGACGCCACATTGTGTA
MDM2	CCATGATCTACAGGAACTTGG	GACACCTGTTCTCACTCACA
TP53	GCGTGTTTGTGCCTGTCCTG	TGGTTTCTTCTTTGGCTGGG
FAS	TGAAGGACATGGCTTAGAAGT	GGTGCAAGGGTCACAGTGTT
TNFRSF10B	GCACCACGACCAGAAACAC	ACAATCACCGACCTTGACCAT
TRAF4	AGGAGTTCGTCTTTGACACCAT	CTTTGAATGGGCAGAGCACC
TBP	CCACTCACAGACTCTCACAAC	CTGCGGTACAATCCCAGAACT
HPRT1	TGCAGACTTTGCTTTCCTTGGT	CCAACACTTCGTGGGGTCCTT

2.13. RNA isolation, miRNA sequencing, and data processing

Total RNA from cell lines was isolated using an RNAzol® RT (Molecular Research Center) reagent according to the manufacturer's instructions. RNA purity and concentration were assessed using NanoDrop (ThermoFisher Scientific). The integrity was assessed using an Agilent 2100 Bioanalyzer using Agilent RNA 6000 Nano Kit (Agilent) or agarose (1%) gel electrophoresis. To avoid DNA contamination before reverse transcription reaction, RNA samples were treated with DNase I (ThermoFisher Scientific) according to the manufacturer's instructions.

Complementary DNA (cDNA) libraries for sequencing were prepared using the NEXTflex Small RNA-Seq v3 kit (PerkinElmer) according to the manufacturer's instructions. Ligation reactions of 3′ and 5′ adapters were performed using 1.2 µg total RNA. The cDNA was amplified by 16 PCR cycles. PCR products were analyzed with Bioanalyzer (Agilent technologies) using DNA High sensitivity chip (Agilent Technologies) and were quantified by KAPA Library Quantification Kit (Roche). Libraries pooled for multiplexed sequencing (5–6 libraries per run), hybridized to Illumina MiSeq flow cell (Illumina) and subsequently sequenced using Illumina MiSeq instrument and MiSeq Reagent Kit v2 chemistry (Illumina) for 50 sequencing cycles.

Sequencing data analysis was performed using CASAVA v1.8 (Illumina) and read sequences were outputted in FASTQ format. Quality control of raw sequences was checked using FastQC v0.11.7. Reads were used when quality retain ≥Q30. Next, raw data of FASTQ files were processed with custom R scripts. Briefly, identical sequences were counted and collapsed, adapter sequences were trimmed and reads shorter than 16 nt and longer than 28 nt were removed. The remaining reads were aligned to human miRNA hairpin sequences from miRBase v22 with Bowtie 1.1.2. Additional

alignment cycles with modified parameters were performed to include miRNA sequences with 1, 2 or 3 non-template 3'-terminal nucleotides. Besides, any aligned sequence was accepted as mature miRNA if it's 5'-terminal mapped to hairpin no further than 1 nt in either direction from the 5' start position of corresponding mature miRNA. Data normalization and differential miRNA expression analyses were performed with R package DeSeq2. After alignment of the reads to currently known pri-miRNAs hairpin precursors annotated in the miRBase database Release 22, a total of 734 and 802 unique miRNA species have been detected in HCT-P, HCT-Oxa, respectively.

2.14. miRNA target analysis

miRNA–mRNA interaction scores were generated by compiling data from eight interaction databases, which use different interaction prediction algorithms. Data from databases, which contained interaction probability values, were converted to percentiles resulting in arbitrary values from 0 to 1 (or 0.5 to 1 in the case were database contained only set of highly probable interactions). Data from databases without any interaction probability values were assigned equal scores by assessing the ratio of all interactions in that database to the count of interactions in our compound database. In the case of the database with experimental data, interactions with strong experimental evidence were given score 3, and interactions with weak experimental evidence were given score 1. Thus, the scores of resulting 11,592,145 interactions were generated by summing values from RepTar, MiRTar, MiRanda, PicTar2, MiRMap, miRTarget3, TargetScan7, and experimental database miRTARbase.

2.15. Sample preparation for mass spectrometry analysis

Cells were lysed with 0.5 mL of urea/thiourea lysis buffer (7 M urea, 2 M thiourea, 40 mM DTT, Protease Inhibitor Cocktail (Thermo Fisher Scientific)). The lysates were sonicated for 1 min at the amplitude of 20% and 0.4 s pulsations on/off cycles (Sonopuls HD 2070, Bandelin). Homogenized lysates were centrifuged at 20000 g for 15 min at 4 °C, and the supernatants were collected. The lysates then were stored at −86 °C.

Trypsin digestion was done according to a modified filter-aided sample preparation (FASP) protocol as described by Wisniewski et al. [54]. Briefly, proteins were diluted in 8 M urea and loaded on Amicon Ultra-30 kDa filters. Following two washes with urea, proteins were alkylated with 50 mM

iodoacetamide. Filters were washed twice with urea and twice with 50 mM NH_4HCO_3. Proteins digested overnight with TPCK Trypsin 20233 (Thermo Scientific). After overnight digestion, peptides were recovered by centrifugation and then two additional washes using 50% CH_3CN were combined, acidified, lyophilized, redissolved in 0.1% formic acid and then fractionated off-line.

2.16. Multiplexed inhibitor bead affinity extraction

Cells were lysed in low-salt lysis buffer (50 mM Tris-HCl (pH 7.5), 0.5% Triton X-100, 150 mM NaCl, 1 mM EDTA, 1 mM EGTA, 10 mM sodium fluoride, 2.5 mM sodium orthovanadate, 1 mM PMSF) supplemented with Protease Inhibitor Cocktail (Thermo Scientific) and Phosphatase Inhibitor Cocktail 2 (Sigma-Aldrich). Lysates were sonicated 1 min at the amplitude of 20% and 0.4 s pulsations on/off cycles (Sonopuls HD 2070, Bandelin) on ice and centrifuged at 22,000 g for 15 min at 4 °C. The supernatant was collected and protein quantity was assessed using Bio-Rad Protein Assay (Bio-Rad). Approximately 10 mg of protein per sample was brought to 1 M NaCl and incubated with 100 µL multiplexed inhibitor-conjugated beads (MIB) consisting of sepharose-conjugated Bisindoylmaleimide-X, dasatinib, Purvalanol B, PP58, and VI16832. MIBs were kindly supplied by dr. Lee M. Graves laboratory (Department of Pharmacology, the University of North Carolina at Chapel Hill). The MIBs were washed three times with high-salt and low-salt buffers (50 mM Tris-HCl (pH 7.5), 0.5% Triton X-100, 1 mM EDTA, 1 mM EGTA, and 10 mM sodium fluoride, and 1 M NaCl or 150 mM NaCl, respectively). Proteins were eluted from MIBs with elution buffer containing 8 M urea, 2 M thiourea, and 40 mM DTT and processed according to FASP protocol.

2.17. Phosphoproteome

Cells for phosphoproteome were lysed with phosphoproteome lysis buffer (10 mM Tris/HCl (pH 7.6), 2% SDS, 0.1 M DTT) supplemented with Protease Inhibitor Cocktail (Thermo Scientific) and Phosphatase Inhibitor Cocktail 2 (Sigma-Aldrich). Lysates were sonicated for 2 min at the amplitude of 15% and 0.4 s pulsations on/off cycles (Sonopuls HD 2070) and heated for 3 min at 95 °C. Homogenized lysates were centrifuged at 20000 g for 15 min at 4 °C, the supernatants were collected and the peptides were prepared by FASP protocol.

Peptide mixture from biological replicates was fractionated by basic reversed-phase (HpH) high-pressure liquid chromatography (HPLC). For all experiments, phosphopeptides from each HpH fraction were enriched using Titanium dioxide (TiO_2) Phosphopeptide Enrichment Kit (Thermo Scientific) following the manufacturer's protocol.

2.18. Computational functional analysis of proteomic data

For quantitative analysis of the global proteome, a statistically significant increase or decrease in protein level was considered as upregulation or downregulation, respectively. The protein-protein interaction network of differentially expressed proteins was built in Cytoscape software [55] using the stringApp plugin. Physical interaction data only was used for network generation; no related genes were added to the network. Gene Ontology (GO) Biological process annotations from stringApp were used for enrichment analysis of global proteome changes. Kinome and phosphoproteome biological functions were annotated using a combination of GO enrichment and biocuration (database and literature search).

In-depth bioinformatic analysis was performed using ClueGO and CluePedia Cytoscape plug-ins [56], [57]. GO Biological process, GO Molecular function and KEGG pathways enrichment examination of miR-23b *in silico* predicted targets and differentially expressed proteins in miR-23b knockout cell line were performed. 601 *in silico* predicted miR-23b target proteins, 141 upregulated and 187 downregulated proteins in Oxa-23b$^{-/-}$ versus HCT-Oxa cell lines were subjected to the extensive bioinformatic analysis. A term was considered enriched if at least 10% of the proteins in this population were predicted *in silico* as miRNA targets or at least 4% of proteins were differentially expressed in our proteomics dataset. A term was considered specific to one of the input lists (that is *in silico* targets, upregulated or downregulated proteins) if more than 50% proteins in that term occur in one of the input lists. Terms were connected into groups according to their Kappa score with a 0.4 threshold.

3. RESULTS AND DISCUSSION

3.1. Generation of resistant cell lines

For cell resistance research two different systems were used (Table 3). One of them was metastatic mammary gland adenocarcinoma cell line MDA-MB-231 used as a model for triple-negative late-stage breast cancer. Breast cancer is most common among women and accounts for about 15% of deaths of cancer patients [58]. Triple-negative breast cancer (TNBC), in particular, is more aggressive, has an increased likelihood of distant recurrence and limited treatment options and, therefore, a worse prognosis [59]. In such cases, new novel therapeutic options are needed to target this type of cancer. One of the promising strategies is to attack cancer cells based on distinct cancer cell properties. One of these cancer cell-specific drugs is 2,5-diaziridinyl-3-(hydroxymethyl)-6-methyl-1,4-benzoquinone (RH1), a novel aziridinyl benzoquinone-based cytotoxic compound that has shown promising results as an antitumor agent during phase I trials and has been recommended for the phase II trials [51]. RH1 is a prodrug that is activated by two-electron reductase NAD(P)H:quinone oxidoreductase (NQO1) or one-electron reductases, such as NADPH cytochrome P450 reductase, to cause DNA alkylation, crosslinking or oxidative stress via generation of free radicals [60], [61]. In this study, we generated the MDA-MB-231 cell line resistant to RH1 as a system for RH1 resistance research.

Table 3. Cell lines and therapeutic agents used for cancer cell resistance research

Cell line	Cancer type	Therapeutic agent	Name of resistant cell line
MDA-MB-231 (MDA-P)	Triple-negative breast cancer (TNBC)	2,5-diaziridinyl-3-(hydroxymethyl)-6-methyl-1,4-benzoquinone (RH1)	MDA-R
HCT116 (HCT-P)	Colorectal cancer (CRC)	5-fluorouracil (5-FU)	HCT-FU
		Oxaliplatin (OxaPt)	HCT-Oxa

The second system we have chosen for our cancer cell resistance mechanisms research was colorectal carcinoma cell line HCT116 as a model for colorectal cancer (CRC). CRC is the third of the most frequently diagnosed and one of the most significant causes of cancer death both in men and women [58]. Even though surgery represents the only curative treatment in 75–80% of cases, postoperative adjuvant chemotherapy has been shown to

improve progression-free and overall survival and is used to destroy microscopic metastases that may be already present and to reduce the risk of recurrence [62]. The most commonly used adjuvant chemotherapy for CRC patients named FOLFOX consists of 5-fluorouracil, leucovorin, and oxaliplatin [63]. As a second research system, we generated two HCT116 cell lines resistant to either 5-fluorouracil or oxaliplatin.

Two different strategies were approached to derive resistant cell lines (Figure 8). The first strategy was to use increasing drug concentration in growing medium to get the cell line with high drug tolerance (continuous treatment). The second strategy was to mimic physiological conditions of treatment and administer the drug in higher concentrations for short periods and letting cells to recover (pulse treatment).

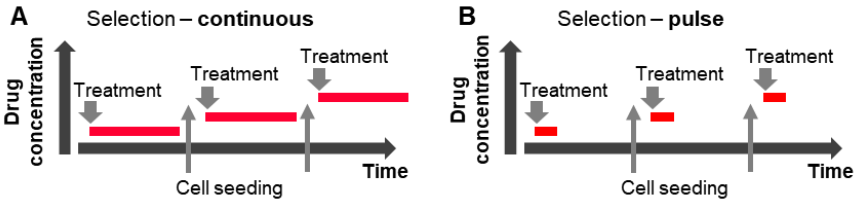

Figure 8. Schematic representation of strategies used to derive resistant cell lines. **A.** Scheme of continuous treatment approach. **B.** Scheme of pulsed treatment approach.

3.2. Characterization of RH1-resistant breast cancer cell line

RH1-resistant MDA-MB-231 (designated as MDA-R) was derived from parental MDA-MB-231 (designated as MDA-P) cell line by 2 h pulse treatment with increasing RH1 concentrations and subsequent recovery and repopulation. The IC_{50} values have been measured for MDA-P and MDA-R cells by the MTT test after 9 months of selection. Results of the MTT test showed that the MDA-R cell line gained a 14-fold increase of RH1 resistance compared to the parental cell line (Figure 9 A and B). Moreover, the fraction of apoptotic cells was evaluated after RH1 treatment using flow cytometric nexin-based apoptosis assay. Nexin assay measures membrane changes associated with apoptosis using Annexin V-PE, and 7-AAD to identify dead cells. The results of this assay show a significant increase in apoptotic cells in the MDA-P cell line after RH1 treatment, but no significant increase of apoptotic cells in the MDA-R cell line (Figure 9 C).

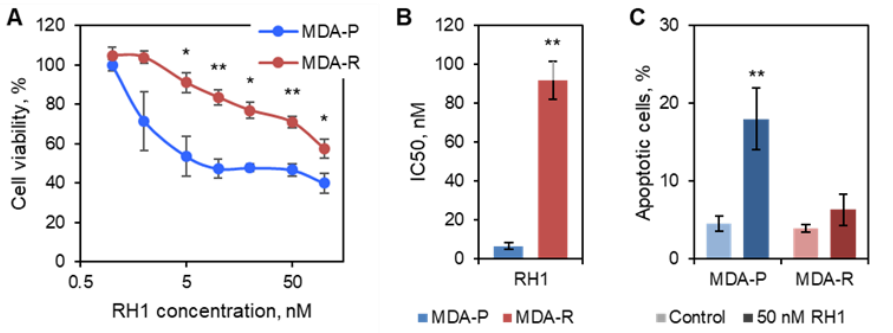

Figure 9. Characterization of RH1 resistant cells. **A.** Viability test. MDA-P and MDA-R cells were treated with increasing concentrations of RH1 for 2 h. Cell survival after 96 h was estimated by MTT assay. Bars are ± SD, significant differences are marked by asterisks: * $p < 0.05$, ** $p < 0.01$, t-test, n = 3. **B.** Estimation of IC50 values from cell viability tests. Bars are ± SD, significant differences are marked by asterisks: * $p < 0.05$, ** $p < 0.01$, ANOVA, n = 3. **C.** Quantification of flow cytometric nexin-based apoptosis assay. Cells were untreated or treated with 50 nM RH1 for 2 h and stained with Guava Nexin reagent after 48 h. Bars are ± SD, significant difference is marked by asterisks: ** $p < 0.01$, t-test, n = 3.

These results confirmed that RH1-resistant cells were derived from the RH1-sensitive parental cell line during the selection process and further experiments can be done with this cell line.

Earlier results in our laboratory suggested that the MDA-P cell line bears low or no activity of two major RH1 bio-activating enzymes NQO1 and NQO2 which are implicated in acquired resistance to RH1. Moreover, inhibition of ROS using ROS scavengers did not show any significant changes in MDA-P and MDA-R cell line resistance suggesting the alternative mechanism for the RH1 means of action and, therefore, acquirement of resistance.

To elucidate resistance mechanisms of RH1-resistant MDA-MB-231 cell line differential global proteomic, kinomic and phosphoproteomic analyses were conducted in our laboratory.

3.2.1. Combined kinome and phosphoproteome analysis

Parental and RH1-resistant cell lines were subjected to multiplexed kinase inhibitor bead (MIB) analysis to examine differences in the active kinases. Kinases were isolated from MDA-P and MDA-R cell lysates using MIB enrichment, which captures a broad range of active protein kinases by five different inhibitors covalently coupled to beads [64]. Results of kinome analysis were supplemented with phosphoproteome analysis data.

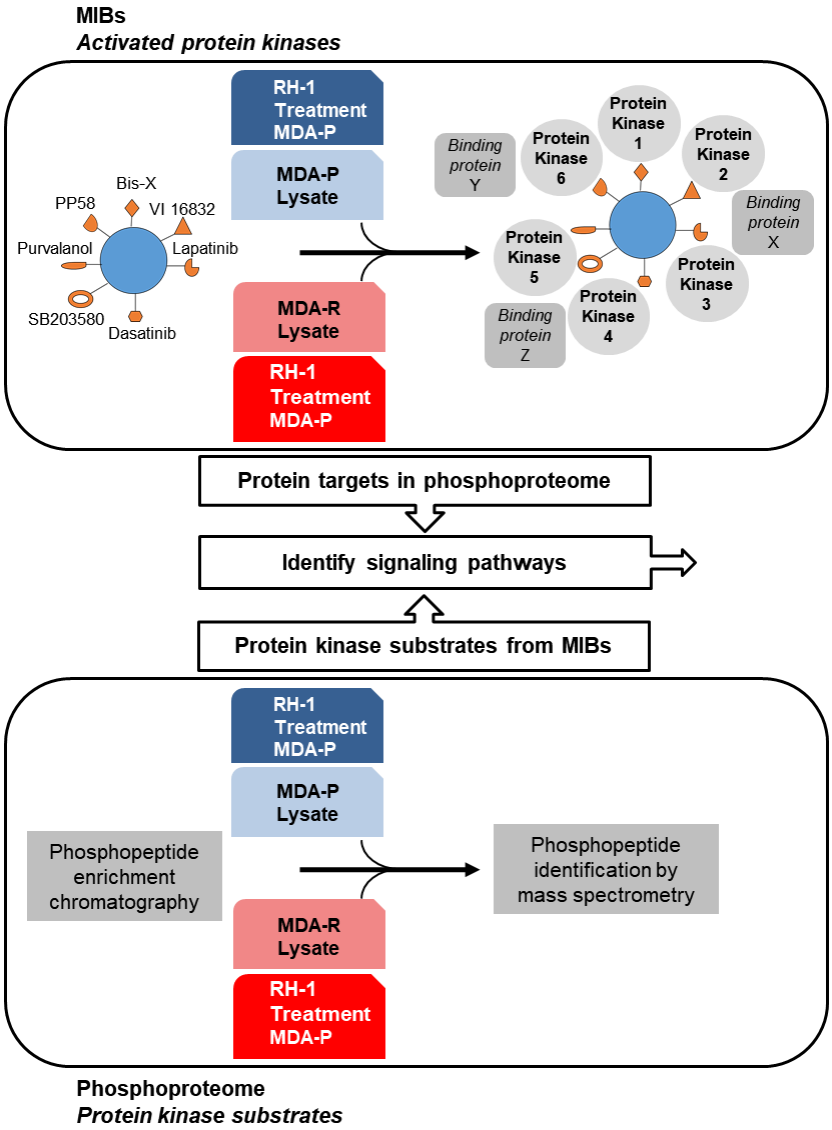

Figure 10. Experimental workflow for kinome and phosphoproteome analysis.

Phosphoproteome analysis was conducted using the phosphopeptide enrichment technique combined with quantitative mass spectrometry. Both datasets produced a vast amount of information, thus, we decided to identify signaling pathways involved in RH1 resistance by combining data from two assays. We applied bioinformatics and biocuration analysis to identify protein targets of activated protein kinases from the MIB dataset and merged that data with protein kinase substrates from the phosphoproteome dataset

(Figure 10). This approach led us to the establishment of possible signaling pathways responsible for the RH1 resistance.

One of the most prominent downregulated pathways in the RH1-resistant cell line was the JNK signaling pathway. First, we observed a decrease in JNK1 activity in the MDA-R cell line according to the MIB data and, therefore, searched JNK target phosphopeptides in the phosphoproteome dataset (Figure 11). Eight phosphosites belonging to seven proteins were identified using PhosphoSitePlus resource data [65]. This includes mTOR interaction partner RPTOR, and the prominent JNK targets JUN and STAT1, all of which are related to the induction of apoptosis, cell cycle arrest and transcription control [66]–[68]. Other JNK targets that are less phosphorylated in the drug-resistant cells include LMO7, DCP1A, and STMN1 which are involved in metabolism and other related processes.

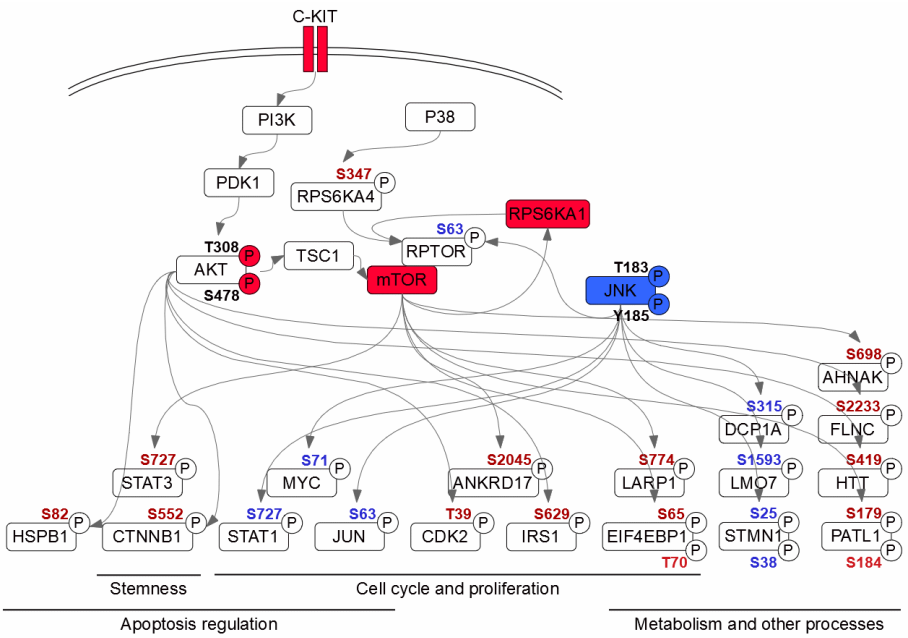

Figure 11. JNK1 and c-KIT-AKT-mTOR signaling pathways. Most biologically important pathways were analyzed combining MIB and phosphoproteome datasets. Red node color indicates increased activity of MIB dataset kinases, blue —decreased. Red phosphosite color indicates increased phosphorylation in the phosphoproteome dataset, blue—decreased. AKT and JNK phosphosites were identified by western blot. Nodes without color indicate proteins that belong to the pathway but have neither been identified nor their phosphorylation changes were observed in either of datasets.

The results of MIB data were validated by western blot analysis of JNK and phosphorylated JNK proteins. Data showed no changes in JNK1/2

quantities, but a significant decrease in phosphorylation of threonine 183 and tyrosine 185 residues of JNK1/2 protein in MDA-R cell line (Figure 12 A). Phosphorylation of JNK at both Thr183 and Tyr185 is required for its full activation and its apoptosis-related activities [69]. Furthermore, inhibition of JNK activity by its specific inhibitor SP600125 increased resistance to RH1 treatment of MDA-P, but not MDA-R cells (Figure 12 B). It is already known that JNK is an important mediator of RH1-induced mitochondrial apoptotic cell death in NQO1-expressing cell lines [70]. Our results indicate that JNK activation is equally important for RH1 cytotoxic function in cells that lack NQO1 and NQO2 activity.

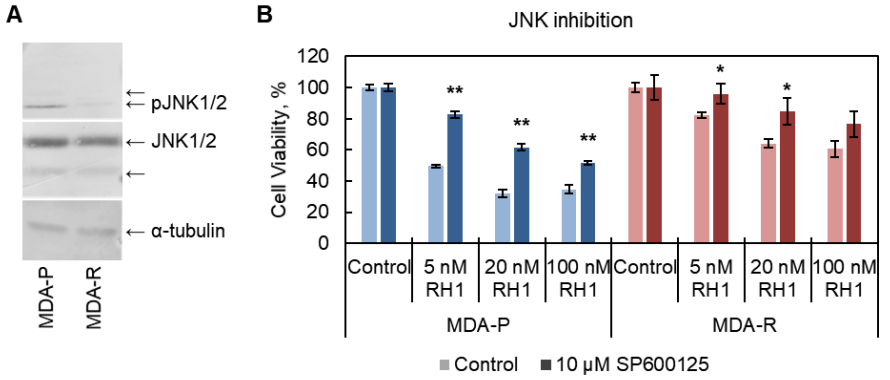

Figure 12. The decrease in JNK activation is related to RH1 resistance. **A.** Western blot analysis showing the level of pJNK (Thr183/Tyr185) in MDA-P and MDA-R cells. α-tubulin is shown as a loading control. **B.** Viability test after JNK inhibition. MDA-P and MDA-R cells were pre-treated with JNK inhibitor SP600125 for 1 h and then treated with increasing concentrations of RH1 for 2 h. Cell survival after 96 h was estimated by MTT assay. Bars are ± SD, significant differences are marked by asterisks: * $p < 0.05$, ** $p < 0.01$, ANOVA, $n = 3$.

Another signaling pathway highlighted by a combination of kinome and phosphoproteome datasets was the c-KIT-AKT-mTOR axis. MIB analysis pointed out a differential activation of at least three members involved in this signaling pathway, namely c-KIT tyrosine kinase, mTOR serine/threonine kinase and one of the mTOR pathway regulators RPS6KA1 (Figure 11). Moreover, we identified increased phosphorylation in drug-resistant cells of seven proteins from the phosphoproteome dataset which can be phosphorylated by mTOR kinase. Remarkably, these proteins include EIF4EBP1 and ANKRD17 which are involved in G1/S transition of the mitotic cell cycle [71], [72]. Additionally, we spotted changes in STAT3 phosphorylation, which can be associated with negative regulation of

apoptosis, positive regulation of cell cycle, and be involved in the regulation of the cancer cell stemness [73].

Since neither kinome nor phosphoproteome datasets revealed a direct link between c-KIT and mTOR activation, thus, we decided to analyze phosphorylation of the most prominent mTOR upstream kinase AKT activity. Immunoblot analysis of AKT phosphorylation in both MDA parental and resistant cell lines indicated increased phosphorylation of Thr308 and Ser473 residues (Figure 13 A). Moreover, AKT target phosphopeptides belonging to six proteins were identified in the phosphoproteome dataset (Figure 11). Notably, AKT phosphorylation target CDK2 is known as a key cell cycle regulator, controlling both G1/S and G2/M transitions [74].

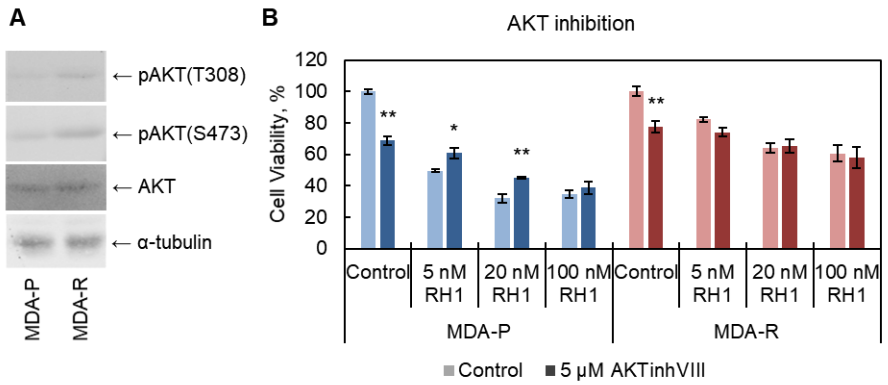

Figure 13. RH1-resistant cells exhibit higher levels of AKT phosphorylation. **A.** Western blot analysis showing the level of pAKT (Thr308/Ser473) in MDA-P and MDA-R cells. α-tubulin is shown as a loading control. **B.** Viability test after AKT inhibition. MDA-P and MDA-R cells were pre-treated with AKT inhibitor VIII for 1 h and then treated with increasing concentrations of RH1 for 2 h. Cell survival after 96 h was estimated by MTT assay. Bars are ± SD, significant differences are marked by asterisks: * $p < 0.05$, ** $p < 0.01$, ANOVA, n = 3.

We also identified an increase in β-catenin (CTNBB1) phosphorylation leading to the augmented transcriptional activity and maintenance of cancer cell stem-like properties, such as tumor initiation, proliferation, and invasion [75], [76]. Moreover, other AKT targets that could be important for cancer cell resistance were identified, such as IRS1, the regulator of cell proliferation and invasion [77], and HSPB1, which can function as apoptosis regulator [78]. However, the inhibition of AKT kinase had no significant impact on resistance to RH1 in the RH1-resistant cell line and promoted cell viability of the RH1-sensitive cell line after treatment (Figure 13 B). On the

other hand, both cell lines were sensitive to AKT inhibition alone showing the involvement of AKT kinase in complex regulation of cell viability in both presence and absence of drug treatment.

To prove the connection between c-KIT and AKT-mTOR axis activation we performed binary combinatorial inhibitory analysis (Figure 14 A). The rationale of this approach was to check if the combined inhibition of both c-KIT and AKT-mTOR pathways facilitate the effect on cell viability. Results of the MTT test performed after combined treatment with inhibitors showed a significant decrease in cell viability compared with single inhibitor treatment (Figure 14 B). Four different inhibitors of the AKT-mTOR axis were used for analysis, namely, LY294002 inhibiting upstream kinase PI3K, AKT inhibitor VIII, INK128 inhibiting both mTORC1 and mTORC2 complexes and rapamycin inhibiting only mTORC1 complex. Most of these inhibitors effectively decreased the viability of MDA-P and MDA-R cells and facilitated each other's inhibitory effect.

Moreover, we tried two different c-KIT inhibitors, more specific AB1010, and less specific XL184, which showed similar results. Both of these inhibitors strengthened the negative effect on the cell viability of most of AKT-mTOR axis inhibitors. On the other hand, we used inhibitor of c-MET receptor tyrosine kinase PHA-665752, which was upregulated according to the MIB dataset, and it did not facilitate the effect of AKT-mTOR axis inhibitors. These results confirmed that facilitated decrease of cell viability after combinatorial inhibitor treatment is reserved for c-KIT receptor tyrosine kinase.

Altogether, the results of the binary combinatorial inhibitory analysis showed interplay between c-KIT and AKT-mTOR axis activation confirming the previous assumption that the AKT-mTOR pathway is specifically activated by c-KIT receptor tyrosine kinase.

In summary, the integration of kinome and phosphoproteome datasets emphasized JNK pathway downregulation and c-KIT-AKT-mTOR axis upregulation as an important feature for the acquisition of resistance to RH1. Both these pathways are involved in cell cycle and apoptosis regulation and can be associated with stemness of cancer cells.

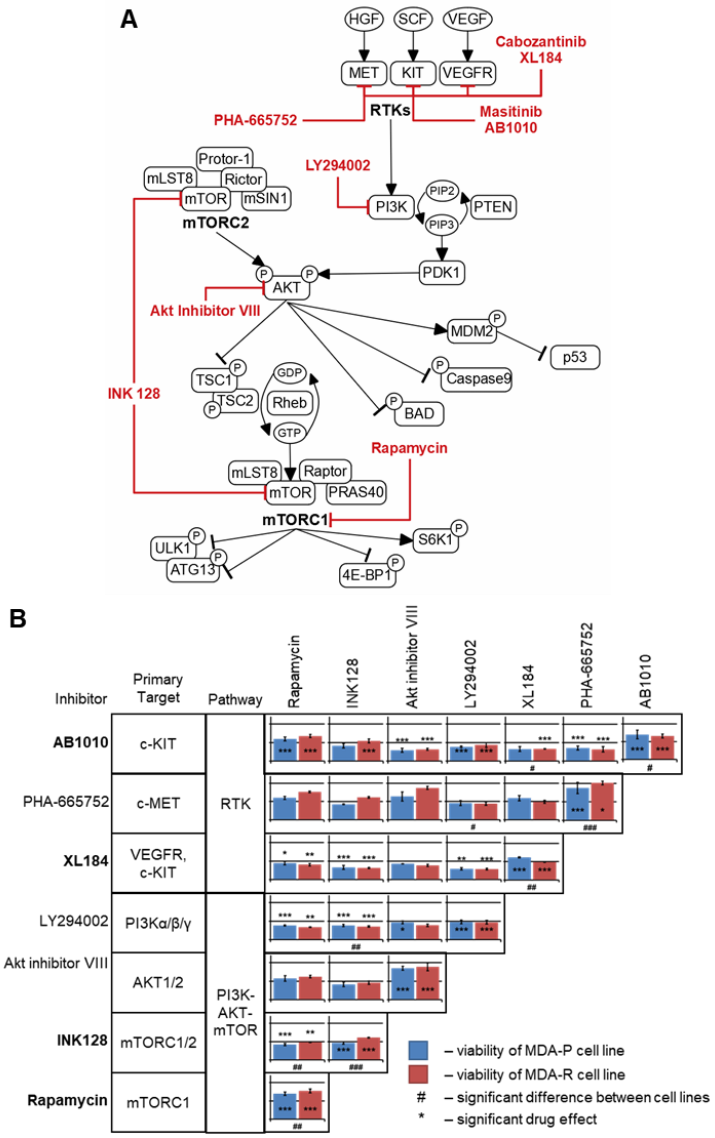

Figure 14. Combined inhibition of c-KIT and the AKT-mTOR axis facilitates the effect on cell viability. **A.** Scheme of the c-KIT-AKT-mTOR signaling pathway. Inhibitors used for binary combinatorial inhibitory analysis are designated in red. **B.** Cell viability results after combinatorial inhibitory analysis. MDA-P and MDA-R cells were treated with a combination of two inhibitors for 48 h. Cell survival after 96 h was estimated by MTT assay. Bars are ± SD, significant differences between cell lines are marked by hash symbols: # $p < 0.05$, ## $p < 0.01$, significant drug effects on cell viability are marked by asterisks: * $p < 0.05$, ** $p < 0.01$, ANOVA using Post-Hoc interaction analysis, n = 3.

3.2.2. Assessment of cell cycle changes

Global proteomic analysis revealed changes in proteins involved in G1/S and G2/M transition of the RH1-resistant cell line compared to the RH1-sensitive parental cell line. The differential expression becomes more prominent after short-term treatment with RH1. Moreover, changes in receptor tyrosine kinases and AKT-mTOR axis as observed from the combination of kinome and phosphoproteome analyses can result in perturbations of the cell cycle.

To confirm cell cycle changes in the MDA-R cell line, we performed a propidium iodide-based cell cycle assay using both MDA-P and MDA-R cell lines without or with RH1 treatment. Results of this assay verified proteomic results and revealed perturbations of cell cycle progression caused by RH1. RH1 causes cell cycle arrest in the G2/M phase in MDA-P, but not the MDA-R cell line (Figure 15 A).

These results were further substantiated by immunofluorescent staining of histone-H3 phosphorylation at serine 10 residue. Histone-H3 gets phosphorylated in the G2-early mitosis interface and is associated with chromatin condensation during mitosis [79]. Staining of MDA-P cell line before and after RH1 treatment showed increased quantities of histone-H3 Ser10 phosphorylation indicated an increased amount of cells at the G2/M checkpoint (Figure 15 B). Moreover, there were no signs of mitotic cells implying that cell cycle arrest happens before cells can enter the active mitotic state. No such effects were observed after the staining of the MDA-R cell line supporting the notion that the RH1-resistant cell line bypasses cell cycle arrest at the G2/M interface after RH1 treatment.

To determine which signaling pathways could be responsible for such differences in the cell cycle, we analyzed our phosphoproteome data searching for phosphorylation changes in proteins involved in cell cycle regulation. Previous analysis already showed differential AKT phosphorylation in the RH1-resistant cell line and CDK2 was identified as one of AKT targets (Figure 11). CDK2 is one of the major regulators of G1/S cell cycle transition and its interaction with cyclin E and A is necessary for normal cell cycle progression. Moreover, the AKT-mediated CDK2 phosphorylation on threonine 39 residue is important for regulating the subcellular distribution of CDK2. CDK2 Thr39 phosphorylation not only increases its affinity to cyclin A but translocation to cell cytoplasm after phosphorylation could be necessary to smooth transition from S to G2/M phases of the cell cycle [80].

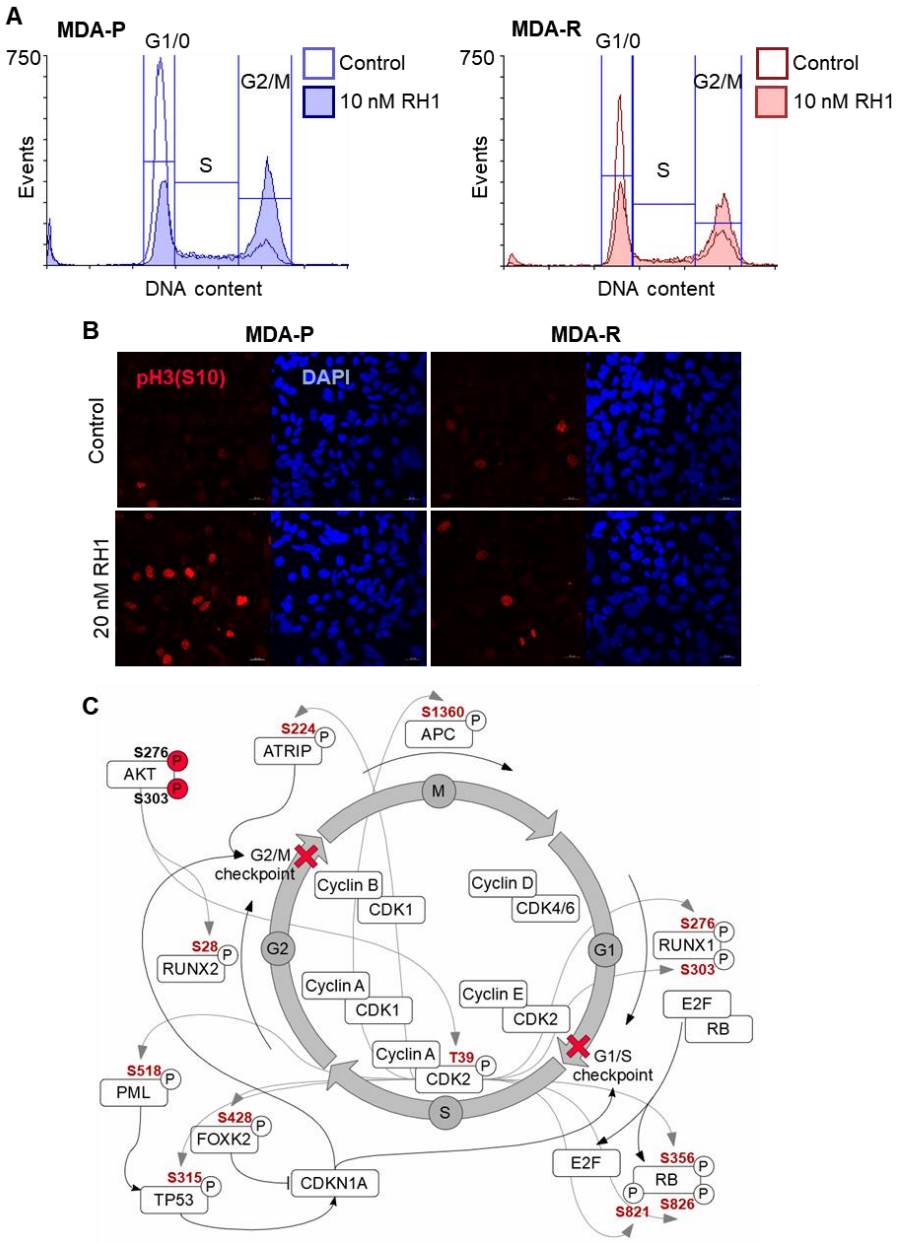

Figure 15. RH1 treatment affects the RH1-sensitive breast cancer cell cycle. **A.** Flow cytometry analysis of cell cycle. MDA-P and MDA-R cells were untreated or 2 h pulse treated with 10 nM RH1 and then incubated for 24 h until propidium iodide staining and flow cytometry cell cycle analysis. **B.** Representative confocal microscopy images of cells stained with antibody against phosphorylated histone-H3 Ser10 (red channel) and DNA dye DAPI (blue channel). Cells were untreated or treated with 20 nM RH1 for 2 h pulse and stained after 24 h. **C.** Cell cycle-related protein phosphorylation changes detected in the phosphoproteome dataset. Red phosphosite color indicates increased phosphorylation, AKT phosphosites were

identified by western blot. Nodes without color indicate proteins that belong to the pathway but have neither been identified nor their phosphorylation changes were observed in the dataset.

Additionally, phosphoproteome analysis revealed targets of CDK2 kinase involved in cell cycle progression, such as retinoblastoma protein which phosphorylation is necessary to overcome G1/S cell cycle checkpoint [81]. Furthermore, phosphorylation of some transcription factors and repressors implicated in cell cycle regulation was found in proteome dataset, involving RUNX1 and FOXK2 phosphorylated by CDK2 [82], [83] and RUNX2 phosphorylated by AKT [84]. Interestingly, ATRIP was found as one of the CDK2 phosphorylation targets. CDK2–dependent phosphorylation of ATRIP regulates the G2-M checkpoint response to DNA damage [85] and, thus, can be associated with acquired resistance to RH1.

Considering all the results of cell cycle-related experiments on MDA-P and MDA-R cells, we propose that cell cycle perturbations caused by RH1 can be bypassed by RH1-resistant cells via differential activation of AKT kinase resulting in differential phosphorylation of cell cycle regulating proteins.

3.2.3. Evaluation of cancer stem cell population

Acquired cancer drug resistance is linked to the expansion of the cancer stem cell (CSC) population [86]. Moreover, our differential global proteomic data pointed to the increase of stemness-related proteins in the RH1-resistant cell line. Therefore, we analyzed how stem cell-specific features manifest in drug-resistant cells.

First of all, we analyzed MDA-P and MDA-R cell lines for a set of known CSC biomarkers, such as DPP4, CD44, MSI1/2, ALCAM, CD133, CD29, and CD24, using RT-qPCR. The expression of DPP4, CD44, MSI1/2, and ALCAM was significantly increased in RH1-resistant cells and the expression of only one marker CD24 was significantly decreased (Figure 16 A). Besides, we checked our global proteomics data for the same markers. Few of them, namely, CD44, MSI1/2, and ALCAM were detected in the global proteome dataset and the amount of their protein level correlated with the results of RT-qPCR (Figure 16 B).

A

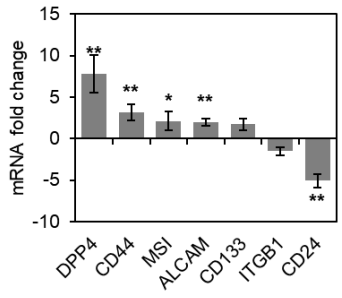

B

Gene	Protein	qPCR fold change	Proteomics fold change
DPP4	Dipeptidyl peptidase 4	11.28	Not detected
CD44	CD44 antigen	3.18	1.74
MSI1/2	RNA-binding protein Musashi homolog 1/2	2.13	1.79
ALCAM	CD166 antigen	1.99	1.68
PROM1	Prominin-1 (CD133)	1.72	Not detected
ITGB1	Integrin beta 1 (CD29)	-1.52	Not detected
CD24	Signal transducer CD24	-5.09	Not detected

C

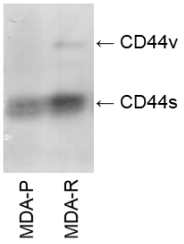

D

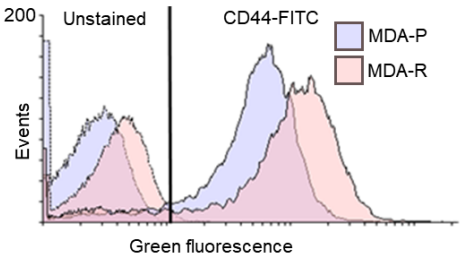

E

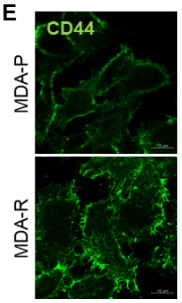

Figure 16. RH1 resistant cells show an increased level of CSC markers. **A.** Relative expression of selected CSC markers measured by RT-qPCR in MDA-R compared to MDA-P. Bars are ± SD, significant differences are marked by asterisks: * $p < 0.05$, ** $p < 0.01$, ANOVA, n = 3. **B.** Comparison of CSC markers detected by RT-qPCR with quantitative proteomic analysis results. **C.** Western blot analysis of various isoforms of CD44 expression in MDA-P and MDA-R cell lines. **D.** Flow cytometry data graph showing CD44 expression in MDA-P and MDA-R cells. Data combined from unstained and CD44-FITC antibody-stained samples. **E.** Representative comparative confocal images of CD44 (green channel) expression in MDA-P and MDA-R cells.

Second, in light of significant mRNA changes and detectable protein levels through proteomic analysis, we chose CD44 as a marker for the CSC population in drug-resistant cell line and validated its differential expression by flow cytometry, western blot, and confocal microscopy. CD44 is a known marker of CSCs in breast cancer and, more importantly, breast cancer cells bearing $CD44^{+}/CD24^{-}$ phenotype exhibit properties of cancer stem cells and high tumor-initiating capacity [87]. Interestingly, western blot analysis of CD44 protein in drug-sensitive and drug-resistant cell lysates showed an increase not only in CD44 standard isoform but also in CD44 variant isoform formed by alternative splicing (Figure 16 C). Different CD44 isoforms may have distinct roles in different breast cancer subtypes and can be involved in specific oncogenic signaling [88]. Moreover, flow cytometric

analysis confirmed higher levels of CD44 in MDA-R cell line and immunofluorescent staining revealed membrane localization of CD44 protein (Figure 16 D and E).

Altogether, these results demonstrate that RH1-resistant cells exhibit elevated levels of multiple CSC markers. Therefore, acquired resistance to RH1 of these cells can be at least partially explained by the enrichment of the CSC population.

3.2.3.1. Analysis of ABC transporters

Cancer stem cells are likely to gain resistance to drugs and toxins through the expression of ATP-binding cassette (ABC) transporters responsible for the removal of cytotoxic substances from cells [2]. To examine levels of ABC transporters in MDA-P and MDA-R cell lines, we looked through our global proteomics dataset. Differential global proteome analysis detected the presence of 10 ATP-binding cassette family members, only two of which, ABCC1 and ABCC4, are associated with drug transport (Figure 17 A). As the quantity of ABCC1 protein in the drug-resistant cell line was decreased, only ABCC4 was chosen for further investigations. Furthermore, we included analysis of P-glycoprotein, the most extensively studied ABC transporter, implicated in drug efflux of many cytotoxic compounds and associated with the development of multi-drug resistance [89].

Rhodamine123 is often used as a tracer dye to determine the rate of P-glycoprotein-mediated transport. Thus, we used flow cytometry analysis to determine the fraction of cells actively exporting rhodamine123 dye. The results show no difference in the Rho123low population in the RH1-sensitive and the RH1-resistant cell lines suggesting no changes in P-glycoprotein-mediated transport (Figure 17 B and C).

Next, we analyzed the role of the ABCC4 transporter in RH1 resistance. ABCC4 is ABC transporter involved not only in drug transport but in the transport of a wide range of endogenous molecules that have a key role in cellular communication and signaling [90]. As a means to demonstrate the importance of ABCC4 for RH1 resistance, we inhibited this transported with specific inhibitor Ceefourin1. The results of the cell viability test after RH1 treatment showed no impact of ABCC4-mediated transport inhibition on cell resistance to the drug (Figure 17 D).

A

Gene	Protein	Proteomics fold change	Drug transport
ABCB7	ATP-binding cassette sub-family B member 7, mitochondrial	1.13	-
ABCB10	ATP-binding cassette sub-family B member 10, mitochondrial	1.28	-
ABCC1	Multidrug resistance-associated protein 1	-1.30	+
ABCC4	Multidrug resistance-associated protein 4	2.60	+
ABCD1	ATP-binding cassette sub-family D member 1	7.27	-
ABCD3	ATP-binding cassette sub-family D member 3	1.11	-
ABCE1	ATP-binding cassette sub-family E member 1	-1.64	-
ABCF1	ATP-binding cassette sub-family F member 1	-1.39	-
ABCF2	ATP-binding cassette sub-family F member 2	1.05	-
ABCF3	ATP-binding cassette sub-family F member 3	-1.11	-

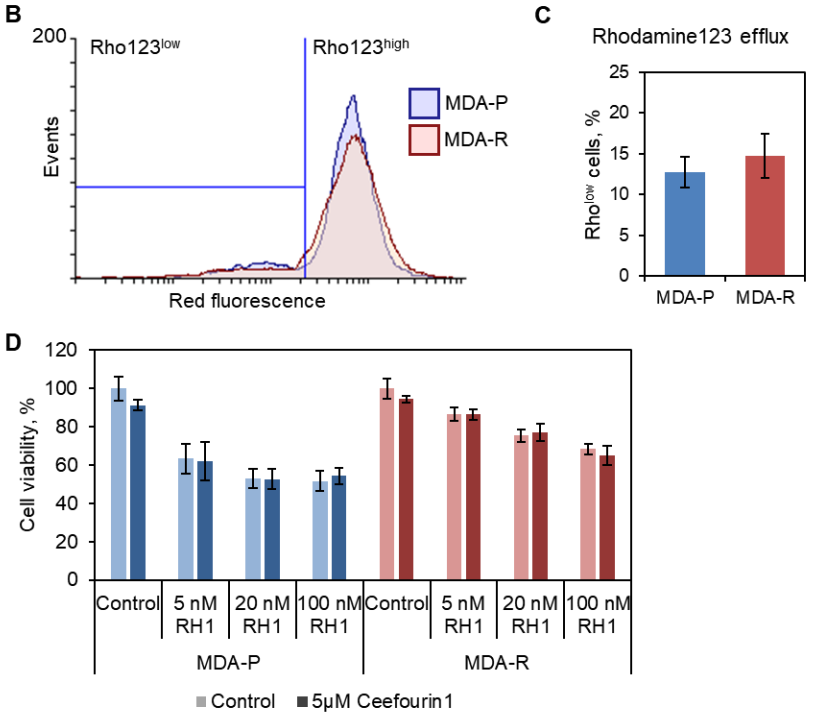

Figure 17. Resistance to RH1 of MDA-R cannot be attributed to changes in ABC transporters' activity. **A.** Differential expression of ABC transporters in the global proteomics dataset and their involvement in drug trafficking. **B.** Flow cytometric analysis of rhodamine123 from MDA-P and MDA-R cells. Cels were treated for 1 h with rhodamine123 and then subjected to the analysis. **C.** Evaluation of rhodamine123 cell population after flow cytometric analysis. Bars are ± SD, significant differences are marked by asterisks: * $p < 0.05$, ** $p < 0.01$, ANOVA, n = 3. **D.** Viability test after ABCC4 inhibition. MDA-P and MDA-R cells were pre-treated with Ceefourin1 for 1 h and then treated with increasing concentrations of RH1 for 2 h. Cell survival after 96 h was estimated by MTT assay. Bars are ± SD, significant differences are marked by asterisks: * $p < 0.05$, ** $p < 0.01$, ANOVA, n = 3.

These results suggested that resistance of CSC-enriched MDA-R cells cannot be attributed to the increase of drug efflux out of the cells mediated by ABC transporters.

3.2.3.2. Role of stem cell factor receptor c-KIT

Data from our combined kinomic and phosphoproteomic approach indicated that the CSC phenotype of the RH1-resistant cell line could arise from the activation of known CSC marker c-KIT. Stem cell factor (SCF), a sole ligand of c-KIT, plays a vital role in maintaining survival, promoting proliferation, and regulating the growth and development of human stem cells [31]. To assess expression levels of the c-KIT receptor and its ligand SCF, RT-qPCR analysis was performed. The results revealed elevated expression of SCF in drug-resistant cells, but no significant changes in c-KIT expression (Figure 18 A). However, MIB assay showed increased c-KIT kinase activity in MDA-R cells leading to the assumption that these cells have enhanced autocrine-stimulated c-KIT receptor.

Since continuous autocrine stimulation via the c-KIT receptor could promote the expansion of the CSC population, we investigated how the prolonged treatment with specific c-KIT inhibitor masitinib affects $CD44^{high}$ population in MDA-P and MDA-R cell lines. Two week-long selection was performed on both cell lines exposing cells to sub-lethal RH1 concentration, letting them recover and repopulating without or with supplementary masitinib treatment (Figure 18 B). The expansion of the $CD44^{high}$ population was evaluated by flow cytometry after this short-term selection.

The prolonged treatment with RH1 led to the selection of MDA-P cells with an increased level of CD44 (Figure 18 C). However, the combined treatment of RH1 and c-KIT inhibitor dramatically reduced the expansion of the $CD44^{high}$ CSCs population. No changes in the $CD44^{high}$ population during this short-term selection assay was observed in MDA-R cells. This might be explained that previous long-term treatment of cells with the drug, which has led to the RH1-resistant cell line generation, cannot produce more $CD44^{high}$ cells during this short-time selection experiment.

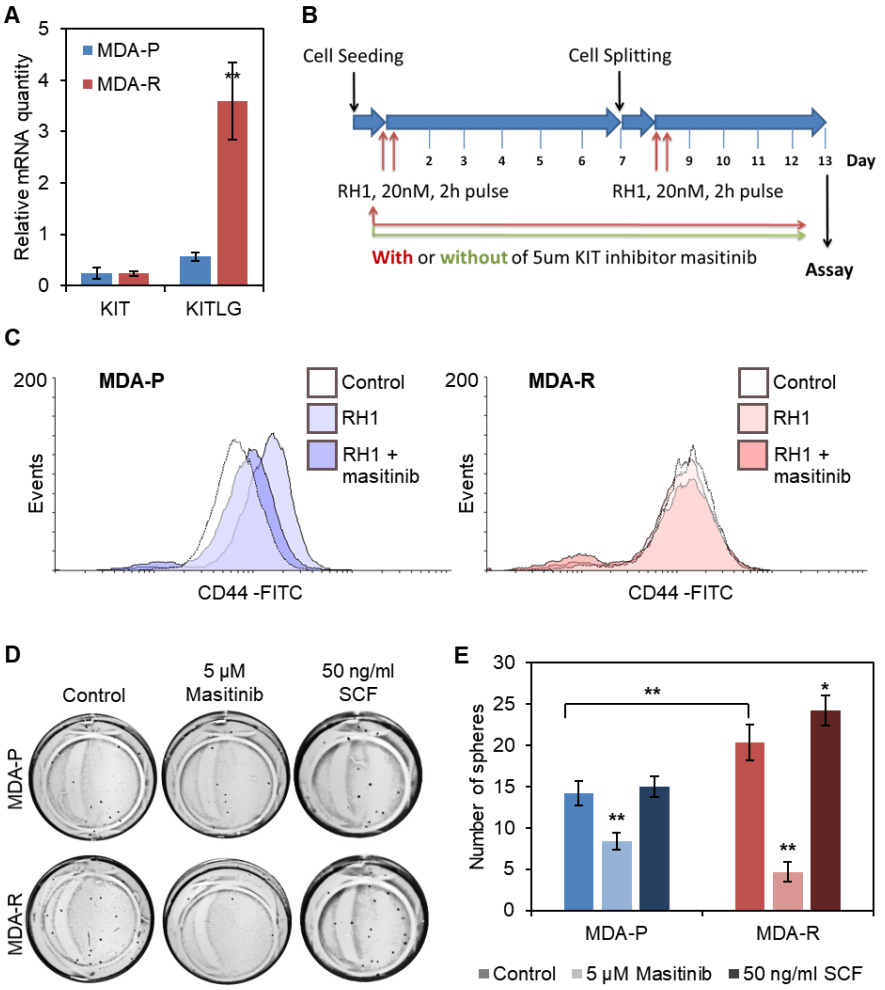

Figure 18. c-KIT inhibition attenuates MDA-P cells selection toward CSC and suppresses tumor-initiating capacity of MDA-R cells. **A.** Relative expression levels of c-KIT receptor and its ligand KITLG in MDA-P and MDA-R cells measured by RT-qPCR. Bars are ± SD, significant differences are marked by asterisks: * $p < 0.05$, ** $p < 0.01$, ANOVA, n = 3. **B.** Experimental time chart of cells short-time selection without and with c-KIT inhibition. **C.** Flow cytometry analysis of $CD44^{high}$ population in MDA-P or MDA-R cell lines which were pulse exposed or not exposed twice to 20 nM RH1 with or without continuous treatment with 5 µM c-KIT receptor inhibitor masitinib. **D.** MDA-P and MDA-R cells were subjected to the sphere-forming assay with or without 5µM masitinib or 50 ng/mL SCF treatment. **E.** Evaluation of sphere-forming assay results. Spheres were stained with MTT dye and counted using ImageJ software. Bars are ± SD, significant differences are marked by asterisks: * $p < 0.05$, ** $p < 0.01$, ANOVA, n = 3.

As the results of short-term selection showed the importance of SCF-c-KIT loop activation for the expansion of $CD44^{high}$ CSCs population, we decided to examine the tumor-initiating capacity of the RH1-sensitive and

the RH1-resistant cells without or with c-KIT inhibition. Ability to initiate tumors and form mammospheres *in vitro* is one of the major characteristics of breast cancer stem-like cells as demonstrated with highly malignant $CD44^{-}/CD24^{+}$ cells [91]. To evaluate the tumor-initiating capacity of the RH1-resistant cell line and to elucidate the role of c-KIT activation in the maintenance of a stem-like state, we performed the cell sphere-forming assay. MDA-P and MDA-R cells were suspended in a non-adherent agarose matrix containing a limited resource of growth factors that resemble similar tumor formation conditions *in vivo*. Under these unfavorable conditions, only stem-like cells can proliferate and form colonies.

The sphere-forming assay revealed the increased capability of CSC-enriched MDA-R cells to form spheres from a single cell (Figure 18 D and E). Equally important, that c-KIT inhibition by masitinib during the formation process diminished sphere-forming capability and this effect was more profound in the RH1-resistant cell line. Moreover, c-KIT stimulation with its ligand SCF slightly increased the sphere-forming capacity of the RH1-resistant but did not affect the sphere-forming capacity of the RH1-sensitive cell line. These data suggest that the tumor-initiating capacity of the MDA-R cell line is highly dependent on c-KIT activation.

Altogether, these results show that the drug-resistant cell line can be characterized by elevated SCF expression and SCF-c-KIT signaling loop activation promotes accumulation of $CD44^{high}$ cell population with more pronounced stem-like features. Integrating RH1 treatment with c-KIT inhibitors might prevent the expansion of the RH1-resistant CSC population and modulate acquired resistance to RH1 in breast cancer therapy.

3.3. Characterization of 5-fluorouracil-resistant colorectal cancer cell line

The 5-fluorouracil-resistant cell line (designated as HCT-FU) was derived from the parental HCT116 colorectal cancer cell line (designated as HCT-P) by continuous treatment with 5-fluorouracil. Cell viability test results measured by MTT assay after selection revealed a 7.5-fold increase in resistance to 5-fluorouracil (Figure 19 A). Moreover, as standard adjuvant treatment for colorectal cancer is FOLFOX, consisting of combinatorial treatment with 5-fluorouracil and oxaliplatin, cell viability after oxaliplatin treatment was evaluated too. Results of the cell viability test after oxaliplatin treatment indicated that there was no increase in resistance to oxaliplatin suggesting the 5-fluorouracil-specific resistance mechanism (Figure 19 B).

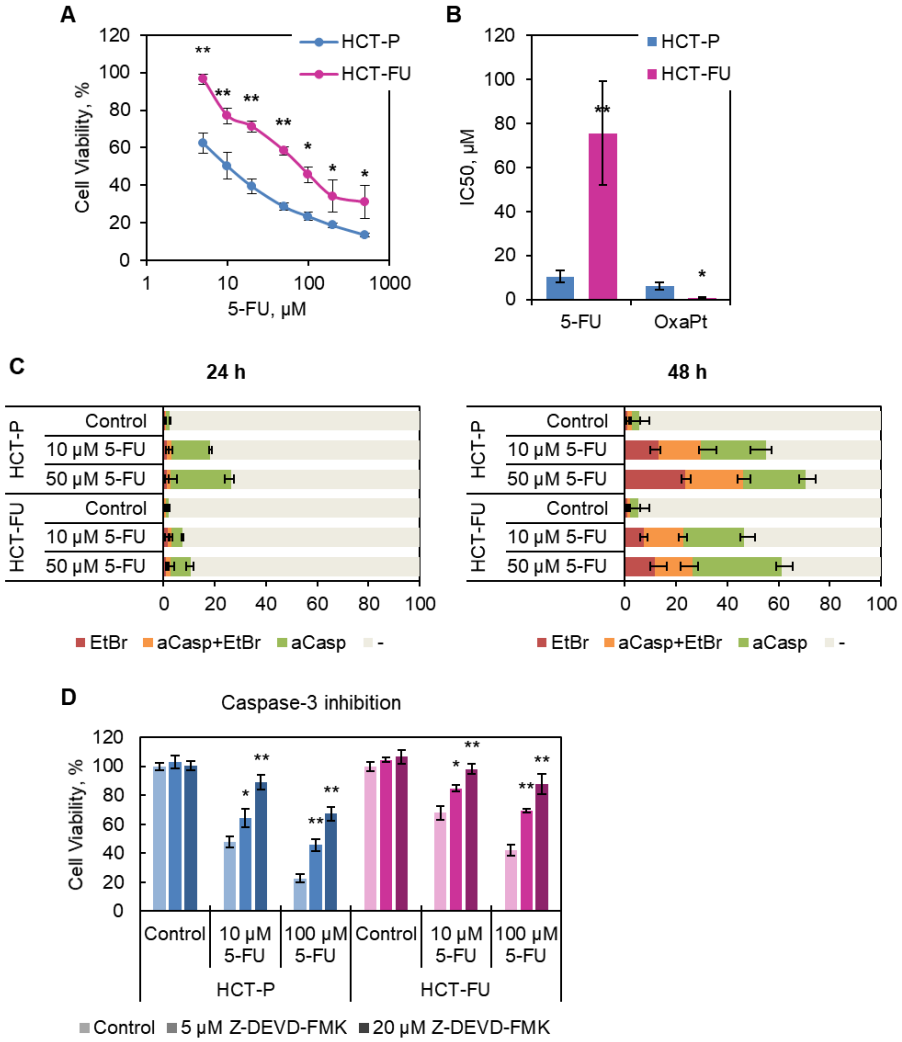

Figure 19. Characterization of 5-fluorouracil resistant cells. **A.** Viability test. HCT-P and HCT-FU cells were treated with increasing concentrations of 5-fluorouracil for 48 h. Cell survival after 96 h was estimated by MTT assay. Bars are ± SD, significant differences are marked by asterisks: * $p < 0.05$, ** $p < 0.01$, t-test, n = 3. **B.** Estimation of IC50 values from cell viability tests. Bars are ± SD, significant differences are marked by asterisks: * $p < 0.05$, ** $p < 0.01$, t-test, n = 3. **C.** Quantification of flow cytometric cell death analysis. Cells were untreated or treated with 10 μM or 50 μM 5-fluorouracil for 24 h or 48 h and stained with ethidium bromide and active caspase-3/7 dye. Bars are ± SD, n = 3. **D.** Viability test after caspase-3 inhibition. HCT-P and HCT-FU cells were pre-treated with Z-DEVD-FMK for 1 h and then treated with increasing concentrations of 5-fluorouracil for 48 h. Cell survival after 96 h was estimated by MTT assay. Bars are ± SD, significant differences are marked by asterisks: * $p < 0.05$, ** $p < 0.01$, ANOVA, n = 3.

Cell viability was further assessed by cell staining with ethidium bromide (EtBr) as an indicator of the ruptured membrane and active executive caspase-3/7 dye. The results of this assay showed a higher amount of viable cells in 5-fluorouracil-resistant cell line after drug treatment, however, this difference was more prominent after 24 h treatment (Figure 19 C). Moreover, results indicated that most of the cells undergo traditional caspase-3/7-mediated apoptosis as a major form of cell death. Given these results, we performed cell viability assay after caspase-3 inhibition with its specific inhibitor Z-DEVD-FMK and showed that caspase-3 inhibition effectively rescues both parental and resistant cells from cell death after 5-fluorouracil treatment (Figure 19 D).

Altogether, this data suggests a standard mechanism of action in both parental and 5-fluorouracil-resistant cell lines. 5-fluorouracil acts as uridine analog, thus, is incorporated in DNA causing DNA damage and activating conventional apoptotic pathways [8].

3.3.1. Assessment of 5-fluorouracil caused DNA damage

Since drug-specific resistance mechanisms are usually associated with changes in drug transport or metabolic processes, we decided to check for protein changes involved in these processes. Quantitative global differential proteomic analysis of parental and 5-fluorouracil-resistant cell lines was performed using label-free high-definition mass spectrometry technology. Proteomic analysis has led to the identification and quantification of 5006 proteins, 238 proteins of which were differentially expressed in HCT-FU versus HCT-P cells. Proteins whose levels were significantly increased or decreased were subjected to GO Biological Process enrichment analysis using ClueGO and CluePedia Cytoscape plugins [56], [57] and revealed changes in nucleobase metabolic process (GO:0009112) (Figure 20). Given that 5-fluorouracil is an antimetabolite exerting its cytotoxic function by disrupting thymidine metabolism and, thus, disrupting DNA synthesis and causing DNA damage [8], changes in nucleotide metabolism could lead to 5-fluorouracil resistance. Moreover, to cause DNA damage 5-fluorouracil should be converted to its active metabolites fluorodeoxyuridine monophosphate and fluorodeoxyuridine triphosphate [8]. One of the most important proteins involved in this process, thymidine phosphorylase, is downregulated in drug-resistant cells according to our proteomics dataset.

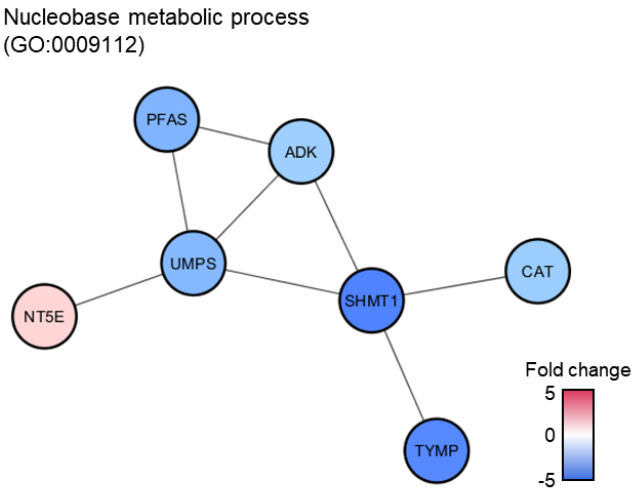

Gene	Protein	Pathway
ADK	Adenosine kinase	AMP biosynthesis via salvage pathway
TYMP	Thymidine phosphorylase	dTMP biosynthesis via salvage pathway
SHMT1	Serine hydroxymethyltransferase	Tetrahydrofolate interconversion
NT5E	5'-nucleotidase	
PFAS	Phosphoribosylformylglycinamidine synthase	IMP biosynthesis via de noo pathway
CAT	Catalase	
UMPS	Uridine 5'- monophosphate synthase	UMP biosynthesis via de novo pathway

Figure 20. Functional analysis of global proteome changes between HCT-P and HCT-FU cells revealed changes in nucleobase metabolism. HCT-P and HCT-FU were subjected to in-depth quantitative proteomic analysis. Protein differential expression, interaction and functional annotation network were built using Cytoscape software with ClueGO and CluePedia plugins. The color of the nodes demonstrates protein level change in the 5-fluorouracil-resistant cells.

Taken together, these data suggest that HCT-FU cells gained resistance to the drug via altering its metabolic pathway and preventing DNA damage. To test this hypothesis, we assessed the occurrence of DNA damage after 5-fluorouracil treatment in HCT-P and HCT-FU cell lines using immunostaining analysis of two proteins activated by DNA damage. One of the proteins chosen as DNA damage indicator was p53 protein which gets phosphorylated and, therefore, becomes more stable upon DNA damage [22]. The increase of p53 protein quantity after 5-fluorouracil treatment in parental cell line indicated occurring DNA damage, however, there were only minor changes in p53 quantity in the drug-resistant cell line (Figure 21 A). Furthermore, results of immunostaining of other DNA damage sensor,

phosphorylated ATM, were very similar supporting the notion that the HCT-FU cell line avoids DNA-damaging effects of 5-fluorouracil.

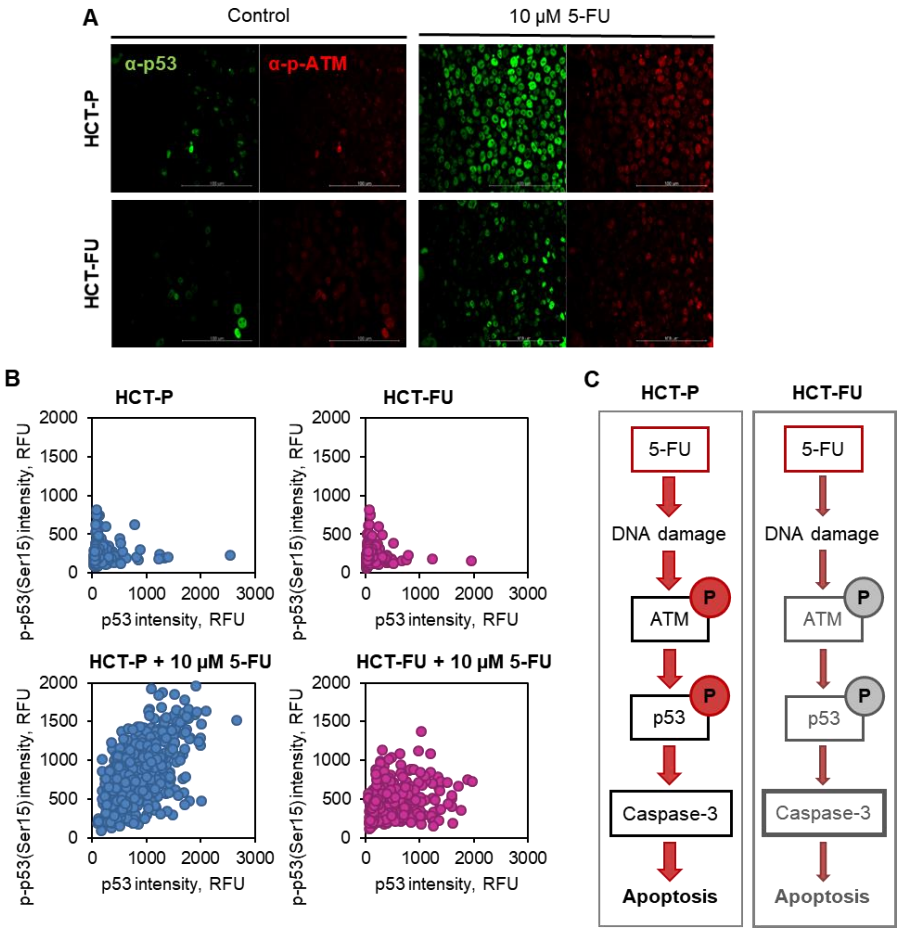

Figure 21. 5-fluorouracil-resistant cells are less susceptible to DNA damage after 5-fluorouracil treatment. **A.** Representative confocal microscopy images of cells stained with antibodies against p53 (green channel) and ATM (red channel) DNA damage sensors. Cells were untreated or treated with 10 μM 5-fluorouracil for 24 h. **B.** Analysis of whole and Ser15 phosphorylated p53 protein in each cell from confocal microscopy images. Cells were untreated or treated with 10 μM 5-fluorouracil for 24 h and stained with p53 and p-p53(Ser15) antibodies. Fluorescence intensity in each cell was estimated using ImageJ software. **C.** Scheme of proposed resistance to the 5-fluorouracil mechanism of HCT-FU cells.

As p53 phosphorylation increases its stability, we decided to test levels of phosphorylated p53 at serine 15 residue in relation to the whole p53 level. Ser15 is the primary target of the DNA damage response on the p53 protein and is phosphorylated by both DNA damage-sensing protein kinases ATM and ATR. Moreover, Ser15 phosphorylation facilitates p53 interaction with

DNA and is crucial for p53 transcriptional function regulation [92]. P53 protein phosphorylation at Ser15 was assessed using immunostaining and confocal microscopy analysis and level of whole and phosphorylated p53 was analyzed in a single cell. The results of this analysis show a significant increase of both p53 and phosphorylated p53 quantity and high correlation between both in 5-fluorouracil treated HCT-P cells (Figure 21 B). However, whole and phosphorylated p53 increase after treatment was far less significant in HCT-FU cells and the correlation between both was much lower.

Considering all the results from 5-fluorouracil-resistant cell line analysis, we propose that HCT-FU cells gained their resistance to the drug as a consequence of changes in nucleotide metabolism. Due to these changes, resistant cells became less susceptible to DNA damage and, therefore, DNA damage sensing proteins are not activated leading to impaired apoptosis induction (Figure 21 C).

3.4. Characterization of oxaliplatin-resistant colorectal cancer cell line

The oxaliplatin-resistant cell line (designated as HCT-Oxa) was derived from HCT116 colorectal carcinoma cell line (designated HCT-P) by continuous treatment with oxaliplatin. The resistant phenotype of the HCT-Oxa cell line was validated by cell viability evaluation after drug treatment using MTT assay. Results show that HCT-Oxa cell line is resistant not only to oxaliplatin treatment (15 times increase of IC50 comparing to parental cell line) but also to 5-fluorouracil (4 times increase of IC50 comparing to parental cell line) another commonly used chemotherapy drug for CRC (Figure 22 A and B).

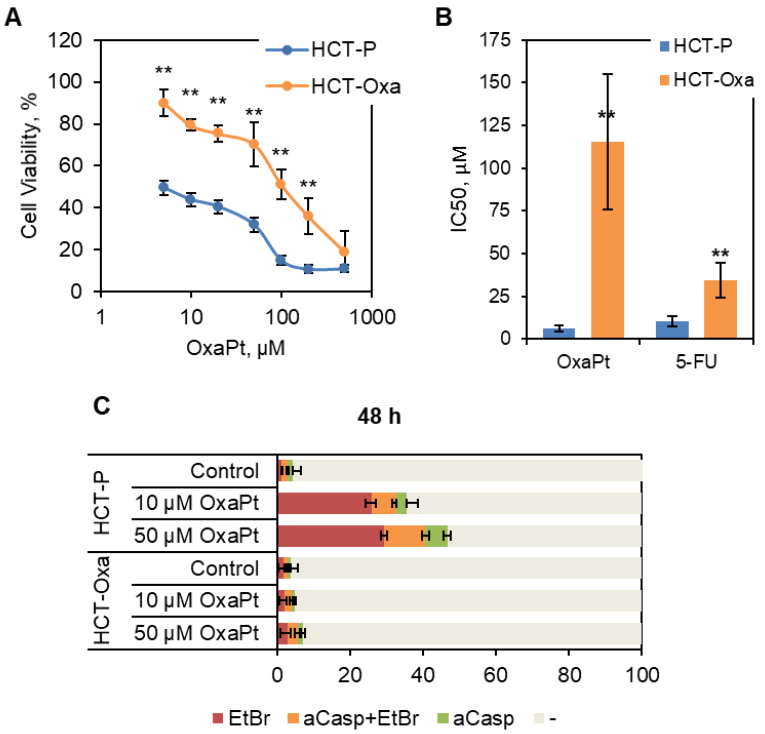

Figure 22. Continuously selected with oxaliplatin HCT-P cells gained resistance to the drug. **A.** Viability test. HCT-P and HCT-Oxa cells were treated with increasing concentrations of oxaliplatin for 48 h. Cell survival after 96 h was estimated by MTT assay. Bars are ± SD, significant differences are marked by asterisks: * $p < 0.05$, ** $p < 0.01$, ANOVA, n = 3. **B.** Estimation of IC50 values from cell viability tests. Bars are ± SD, significant differences are marked by asterisks: * $p < 0.05$, ** $p < 0.01$, ANOVA, n = 3. **C.** Quantification of flow cytometric cell death analysis. Cells were untreated or treated with 10 μM or 50 μM oxaliplatin for 48 h and stained with ethidium bromide and active caspase-3/7 dye. Bars are ± SD, n = 3.

To evaluate cell death occurring after oxaliplatin treatment, we subjected both parental and resistant cell lines to flow cytometry analysis using ethidium bromide (EtBr) as an indicator of the ruptured membrane and active executive caspase-3/7 dye. HCT-P cell line exhibited a moderate amount of active caspase-3/7 staining after 48 h of treatment and most of it coincided with EtBr staining indicating late stages of apoptosis (Figure 22 C). Moreover, about 30% of cells were stained with EtBr alone that implies different cell death mechanisms not involving caspase-3/7 activation. On the other hand, the HCT-Oxa cell line did not exhibit any sensitivity to an administered drug resulting in the absence of both EtBr and active caspase-3/7 staining.

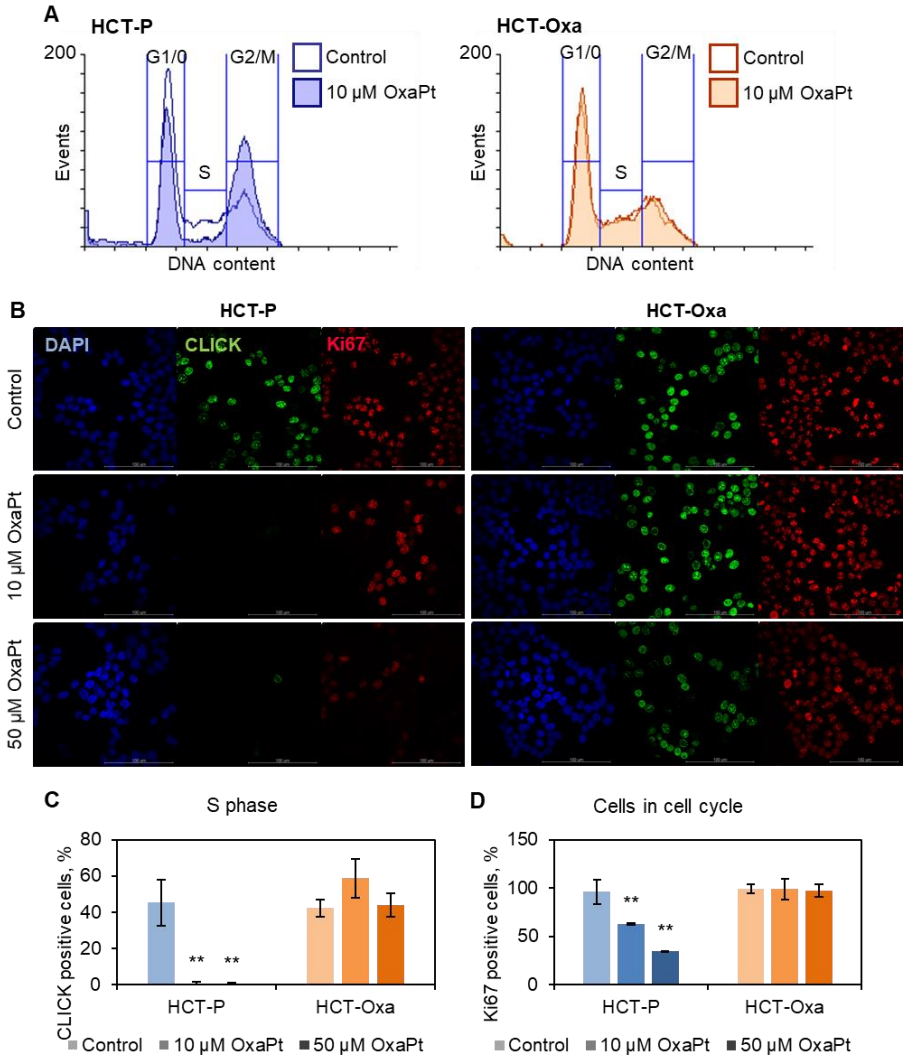

Figure 23. Oxaliplatin-resistant cell line evades the oxaliplatin-induced cell cycle arrest **A.** Flow cytometry analysis of cell cycle. HCT-P and HCT-Oxa cells were untreated or 24 h treated with 10 μM oxaliplatin for 24 h until propidium iodide staining and flow cytometry cell cycle analysis. **B.** Representative confocal microscopy images of cells stained with DNA dye DAPI (blue channel), S phase detecting CLICK-iT EDU analysis kit (green channel) and antibody against Ki67 (red channel). Cells were untreated or treated with 10 or 50 μM oxaliplatin for 24 h. **C.** Analysis of CLICK positive cells from confocal microscopy images. Cells were untreated or treated with 10 or 50 μM oxaliplatin for 24 h and stained with CLICK-iT EDU analysis kit. Fluorescence intensity was estimated using ImageJ software. Bars are ± SD, significant differences are marked by asterisks: * $p < 0.05$, ** $p < 0.01$, ANOVA, n = 3. **D.** Analysis of Ki67 positive cells from confocal microscopy images. Cells were untreated or treated with 10 or 50 μM oxaliplatin for 24 h and stained with antibody against Ki67. Fluorescence intensity was estimated using ImageJ software. Bars are ± SD, significant differences are marked by asterisks: * $p < 0.05$, ** $p < 0.01$, ANOVA, n = 3.

Next, we tried to establish whether oxaliplatin treatment has any impact on the cell cycle of the oxaliplatin-resistant cell line. First, we evaluated cell distribution through cell cycle phases by flow cytometry using propidium iodide stain. In the case of the HCT-P cell line, we noticed an accumulation of cells in both G1 and G2/M phases after low-dose oxaliplatin treatment and a highly decreased amount of cells undergoing S phase. On the contrary, HCT-Oxa cell line did not display any variation in cell cycle distribution independently of oxaliplatin treatment (Figure 23 A). Second, we tried to visualize cells that are in an active DNA synthesis state based on the incorporation of 5-ethynyl-2′-deoxyuridine (EdU), a thymidine analog, and the subsequent reaction of EdU with a fluorescent azide (CLICK) [93]. Notably, in HCT-P cell line active DNA synthesis was completely undetectable after oxaliplatin treatment, whereas the HCT-Oxa cell line didn't exhibit any significant changes in the amount of CLICK positive cells or even slight increase in DNA synthesizing cells after low-dose oxaliplatin treatment (Figure 23 B and C). Third, we demonstrated the proliferative rate of the cells by detecting Ki-67 protein that is present during all active phases of the cell cycle but is absent from resting cells in G_0 [94] as well as is essential for normal cell progression through S phase [95]. Similarly, we determined that Ki-67 positive cells are diminished in the HCT-P cell line after oxaliplatin treatment in a dose-dependent manner while in the HCT-Oxa cell line all cells are Ki-67 positive before and after treatment (Figure 23 B and D).

In summary, cell death and cell cycle analyses reveal the highly resistant phenotype of the HCT-Oxa cell line resulting in evasion of oxaliplatin-induced cell death and cell cycle arrest.

3.4.1. Analysis of miRNA expression profile

To investigate the impact of miRNAs on the emerged insensitivity to oxaliplatin treatment, we performed sequencing of small RNA libraries from the HCT-Oxa cell line and determined miRNA changes compared to the parental HCT-P line. 40 of miRNAs were differentially expressed with high confidence relative to the parental cell line, thereby potentially contributing to drug adaptation in HCT-Oxa cells.

The expression patterns of three groups of the most prominent miRNAs prompted by the differential miRNA sequencing were evaluated by RT-qPCR. MiR-23a-3p, miR-27a-3p, miR-27a-5p, and miR-24-2-5p belonging to the intergenic miR-23a/27a/24-2 cluster and miR-23b-3p, miR-27b-3p,

and miR-27b-5p belonging to the intronic miR-23b/27b/24-1 cluster, as well as miR-181-5p, were selected for further assessment of their potential role in the modulation of oxaliplatin resistance. The expression of all verified miRNAs presented in the miR-23b/27b/24-1 cluster, as well as miR-181-5p, were preferentially enhanced in cells with acquired resistance to oxaliplatin and miRNAs presented in the miR-23a/27a/24-2 cluster were down-regulated (Table 4).

Table 4. Validation of differentially expressed miRNAs in oxaliplatin-resistant cell line by qRT-PCR. Statistically significant changes are marked in bold., n = 3.

miRNA	Expression change	
	RNA-Seq	qPCR
23b-3p	up	**5.2 ± 0.9**
27b-3p	up	**5.9 ± 1.2**
27b-5p	up	**9.1 ± 1.0**
24-3p	constant	-1.1 ± 0.0
23a-3p	down	**-1.9 ± 0.4**
27a-3p	down	**-1.6 ± 0.3**
27a-5p	down	-1.6 ± 0.6
24-2-5p	down	**-1.5 ± 0.1**
181b-5p	up	**2.5 ± 0.4**

As miRNA sequencing data revealed a significant 5–10-fold up-regulation of the miR-23b/27b/24-1 cluster, we induced mutations in miR-23b (coding the miR-23b-3p and miR-23b-5p) or miR-27b (miR-27b-3p and miR-27b-5p) genes using the CRISPR/Cas9 technique in the HCT-Oxa cells to explore its role in chemoresistance. The miR-23b knockout line (designated as Oxa-23$^{-/-}$) completely lacked the expression of miR-23b-3p and also showed a 1.8- and 2.2-fold impaired expression of miR-27b-3p and miR-27b-5p, respectively (Figure 24 A). In contrast, in the miR-27b knockout line (designated as Oxa-27b$^{-/-}$) only the miR-27-3p and miR-27-5p biogenesis was disrupted without interfering with miR-23b-3p expression.

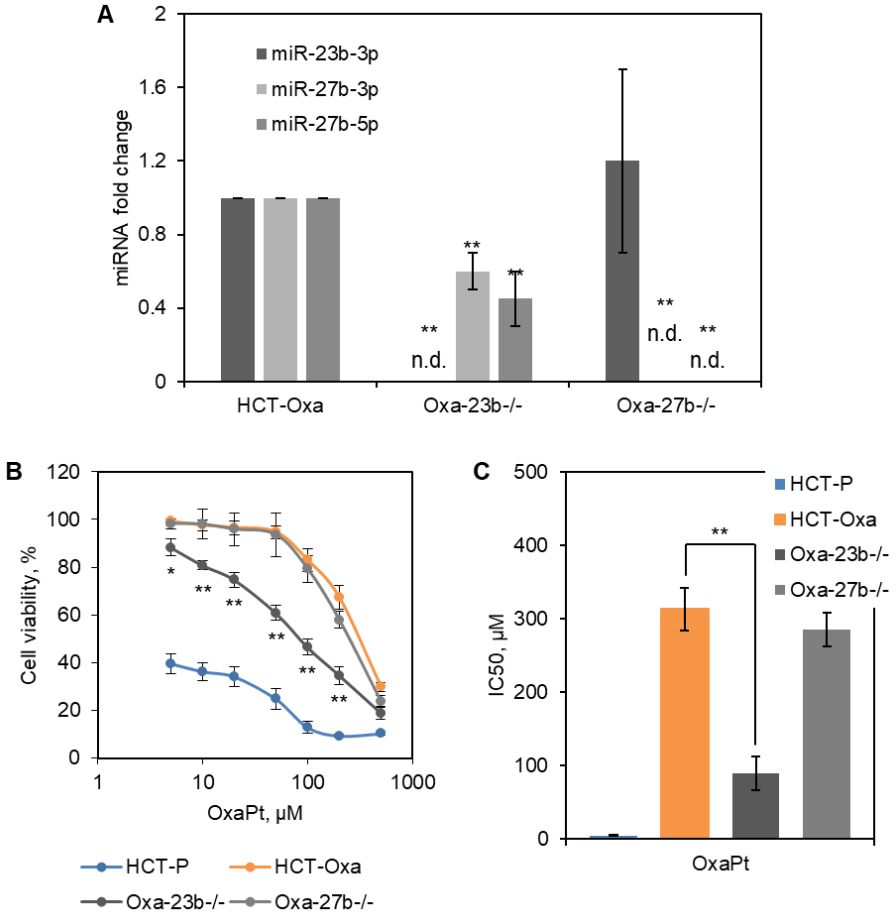

Figure 24. CRISPR/Cas9 mediated knockout of miR-23b, but not of miR-27b, sensitized HCT-Oxa cells to oxaliplatin. **A.** Evaluation of expression of CRISPR/Cas9-targeted miRNA by RT-qPCR analysis. Mutations significantly inhibit the expression of miR-23b-3p, miR-27b-3p and miR-27b-5p. Bars are ± SD, significant differences are marked by asterisks: * $p < 0.05$, ** $p < 0.01$, ANOVA, n = 3. **B.** Viability test after miR-23b and miR-27b knockout. Cells were treated with increasing concentrations of oxaliplatin for 48 h. Cell survival after 96 h was estimated by MTT assay. Bars are ± SD, significant differences are marked by asterisks: * $p < 0.05$, ** $p < 0.01$, ANOVA, n = 3. **C.** Estimation of IC50 values from cell viability tests. Bars are ± SD, significant differences are marked by asterisks: * $p < 0.05$, ** $p < 0.01$, ANOVA, n = 3.

Finally, we estimated the effect of the loss of the miR-23b and miR-27b expression on resistance to oxaliplatin in the CRISPR/Cas9 mutants. The results of the cell viability test showed that miR-23b knockout caused a 3.5-fold increase in sensitivity to the drug, whereas, knockout of miR-27b had no significant effect on cell resistance to oxaliplatin (Figure 24 B and C).

To summarize, changes in miRNA expression detected in the oxaliplatin-resistant cell line can be associated with adaptation to the drug treatment. Besides, knockout of one of the differentially expressed miRNA, miR-23b, resulted in a significant decrease in cell resistance to oxaliplatin suggesting the processes controlled by this miRNA are important for ensuring resistance to the drug.

3.4.1.1. Identification of miR-23b targets and their functional bioinformatics analysis

Since a single miRNA may cause expression changes in hundreds of proteins, it is essential to understand which of these changes are relevant to the acquisition of the resistance. To elucidate processes involved in the acquisition of resistance, we examined changes in the proteome of Oxa-23b$^{-/-}$ cell line to identify the genuine targets of miR-23b and to explore their functional and signaling connections. Thus, to identify direct primary targets and consequential secondary (indirect) targets of miR-23b, global high-throughput differential quantitative proteomic analysis of HCT-P, HCT-Oxa and Oxa-23b$^{-/-}$ cells was performed using label-free high-definition mass spectrometry technology. The protein which quantity negatively correlated with miR-23b expression level were considered as primary miRNA targets and other changes in proteome were considered consequential (Figure 25 A).

To define the gene expression directly affected by the miR-23b-3p or mir-23b-5p, multiple criteria have been set: (I) the gene expression has to be increased in miR-23b knockout cells versus oxaliplatin-resistant cells; (II) the same gene should be down-regulated in oxaliplatin-resistant versus parental cells, which express less of miR-23b. If the gene met both conditions, we assigned it to the strict targets group. Alternately, if the gene met just the first criteria, we added it to the moderate stringency targets group. Also, the gene assignment to the miR-23b targets group was strengthened if it was identified as a possible target *in silico* using our computation approaches. To find out whether our computation approaches predicted miRNA targets *in silico*, we compiled a comprehensive in-house dataset, which consolidated the resources of eight publicly available gene target prediction databases, thereby incorporating the benefits of different target prediction algorithms.

The proteomic analysis led to the identification and quantification of a total of 2750 proteins; 269 of these proteins were differentially expressed in HCT-Oxa versus HCT-P, and 328 proteins were differentially expressed in Oxa-23b$^{-/-}$ versus HCT-Oxa cells.

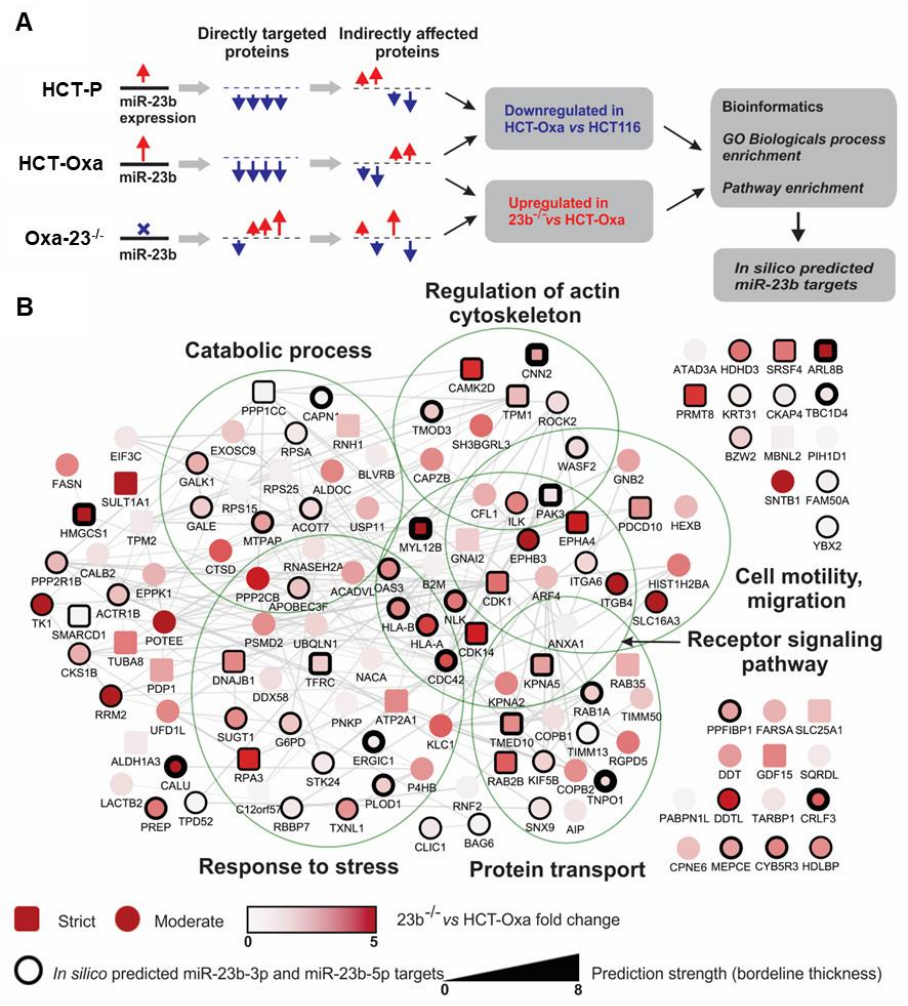

Figure 25. Functional analysis of global proteome changes between HCT-P, HCT-Oxa, and Oxa-23b$^{-/-}$ cells. **A.** The predicted effect of miR-23b on gene expression in various cells and the approach used to analyze the proteomics data. **B.** Protein networks and enriched functional groups from Gene Ontology (GO) Biological process enrichment analysis. HCT-P, HCT-Oxa, and Oxa-23b$^{-/-}$ cells were subjected to in-depth quantitative proteomic analysis. A protein differential expression, interaction and functional annotation network were built using Cytoscape software. The shape of the nodes represents the strength of target selection conditions, the color demonstrates an actual protein-level change in proteomics datasets and the borderline shows mRNA–miRNA interaction stringency predicted *in silico*.

After applying strict and moderate target-sorting conditions, combined with the *in silico* miR-23b predicted targets, the pooled gene sets were further subjected to functional bioinformatics analysis. Protein interaction networks and functional annotations by Gene Ontology (GO) Biological

process enrichment were built and evaluated in Cytoscape software [55] using the stringApp plugin.

The data show changes in the protein levels that are involved in catabolic processes, response to stress, receptor signaling pathways, regulation of actin cytoskeleton and cell motility and migration (Figure 25 B). Interestingly, some strong candidates associated with cell resistance to chemotherapy, such as CAMK2D and SRSF4, have already been implicated in the resistance to platinum compounds [96], [97]. Similarly, PDCD10, a predicted miR-23b target, has been shown to play a dual role in cancer cell drug resistance [98] (Figure 25 B).

Next, having differential proteomes of parental, oxaliplatin-resistant and miR-23b knockout cell lines allowed us to perform an in-depth bioinformatics analysis and to search for the potential mechanisms of the oxaliplatin resistance. To this end, we performed GO biological process, GO Molecular function and KEGG pathway enrichment of in-silico predicted miR-23b targets and differentially expressed proteins in the miR-23b knockout cell line using ClueGO and CluePedia Cytoscape plug-ins [56], [57].

The GO biological process enrichment analysis revealed changes in GO terms of cell polarity, motility and cytoskeleton organization as well as changes in the developmental processes, receptor signaling pathways and RNA splicing regulation (Figure 26).

Processes such as cortical cytoskeleton organization (GO:0030865), the regulation of actin filament depolymerization (GO:0030834) and the establishment or maintenance of epithelial cell apical/basal polarity (GO:0045197) are associated with cells undergoing morphological changes and epithelial-mesenchymal transition (EMT) [99]–[101]. These changes suggest that miR-23b is involved in altering the epithelial-mesenchymal state of oxaliplatin-resistant and miR-23b knockout cells. This prediction is also supported by further bioinformatics data. For instance, development-related proteins, cytoskeleton reorganization or EMT, as well as proteins involved in cell migration, are crucial to the biological processes determined in our bioinformatics analysis such as tissue regeneration (GO:0042246), dendritic spine development (GO:0060996) and neural nucleus development (GO:0048857) [102]–[104].

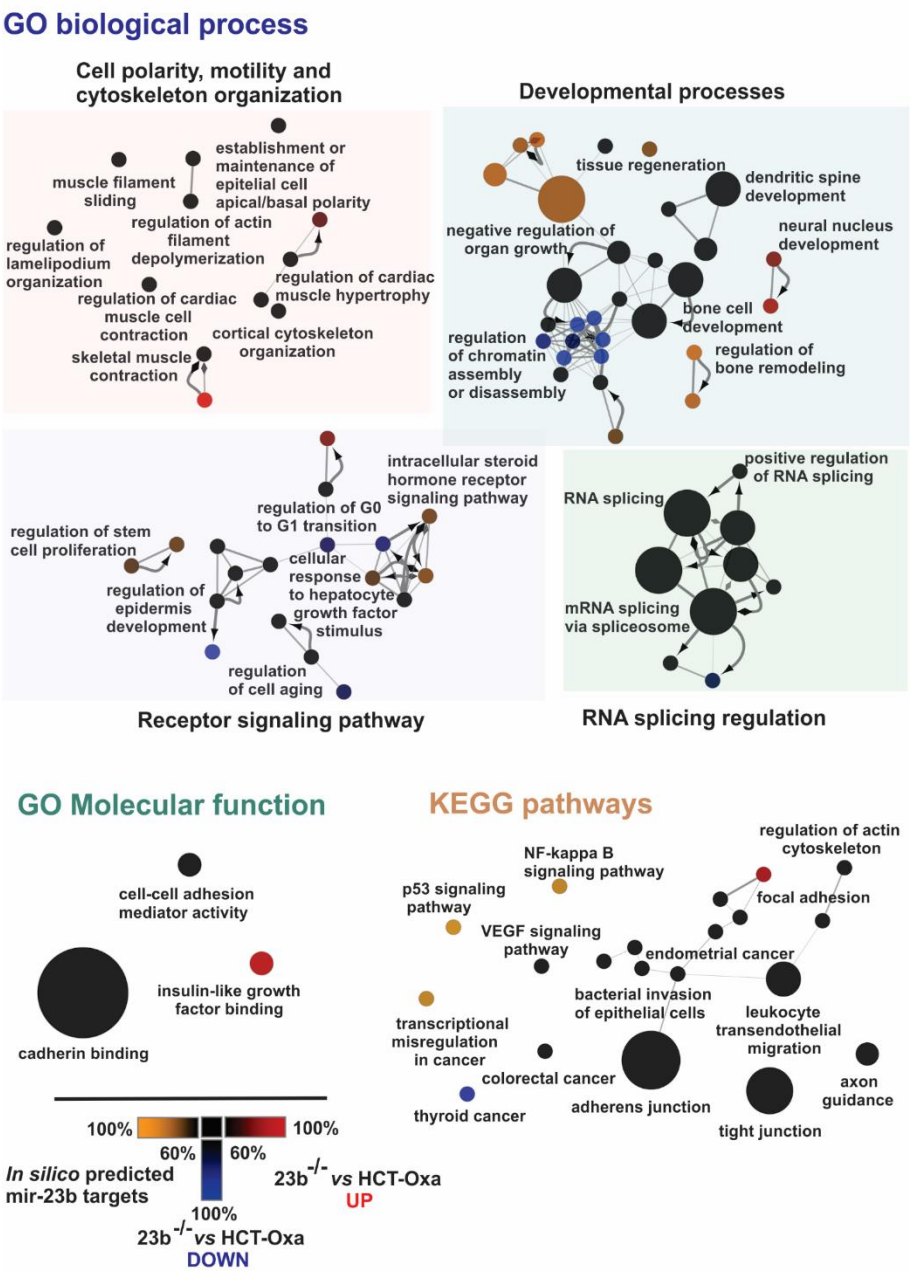

Figure 26. The enrichment of cell motility, migration, cytoskeleton organization, and epithelial-mesenchymal transition-related terms was revealed from in-depth GO biological process, GO molecular function and KEGG pathway enrichment analysis of *in silico*-predicted miR-23b targets and differentially expressed proteins in the miR-23b knockout cell line. Terms specifically enriched by *in silico*-predicted miR-23b targets are designated yellow, terms specifically enriched by Oxa-23b$^{-/-}$ vs. HCT-Oxa upregulated proteins in proteomics data are designated red and terms specifically enriched by Oxa-23b$^{-/-}$ vs. HCT-Oxa

downregulated proteins in proteomics data are designated blue. Terms enriched by all groups are designated black.

Moreover, we identified changes in receptor signaling pathways resulting in the altered regulation of stem cell proliferation (GO:0072091), epidermis development (GO:0045682), cell aging (GO:0090342) or differences in response to growth factor stimuli. Enrichment analysis highlighted changes in RNA splicing (GO:0008380) and RNA splicing regulation (GO:0043484) and also pointed to EMT as it was previously associated with alterations in RNA splicing mechanisms [105], [106]. Furthermore, modified receptor signaling pathways could also result in changes in cell migration and EMT as these processes are regulated by the same receptor tyrosine kinases and other proteins involved in signal transduction [107], [108].

GO molecular function enrichment analysis supplemented GO Biological process data by highlighting changes in cell-cell adhesion mediator activity (GO:0098632) and cadherin binding (GO:0045296). Remarkably, it is well established that the loss of cell-cell junctions and changes in cadherin levels and binding capacity are crucial for EMT [109], [110].

Additionally, KEGG pathway enrichment also demonstrated similar results such as changes in various signaling pathways including (I) the NF-kappa B signaling (KEGG:04064) and VEGF signaling pathways (KEGG:04370), (II) cell-cell and cell-substrate interactions such as in tight junctions (KEGG:04530), adherent junctions (KEGG:04520) or focal adhesion (KEGG:04510) and (III) the regulation of actin cytoskeleton (KEGG:04810). Notably, all these pathways contribute to the EMT in one way or another [99]–[101], [107], [111], [112].

In summary, the bioinformatic analysis of global differential proteomes shows changes in processes, functions, and pathways related to cell motility, migration, cytoskeleton organization, and most importantly related to the epithelial-mesenchymal transition. This allowed us to predict miR-23b involvement in the regulation of complex EMT cellular phenomena contributing to the oxaliplatin resistance mechanism in CRC cells.

3.4.1.2. Evaluation of epithelial-mesenchymal transition

To validate proteomic and bioinformatic data that pointed toward the involvement of miR-23b in the regulation of cell EMT as well as their migration, we evaluated the epithelial-mesenchymal phenotype of parental, oxaliplatin-resistant and miR-23b knockout cell lines.

First, we evaluated cell migration using the wound-healing assay. The wound-healing assay revealed that Oxa-23b$^{-/-}$ cells possess considerably higher migration potential than HCT-Oxa cells and HCT-P, which exhibited the lowest degree of mobility (Figure 27 A and B). Furthermore, we observed that Oxa-23b$^{-/-}$ cells have fewer cell-cell contacts, tend to attach to the surface like fibroblasts and have a higher number of lamellipodia than HCT-Oxa cells (Figure 27 C).

Since the increase in cell migration is frequently attributed to the mesenchymal phenotype [100] and our proteomic data also suggest alterations in the EMT state of oxaliplatin-resistant cells, we have quantitated a few mesenchymal cell markers to relate their phenotype to miR-23b expression. Analysis of microscopy data supported the results of the wound-healing assay showing the greatest amount of vimentin in Oxa-23b$^{-/-}$ cells and a moderately increased amount in HCT-Oxa cells compared with HCT-P cells (Figure 27 D and E).

The EMT marker vimentin [113] expression level determined by confocal microscopy and RT-qPCR, as well as the level of one of the EMT-inducing transcription factors SNAI2 (also known as SNAIL2 or SLUG) [114] determined by RT-qPCR, showed a similar effect (Figure 27 F). Therefore, the acquisition of oxaliplatin resistance coincides with the increase in miR-23b expression, the moderate increase in EMT markers, vimentin and SNAI2, expression. However, the further rise in their expression in the miR-23b deficient cells results in less resistant phenotype.

In summary, these findings show that HCT-Oxa cells acquired a hybrid epithelial-mesenchymal phenotype while obtaining resistance to oxaliplatin. Depleting miR-23b from the resistant cell line resulted in the decrease of drug resistance and a more profound mesenchymal phenotype. This indicates that elevated miR-23b in the oxaliplatin-resistant cells holds them in a hybrid EMT stage and contributes to the cancer cell insensibility to the drug (Figure 27 G).

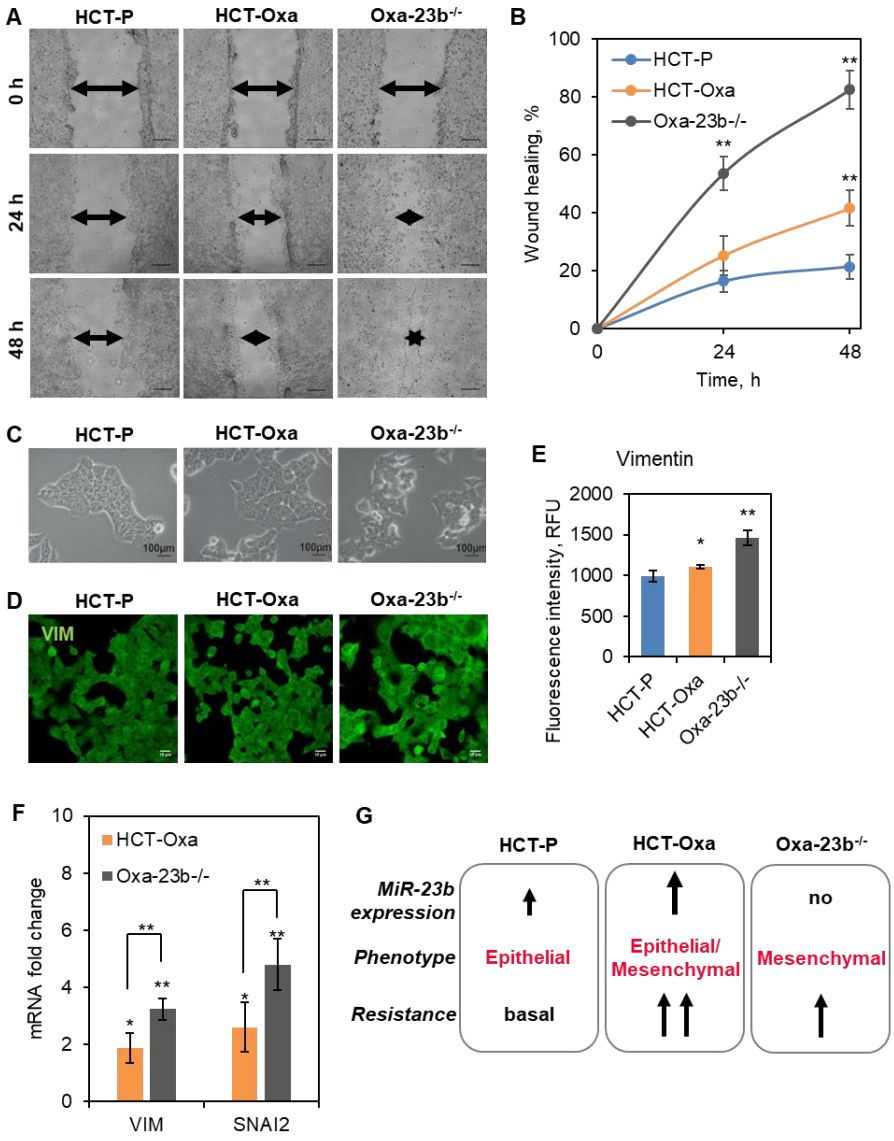

Figure 27. MiR-23b contributes to epithelial-mesenchymal transition. **A.** Bright-field microscopy images of cell migration into the wound area. **B.** Estimation of cell migration capabilities from wound healing images. Bars are ± SD, significant differences are marked by asterisks: * $p < 0.05$, ** $p < 0.01$, ANOVA, n = 3. **C.** Identification of cell morphology by bright field microscopy. **D.** Representative confocal microscopy images of cells stained with antibody against vimentin (green channel). **E.** Analysis of vimentin quantity from confocal microscopy images. Fluorescence intensity was estimated using ImageJ software. Bars are ± SD, significant differences are marked by asterisks: * $p < 0.05$, ** $p < 0.01$, ANOVA, n = 3. **F.** Change of expression of EMT markers measured by RT-qPCR. Bars are ± SD, significant differences are marked by asterisks: * $p < 0.05$, ** $p < 0.01$, ANOVA, n = 3. **G.** Schematic representation of EMT status and resistance of HCT-P, HCT-Oxa and Oxa-23b$^{-/-}$ cells showing the importance of partial EMT for cancer cell resistance.

3.4.1.3. Manipulation of EMT-inducing transcription factor SNAI2

The epithelial-mesenchymal transition is regulated by EMT-inducing transcription factors which usually act in various combinations to induce the expression of genes that promote the mesenchymal cell state or repress the expression of genes that maintain the epithelial state. Some of the EMT-inducing factors directly or indirectly inhibit the function of one of the major regulators of cell adhesion E-cadherin considered as a tumor suppressor in some cancer types [115]. EMT-related proteins play an important role in cancer invasiveness and metastasis, so manipulation of the EMT process and involved proteins became an attractive strategy for cancer therapy.

As our previous findings suggested a hybrid state of EMT as a possible mechanism of maintenance of cell resistance, we decided to induce the mesenchymal phenotype in the parental cell line and check for changes in resistance to oxaliplatin. SNAI2 transcription factor was chosen to manipulate the EMT status of the HCT-P cell line as an increase in this transcriptional repressor was spotted in previous experiments with miR-23b. SNAI2 not only represses epithelial genes by binding to E-box DNA sequences through their zinc-finger domain but can interfere with various signaling pathways involved in the initiation and progression of EMT [100].

Since epithelial-mesenchymal transition is a process requiring time, 7-day or 14-day induction of exogenous SNAI2 protein was performed by using the doxycycline-inducible protein expression system. Induction of the FLAG-tagged SNAI2 transcription factor was evaluated via western blot analysis showing the dose-dependent effect of doxycycline concentration on SNAI2 quantity (Figure 28 A). Moreover, the quantity of E-cadherin which is directly repressed by the SNAI2 transcription factor was evaluated to show the transcriptional activity of exogenously expressed SNAI2 protein. Indeed, the results showed a direct negative correlation between SNAI2 and E-cadherin quantities supporting the notion that exogenously expressed SNAI2 is functional in HCT-P cells and can cause changes in epithelial-mesenchymal phenotype.

Next, we evaluated localization of FLAG-tagged SNAI2, as nuclear translocation is essential for the functionality of all transcription factors. The results of immunofluorescence analysis showed nuclear localization of exogenous SNAI2 protein as was expected (Figure 28 B). Furthermore, RT-qPCR analysis of other EMT-related genes showed a decrease in mRNA encoding proteins ensuring epithelial state such as E-cadherin (*CDH1*) and an increase in miRNA encoding proteins involved in the maintenance of

mesenchymal state such as N-cadherin (*CDH2*) and vimentin (Figure 28 C). Interestingly, SNAI2 quantity negatively correlates with the quantity of another EMT-promoting transcription factor SNAI1 suggesting a negative regulatory feedback loop.

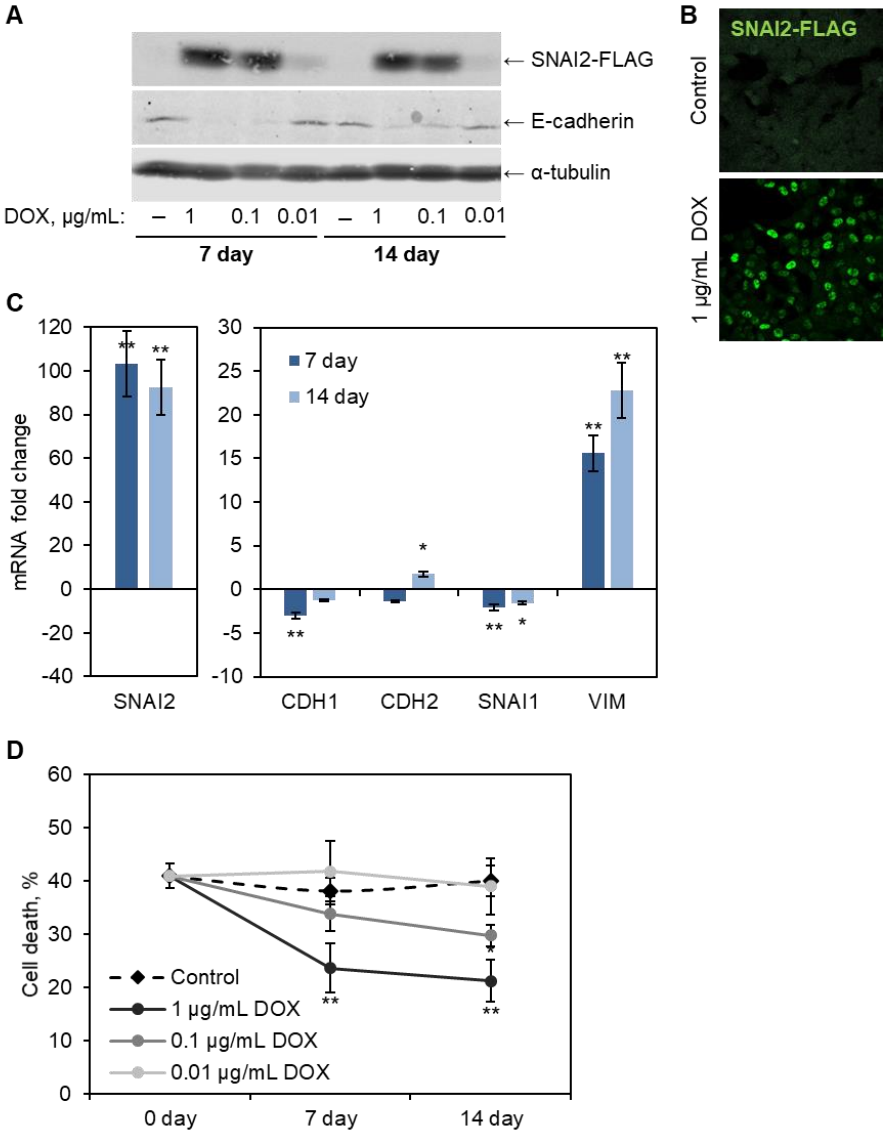

Figure 28. EMT-inducing transcription factor SNAI2 modulates the EMT state and cell resistance to oxaliplatin of the HCT-P cell line. **A.** Western blot analysis of doxycycline-induced FLAG-tagged SNAI2 protein quantity in HCT-P cell line after treatment with various concentrations of doxycycline for 7 and 14 days. α-tubulin is shown as a loading control. **B.** Representative confocal microscopy images of cells stained with antibody against the FLAG tag (green channel). The expression of FLAG-tagged SNAI2 protein was induced by

treatment with 1 μg/mL doxycycline for 72 h before staining. **C.** Change of expression of EMT markers after SNAI2 induction for 7 or 14 days measured by RT-qPCR. Bars are ± SD, significant differences are marked by asterisks: * $p < 0.05$, ** $p < 0.01$, ANOVA, n = 3. **D.** Evaluation of cell resistance to oxaliplatin after 7-day and 14-day SNAI2 induction. Cells were treated with 50 μM oxaliplatin for 48 h and cell death was estimated using propidium iodide staining-based flow cytometric assay. Bars are ± SD, significant differences are marked by asterisks: * $p < 0.05$, ** $p < 0.01$, ANOVA, n = 3.

Finally, the resistance to oxaliplatin treatment of SNAI2 expressing cells was evaluated using propidium iodide staining-based cell death assay. The data showed an increase in HCT-P cell resistance after both 7-day and 14-day induction of exogenous SNAI2 transcription factor in a dose-depended manner, thus, supporting previous results that oxaliplatin-resistant cells gained resistance via adopting mesenchymal phenotype (Figure 28 D).

In conclusion, miRNA expression profile analysis, as well as in-depth analysis of differential global proteomic data of miR-23b knockout cells, pointed out the importance of the EMT state on CRC resistance to oxaliplatin. The experiments with the inducible EMT-promoting transcription factor SNAI2 suggested this protein as one of the major regulators of the resistance-associated hybrid EMT state. Significantly, new data emerge suggesting that SNAI2 expression is more prominent in intermediate-epithelial or intermediate-mesenchymal phenotype bearing cells [116] supporting this hypothesis.

3.4.2. Differential proteomic analysis

To get some insights into the molecular mechanism of HCT-Oxa cells resistance to oxaliplatin, we decided to perform both proteomic and miRNomic analysis of these cells in comparison to the parental cell line.

First, we examined changes in proteome associated with resistance to oxaliplatin by global high throughput differential quantitative proteomic analysis of HCT-P and HCT-Oxa cells performed using label-free high-definition mass spectrometry technology. Proteomic analysis has led to the identification and quantification of 5094 proteins, 375 of which were differentially expressed in HCT-Oxa versus HCT-P. Proteins whose level was significantly ($p \leq 0.05$) increased or decreased 1.5-fold and higher in HCT-Oxa versus HCT-P cells were considered differentially regulated in oxaliplatin-resistant cells and subjected to further analysis.

Next, GO Biological Process enrichment analysis of differentially expressed proteins was performed using ClueGO and CluePedia Cytoscape plug-ins [56], [57]. Bioinformatic analysis indicated changes in biological

processes that could be associated with cancer cell resistance to chemotherapy such as cell cycle phase transition (GO:0044770) and intrinsic apoptotic signaling pathway (GO:0097193) [12], [117].

Since changes in the cell cycle of the HCT-Oxa cell line have been already detected by previous cell cycle analysis, we took particular interest in the possible alteration of apoptotic signaling. To detect changes in the intrinsic apoptotic signaling pathway, we subjected differentially expressed proteins belonging to that term to subsequent GO Biological Process enrichment analysis. This analysis revealed key regulators of the intrinsic apoptotic signaling pathway (GO:0097193) such as *MIF*, *TRIAP1*, and *TP53* (Figure 29 A). Macrophage migration inhibitory factor (MIF) and TP53-regulated inhibitor of apoptosis 1 (TRIAP1) play important roles in DNA damage response and transduction of apoptotic signals [118], [119]. MIF is a known inhibitor of p53 protein [120] and TRIAP1 is transcriptionally regulated by p53 protein [119].

Moreover, differentially expressed proteins involved in the intrinsic apoptotic signaling pathway (GO:0097193) were subjected to transcription factors protein-protein interaction (PPI) analysis using the Enrichr web tool [121]. According to this analysis, p53 protein interacts with most of the proteins in apoptotic signaling pathway differentially expressed in our dataset including MIF and TRIAP1 or well-known regulators of mismatch repair pathway *MSH2* and *MSH6* [122], as well as cell cycle regulator *CDKN1A* [123] and CUL4A, the ubiquitin ligase component of a multimeric complex involved in the degradation of DNA damage response proteins [124] (Figure 29 B).

As proteomic analysis highlighted p53 as a major regulator of oxaliplatin-induced cell apoptosis, we decided to analyze the miRNomics dataset looking for miRNAs involved in p53 pathway regulation. We found multiple changes in p53-associated miRNA confirming the important changes in this pathway (Figure 29 C). Most notably, changes were detected in miR-23a/27a/24-2 cluster which is found to have altered expression in many cancers and has been shown to give rise to contrasting phenotypes in different cell types [125]. The expression level of MiR-27a, a member of this cluster, correlated with the quantity of p53 protein [126] and miR-24-2 affects a variety of p53 proteins, namely, p53 degradation regulator MDM2, cell cycle regulator p21, apoptosis-related protein Bcl-2, and DNA damage sensor H2AX [127].

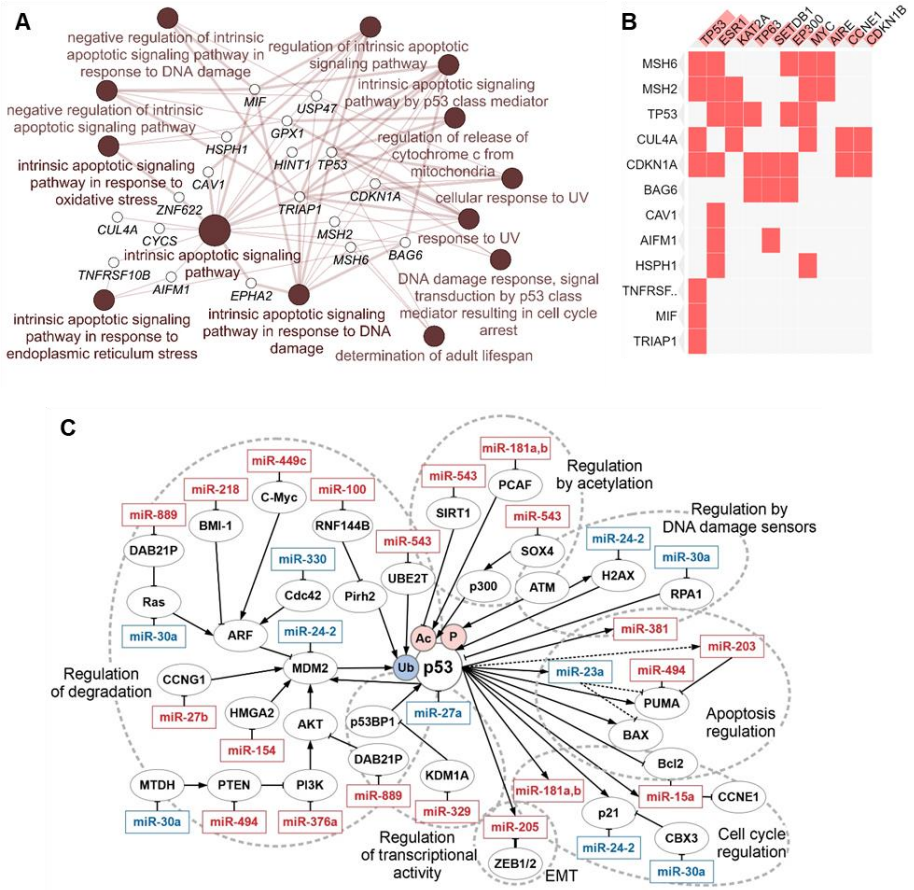

Figure 29. Differential proteomic and miRNomic analysis of parental and oxaliplatin-resistant cell lines reveals changes in the apoptotic signaling pathway and highlights p53 protein as a major regulator. **A.** HCT-P and HCT-Oxa were subjected to in-depth quantitative proteomic analysis. GO Biological Process enrichment analysis of differentially expressed proteins from the intrinsic apoptotic signaling pathway was performed using ClueGO and CluePedia plugins for Cytoscape software. **B.** Differentially expressed proteins belonging to the intrinsic apoptotic signaling pathway were further subjected to transcription factors PPIs analysis using the EnrichrR web tool. **C.** Differentially expressed miRNA dataset was analyzed looking for changes in miRNA involved in p53 pathway regulation.

Altogether, proteomics data implied changes in the apoptotic signaling pathway of the oxaliplatin-resistant cell line regulated by signal transduction mediator p53 protein. Moreover, the analysis of the differential miRNomics dataset revealed changes in p53 pathway regulation highlighting the importance of p53 activation for the sufficient response to oxaliplatin treatment.

3.4.2.1. Transcriptional target and mutational analysis of p53

Two major pathways regulated by p53 during the response to cytotoxic drugs are cell cycle arrest resulting in DNA damage repair and consecutive increase in cell viability or induction of apoptosis (Vousden and Lu, 2002). Upon DNA damage cell cycle arrest is mediated through transcriptional regulation of the *CDKN1A* gene which encodes cyclin-dependent kinase inhibitor p21 [123]. Induction of apoptosis executed either by transcriptionally activating pro-apoptotic Bcl-2 family member BAX or several BH3 domain-only proteins that function upstream of BAX called PUMA and NOXA [128]. The increase in BAX, PUMA and NOXA quantity leads to cytochrome C release from mitochondria and activation of initiator caspase-9 and executive caspase-3 [129], [130] (Figure 30 A).

Since the p53-mediated response to genotoxic stress depends on the ability of p53 to activate gene expression as a transcription factor, we decided to test p53 target gene activation after drug treatment. The results of RT-qPCR analysis of p53 transcriptional targets *CDKN1A* (encoding p21 protein), *BAX*, *BBC3* (encoding PUMA protein), *PMAIP1* (encoding NOXA protein), and *MDM2* pointed out that wild-type p53 in HCT-P cell line effectively increases mRNA levels of its target genes after oxaliplatin treatment (Figure 30 B). However, transcriptional activation of p53 target genes in the oxaliplatin-resistant cell line was not observed. These results were further validated by confocal microscopy analysis of p21 protein quantity, one of the most prominent p53 transcriptional targets. After the oxaliplatin treatment, the HCT-P cell line exhibited a substantial increase in p21 quantity, whereas, in the HCT-Oxa cell line any changes remained undetectable (Figure 30 C and D).

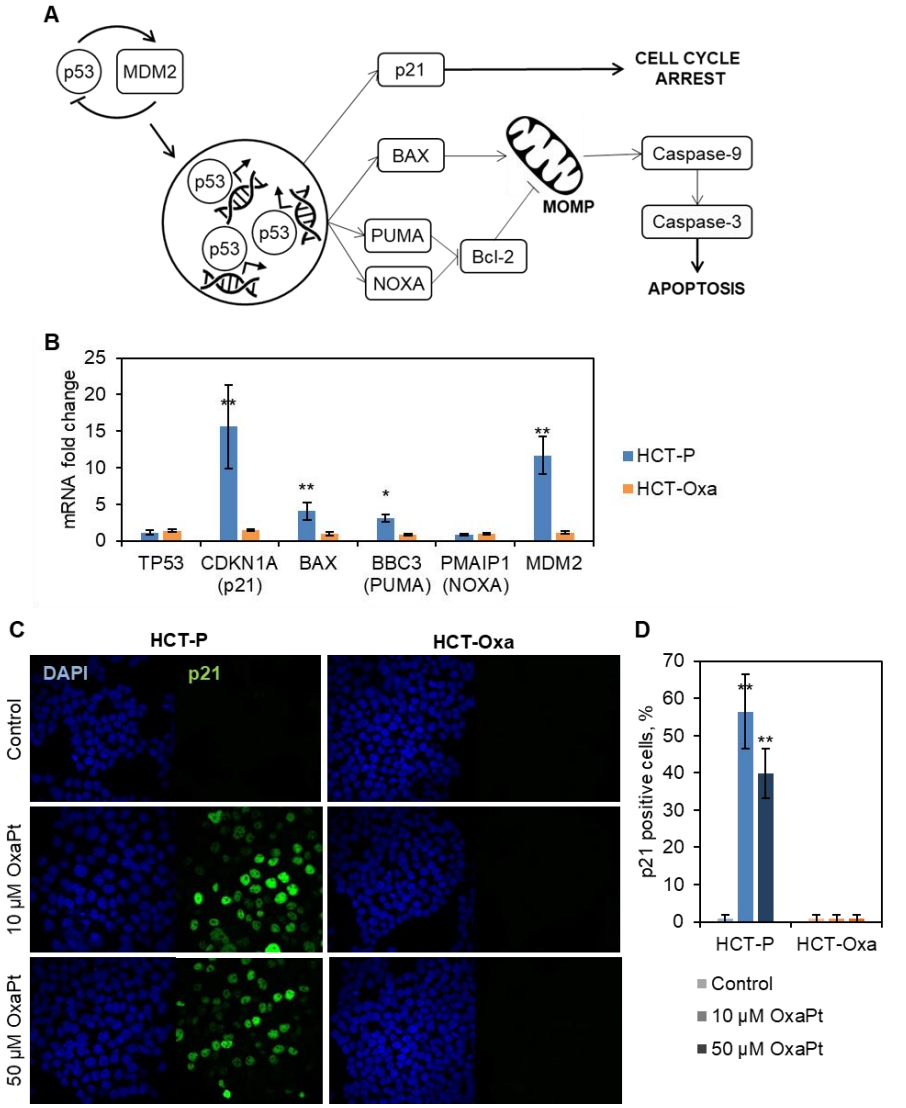

Figure 30. P53 protein does not activate its transcriptional targets in the HCT-Oxa cell line. **A.** Scheme of p53 transcriptionally activated targets and their function. **B.** Change of expression of p53 transcriptional targets measured by RT-qPCR in HCT-P and HCT-Oxa cells after 10 µM oxaliplatin treatment for 24 h. Bars are ± SD, significant differences are marked by asterisks: * $p < 0.05$, ** $p < 0.01$, ANOVA, n = 3. **C.** Representative confocal microscopy images of cells stained with DNA dye DAPI (blue channel) and antibody against p21 (green channel). Cells were untreated or treated with 10 or 50 µM oxaliplatin for 24 h. **C.** Analysis of p21 positive cells from confocal microscopy images. Fluorescence intensity was estimated using ImageJ software. Bars are ± SD, significant differences are marked by asterisks: * $p < 0.05$, ** $p < 0.01$, ANOVA, n = 3.

The impaired signal transduction by p53 protein may be caused by loss of signal from upstream regulators of p53 or loss of p53 ability to transduce signal downstream. Most of the changes in p53 protein functions, such as tumor-promoting or chemoresistance-related, are often attributed to mutations in the *TP53* gene [17]. As mutations in the *TP53* gene can occur in almost every part of the gene [131], full-length gene sequencing of *TP53* was performed. We identified two novel heterozygous point substitutions Tyr236Cys and Ile255Thr in the *TP53* gene that occurred during the selection of oxaliplatin-resistant cell line (Figure 31 A). These mutations are confined to the DNA binding domain, thus implying changes in the DNA binding capabilities and alterations in functioning as a transcription factor.

The mutations of p53 have been divided into two categories: structural mutants that can cause unfolding of the p53 protein, and DNA-contact mutants that affect DNA binding capabilities [17]. To test p53 stability, we analyzed the p53 quantity changes after drug treatment in parental and oxaliplatin-resistant cells. Confocal microscopy, as well as western blot analysis, revealed an increased quantity of p53 in both HCT-P and HCT-Oxa cell lines after treatment with oxaliplatin (Figure 31 B and C). Moreover, these results confirmed previous differential proteomics data that basal p53 level is increased in the oxaliplatin-resistant cell line.

Altogether, the results of transcriptional targets and mutation analyses suggest that mutated p53 in the oxaliplatin-resistant cell line lost its sequence-specific DNA binding. This hypothesis was verified by oligoprecipitation assay of p53 using the p21 promoter sequence as a bait. P21 promoter sequence was chosen due to the highest affinity to p53 [132] and scrambled oligonucleotide, named WRNC, was used as an unspecific binding control. P53 protein was pulled out from nuclear lysate via interaction with biotinylated oligonucleotide and using streptavidin-conjugated agarose as a solid fraction (Figure 31 D). The results of this assay demonstrated the ability of wild-type p53 from HCT-P cells strongly interacts with the target DNA sequence, however, this ability was lost in mutant p53 from HCT-Oxa cells (Figure 31 E).

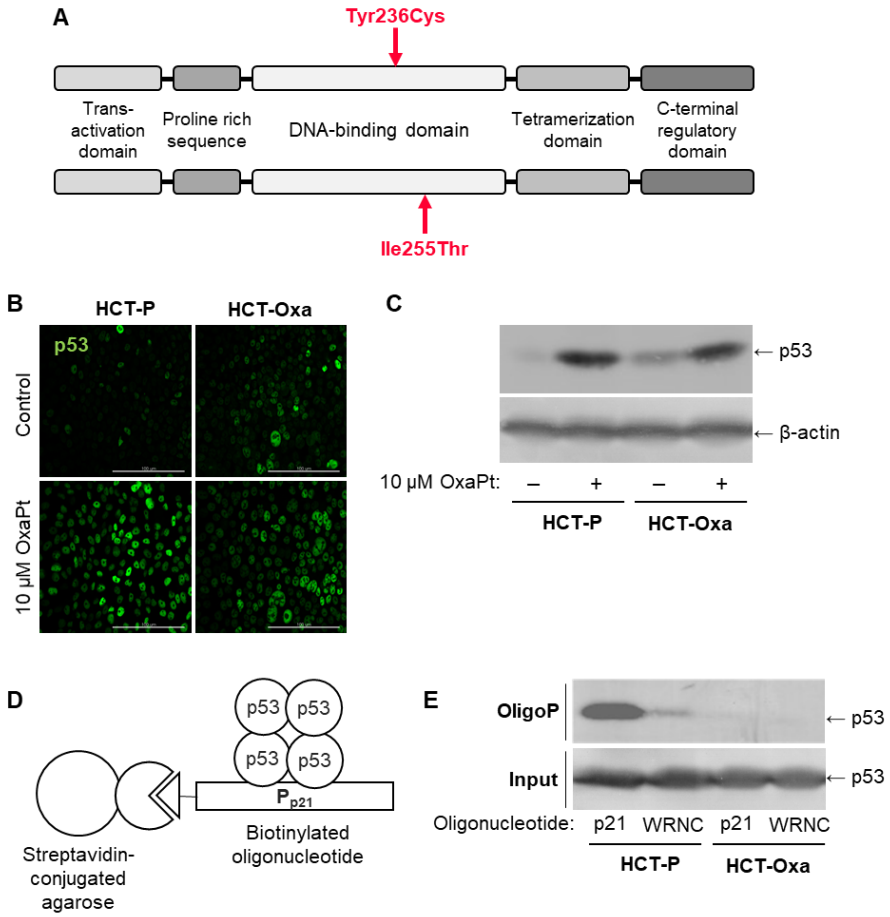

Figure 31. Mutant p53 protein lost its ability to interact with target promoter sequences. **A.** Scheme of p53 domain structure. Detected p53 mutations are signified in red. **B.** Representative confocal microscopy images of cells stained with antibody against p53 (green channel). Cells were untreated or treated with 10 μM oxaliplatin for 24 h before staining. **C.** Western blot analysis of p53 protein quantity in HCT-P and HCT-Oxa cell lines after 10 μM oxaliplatin treatment for 24 h. β-actin is shown as a loading control. **D.** Scheme of oligoprecipitation assay used for p53 and DNA interaction analysis. **E.** Western blot analysis of p53 oligoprecipitation results. P21 promoter sequence was used as a positive control, WRNC oligonucleotide used as a negative control, nuclear lysates before oligoprecipitation used as input control.

In conclusion, mutant p53 protein in the oxaliplatin-resistant cell line is unable to form a stable interaction with its target DNA and, therefore, does not activate its transcriptional targets after drug treatment.

3.4.2.2. Evaluation of p53 knockdown cells resistance

Mutations in the *TP53* gene can result in various outcomes such as loss of transcriptional function or gain of various unique functions that differ from wild-type protein. Mutant p53 can interact with different DNA sequences and/or different proteins and modify their interaction and transcriptional activation of target genes [17]. To elucidate how mutant p53 protein affects the resistance of the HCT-Oxa cell line, we have knockdown p53 protein using shRNA. Five different shRNAs were used yielding different levels of protein quantity decrease validated by western blot analysis (Figure 32 A). From these results, we evaluated the correlation of p53 protein quantity with resistance to oxaliplatin. Data shows a moderate negative correlation of p53 quantity and resistance in the HCT-P cell line with knockdown p53 protein (Figure 32 B). On the other hand, the HCT-Oxa cell line displays no correlation referring to no additional resistance-related functions of mutant p53 protein.

Changes in p53 protein function are related not only to resistance to platinum compounds [133] but to 5-fluorouracil resistance as well [134]. We examined resistance of the most effective p53 knockdown cells to both compounds in the FOLFOX regimen. According to cell viability data, wild-type p53 knockdown cells exhibit an increase in cell resistance to both drugs (Figure 32 C and D). However, mutant p53 bearing HCT-Oxa cells are resistant to both compounds and this resistance is not attenuated by diminished p53 quantity.

One of the most interesting aspects of p53 transcriptional function is coordinated promoter selection, which plays a key role in determining response to p53 protein. It has been shown that some of the p53 mutants retain the ability to induce expression of only a subset of target genes when compared with wild-type p53 [135], [136]. In the light of this data, we performed RT-qPCR analysis of a few of p53 transcriptional target genes. We selected mRNA of proteins involved in various diverse p53-regulated processes such as cell cycle control (*CDKN1A* or p21 and *GADD45A*), apoptosis induction (*BAX*, *BBC3*(PUMA) and *PMAIP1*(NOXA)) or feedback loop (*MDM2*). Analysis of p53 transcriptional targets activation after oxaliplatin treatment revealed that in HCT-P cell line wild-type p53 does not induce synthesis of miRNA of NOXA, moderately induce GADD45, BAX, and PUMA and strongly induce p21 and MDM2 proteins (Figure 32 E). In all cases, the HCT-P p53 knockdown cell line displayed diminished activation of transcriptional p53 targets. On the contrary, there

was no transcriptional target activation by mutated p53 protein both in HCT-Oxa control and p53 knockdown cell lines.

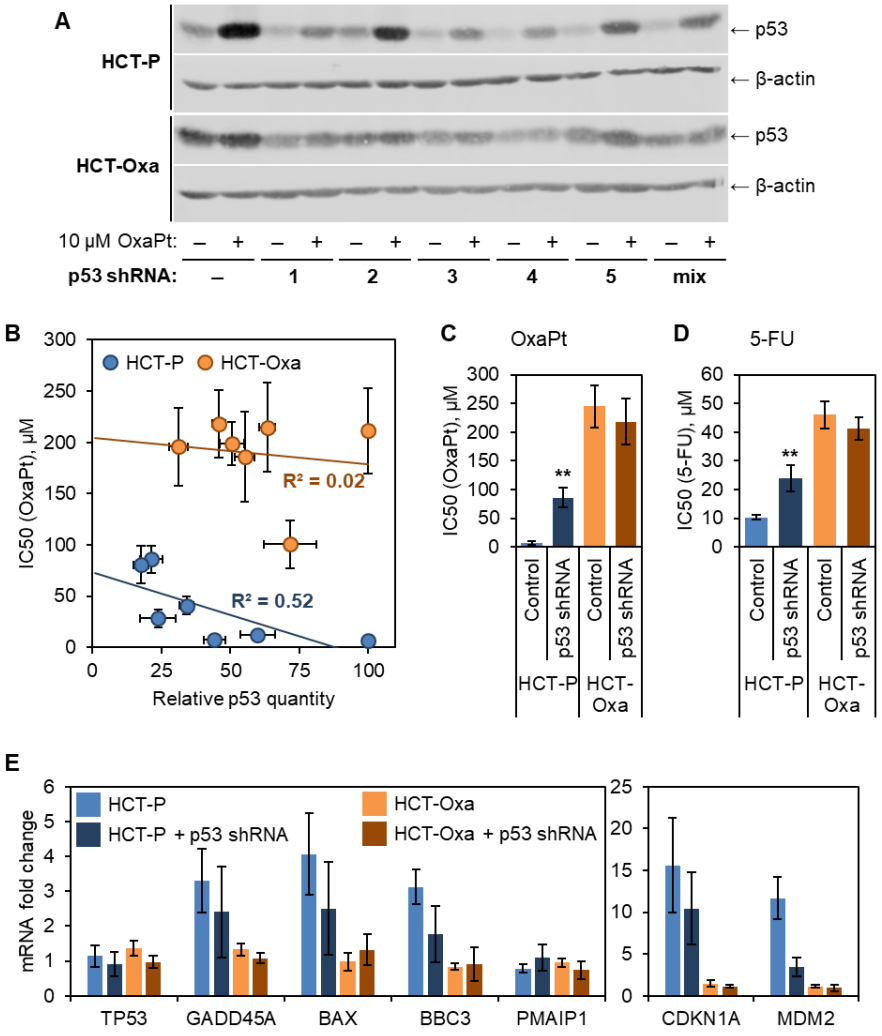

Figure 32. P53 knockdown results in increased resistance and diminished activation of transcriptional targets in HCT-P, but not the HCT-Oxa cell line. **A.** Western blot analysis of p53 protein quantity in HCT-P and HCT-Oxa cell lines expressing scrambled or p53-targeted shRNA after 10 μM oxaliplatin treatment for 24 h. β-actin is shown as a loading control. **B.** Correlation analysis of p53 quantity and oxaliplatin resistance. P53 quantity was evaluated from western blot analysis of cells expressing p53 shRNA relative to cells treated with scrambled shRNA control. IC50 values were estimated from MTT assay by treating cells with increasing concentrations of oxaliplatin for 48 h and evaluating viability after 96 h. Bars are ± SD, n = 3. **C, D.** IC50 value estimation of cells expressing scrambled or p53-targeted shRNA from cell viability tests. Bars are ± SD, significant differences are marked by asterisks: * $p < 0.05$, ** $p < 0.01$, ANOVA, n = 3. **E.** Change of expression of p53 transcriptional targets measured by RT-qPCR in HCT-P and HCT-Oxa cells expressing scrambled or p53-targeted

shRNA after 10 μM oxaliplatin treatment for 24 h. Bars are ± SD, significant differences are marked by asterisks: * $p < 0.05$, ** $p < 0.01$, ANOVA, n = 3.

Altogether, these results show that intact p53 function is essential for cytotoxic effects of both oxaliplatin and 5-fluorouracil - two active compounds of FOLFOX therapy. Moreover, mutated p53 protein in the HCT-Oxa cell line does not confer to resistance by the means of gaining any additional functions as p53 knockdown does not sensitize HCT-Oxa cell line to chemotherapy drugs.

3.4.2.3. Inducible wild-type and mutant p53 expression

Another strategy to elucidate the effect of mutated p53 on cancer cell resistance is to overexpress target protein in both parental and resistant cell lines. As p53 protein is a well-known tumor-suppressor protein, long-term stable expression of this protein can lead to unwanted cell line adaptation to increased p53 quantity or even lethality. Thus, the rtTA-Advanced inducible protein expression system was chosen for this application. If there is no inductor present in growth media cells are expressing only endogenous p53 protein from an endogenous promoter and the doxycycline-induced promoter remains inactive (Figure 33 A). Then doxycycline is added to growth media, it interacts with rtTA protein and expression of exogenous FLAG-tagged p53 protein starts. P53 expression levels after induction were evaluated using western blot analysis showing levels of exogenous p53 are comparable to endogenous p53 (Figure 33 B). Moreover, western blot analysis confirmed that there was no leakage of the doxycycline-inducible promoter in the absence of an inducer.

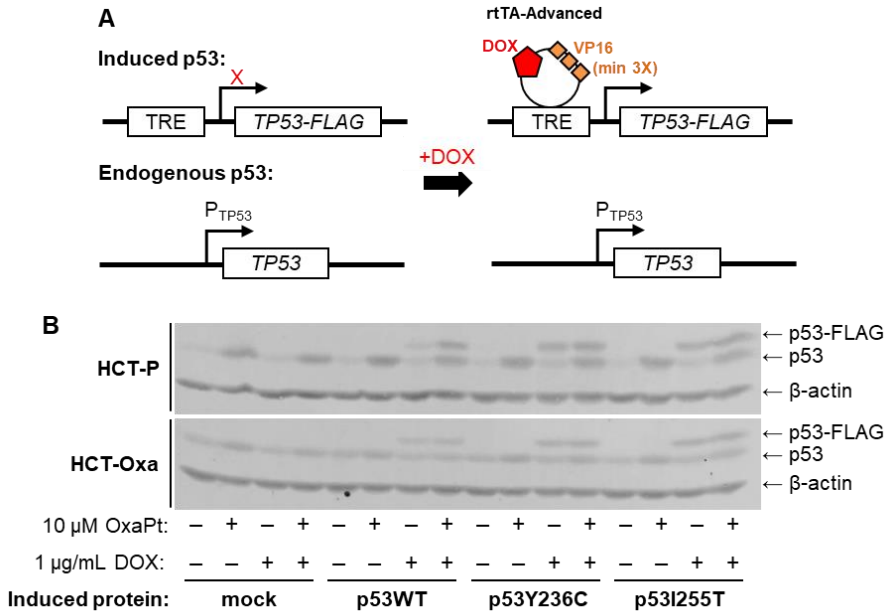

Figure 33. P53 can be successfully induced in both HCT-P and HCT-Oxa cell lines. **A.** Scheme of rtTA-Advanced doxycycline-inducible expression system used for p53 induction. **B.** Western blot analysis of endogenous and doxycycline-induced FLAG-tagged p53 protein quantity in HCT-P and HCT-Oxa cell lines after 1μg/mL doxycycline treatment for 48 h and 10 μM oxaliplatin treatment for 24 h. β-actin is shown as a loading control.

Many mutated p53 isoforms can exert dominant-negative effects over co-expressed wild-type p53, largely by forming mixed tetramers that are incapable of DNA binding and transactivation [18]. Hence, transcriptional activation of the most prominent p53 target protein p21 was evaluated by confocal microscopy after wild-type or mutated p53 induction. The results showed an increase of p21 immunofluorescence after the induction of wild-type p53 in both oxaliplatin-sensitive and -resistant cell lines (Figure 34 A). Furthermore, the induction of mutated p53 reduced transcriptional activation of p21 in HCT-P cells showing dominant-negative effect over the endogenous wild-type p53. The induction of mutated p53 in the HCT-Oxa cell line already bearing mutated p53 did not affect p21 immunofluorescence.

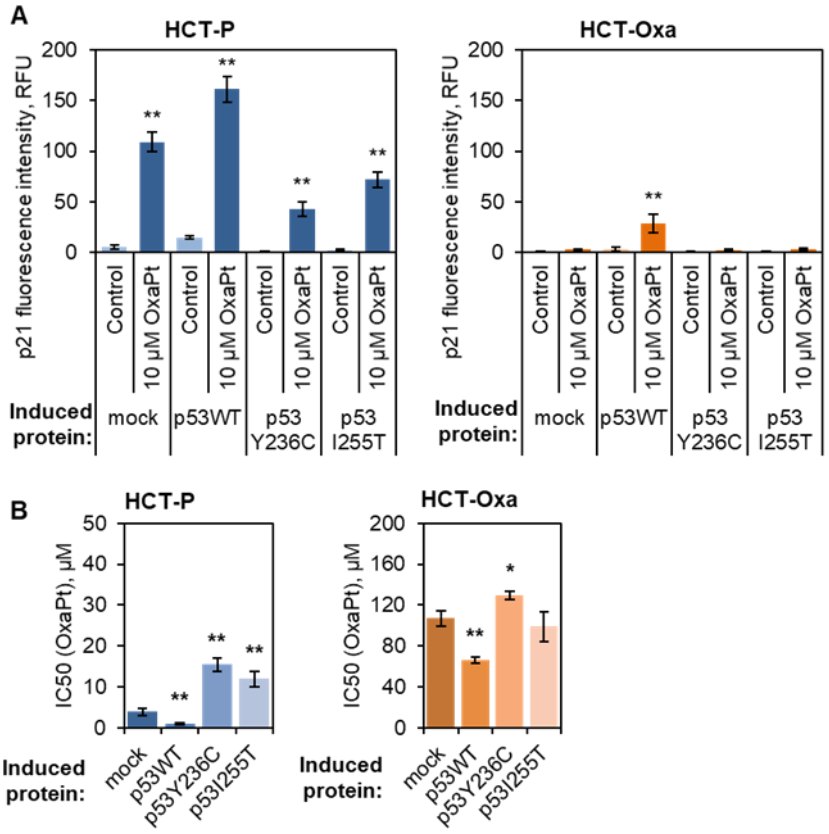

Figure 34. Induction of wild-type p53 protein restores p53 transcriptional activity and sensitizes both HCT-P and HCT-Oxa cells to oxaliplatin. **A.** Analysis of p21 quantity from confocal microscopy images. Wild-type or mutant p53 was induced by 1 μg/mL doxycycline 24 h before oxaliplatin treatment. Cells were treated with 10 μM oxaliplatin for 24h and stained with antibody against p21 protein. Fluorescence intensity was estimated using ImageJ software. Bars are ± SD, significant differences are marked by asterisks: * $p < 0.05$, ** $p < 0.01$, ANOVA, n = 3. **B.** IC50 value estimation of cells expressing induced wild-type or mutant p53 protein from cell viability tests. Wild-type or mutant p53 was induced by 1 μg/mL doxycycline 24 h before oxaliplatin treatment. Bars are ± SD, significant differences are marked by asterisks: * $p < 0.05$, ** $p < 0.01$, ANOVA, n = 3.

The same results were obtained from cell viability analysis of parental and oxaliplatin-resistant cell lines after p53 induction. The induction of wild-type p53 diminished resistance to oxaliplatin treatment in both cell lines, however, the induction of mutated p53 increased resistance of HCT-P cells but had no or slight effect in HCT-Oxa cells (Figure 34 B).

To summarize, the results of the inducible expression of p53 supported the hypothesis that wild-type p53 is essential for a proper oxaliplatin-

induced response. Moreover, mutated p53 exerts dominant-negative effect over wild-type p53 and promotes resistance to oxaliplatin.

3.4.2.4. P53 knockout using CRISPR/Cas9 system

As previous experiments pointed out the importance of wild-type p53 for cell response to oxaliplatin, we decided to analyze the mechanism of action of oxaliplatin in relation to p53 activation. For this purpose, we designed p53 knockout cell lines using the CRISPR/Cas9 system for the negative reference control. Genomes of the parental p53 wild-type bearing and the oxaliplatin-resistant mutated p53 bearing cell lines were edited using p53 exon 2- and 3-targeted CRISPR/Cas9 system (Figure 35 A). After genetic manipulation cells were cloned and p53-negative clones were pooled to create p53 knockout cell lines. P53-negative clones were screened using western blot analysis and only clones with absent p53 were chosen for further experiments (Figure 35 B). 15 different clones were used for each cell line to avoid any off-target effects of CRISPR/Cas9 editing and clone variability due to cell line heterogeneity.

First of all, the resistance to oxaliplatin of newly-derived p53 knockout cell lines was evaluated using the propidium iodide staining-based dead cell detection method. The results showed a decrease in sensitivity to oxaliplatin of parental p53 knockout cell line (designated as HCT-P-p53$^{-/-}$) but no significant changes in oxaliplatin-resistant p53 knockout cell line (designated as HCT-Oxa-p53$^{-/-}$) (Figure 35 C). These results support previous findings that activation of wild-type p53 is necessary for response to oxaliplatin and that mutated p53 in the oxaliplatin-resistant cell line didn't gain any additional functionalities involved in the maintenance of resistance to oxaliplatin.

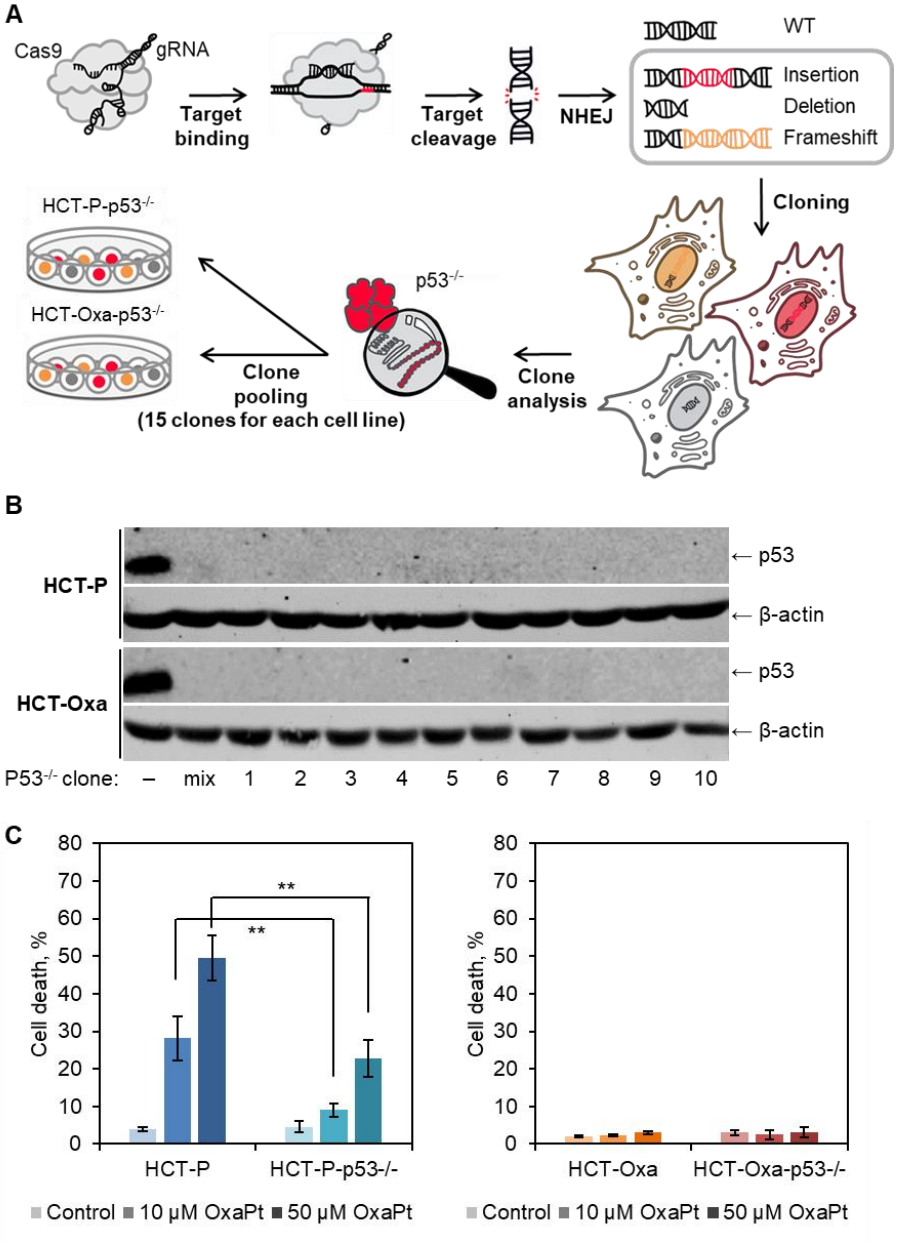

Figure 35. P53 knockout using the CRISPR/Cas9 system causes an increase of resistance to oxaliplatin in the parental cell line. **A.** Scheme of p53 knockout cell line generation using the CRISPR/Cas9 system. **B.** Evaluation of p53-negative clones by western blot analysis after 24 h treatment with 10 μM oxaliplatin. β-actin is shown as a loading control. **C.** Cell death analysis by propidium iodide staining assay after 10 μM or 50 μM treatment with oxaliplatin for 48h. Bars are ± SD, significant differences are marked by asterisks: * $p < 0.05$, ** $p < 0.01$, ANOVA, $n = 3$.

Next, these HCT-P-p53$^{-/-}$ and HCT-Oxa-p53$^{-/-}$ cells were used for the analysis of the mechanism of action of oxaliplatin and the role of p53 in it. For this purpose, the response to DNA damage was tested after oxaliplatin treatment using cisplatin, another DNA-damaging platinum-based compound, and doxorubicin, the DNA-intercalating agent, as the reference drugs. Cisplatin is an agent causing intra-strand or inter-strand DNA adducts which are repaired by mismatch repair (MMR) or nucleotide excision repair (NER) systems [137]. Doxorubicin is a strong DNA-intercalating agent inhibiting the activity of topoisomerase-2 and, hence, causing double-strand DNA breaks [138]. Efficacy of these drugs is known to be reliant not only on DNA-damaging effects but on the efficiency of DNA repair which can be evaluated by histone H2AX phosphorylation. Histone H2AX is a substrate of several DNA damage-activated protein kinases, such as ATM (ataxia teleangiectasia mutated), ATR (ATM and Rad3-related) or DNA-dependent protein kinase (DNA-PK) and can be used as a DNA damage marker [139]. The results of H2AX immunostaining showed a lack of DNA damage response after oxaliplatin treatment in all tested cell lines, however, DNA damage response was detected after both cisplatin and doxorubicin (Figure 36 A). These results suggest unconventional oxaliplatin cytotoxicity mechanism that is not reliant on DNA damage or at least does not evoke H2AX-involved DNA damage response mechanisms.

Moreover, the cell cycle analysis of parental, oxaliplatin-resistant and p53 knockout cell lines showed different cell responses to oxaliplatin and cisplatin implying that different cell cycle checkpoints are activated upon the drug treatment. Cisplatin causes accumulation of cells in the G2/M cell cycle phase and this effect becomes even more overwhelming after p53 knockout in the HCT-P cell line (Figure 36 B). Meanwhile, oxaliplatin has only a minor effect on cell cycle distribution of oxaliplatin-resistant cells independently of p53 status. On the other hand, HCT-P cells in the S phase are almost completely abolished after oxaliplatin treatment and this outcome is determined by the wild-type p53 activation as HCT-P-p53$^{-/-}$ do not exhibit this effect. These findings further support the previous observation that two platinum-based compounds, oxaliplatin, and cisplatin, exert their cytotoxicity differently in HCT116 colorectal cancer cell line with wild-type p53 protein.

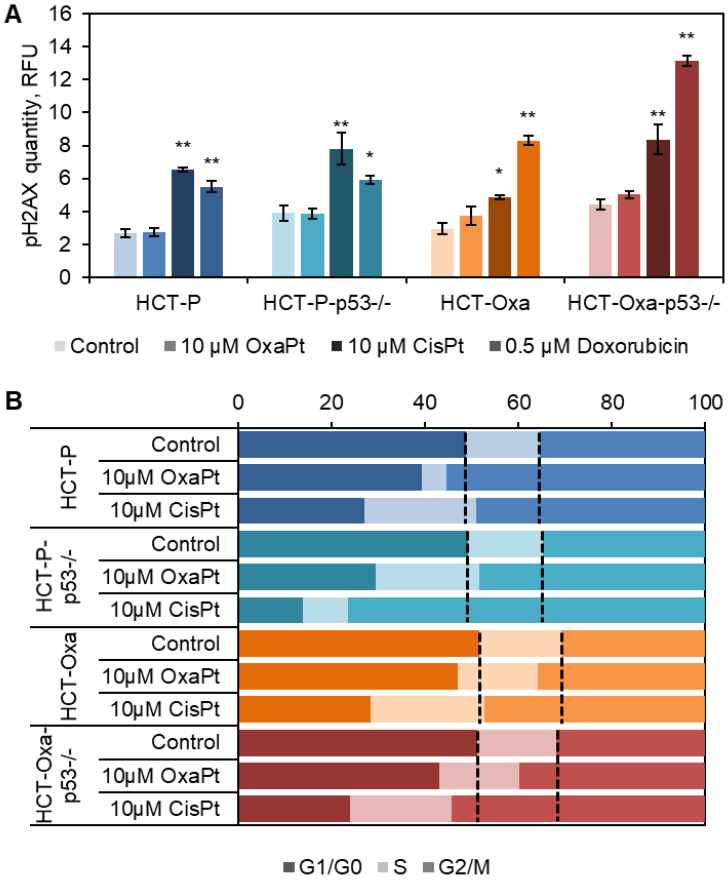

Figure 36. Oxaliplatin treatment does not evoke conventional DNA damage response mechanisms and maintains its cytotoxic effect differently than cisplatin. **A.** Assessment of DNA damage response by phosphorylated H2AX staining after 10 μM oxaliplatin, 10 μM cisplatin or 0.5 μM doxorubicin treatment. Bars are ± SD, significant differences are marked by asterisks: * $p < 0.05$, ** $p < 0.01$, ANOVA, n = 3. **B.** Cell cycle evaluation after 10 μM oxaliplatin or 10 μM cisplatin treatment in p53-positive and p53-negative cell lines.

3.4.2.5. Elucidation of unconventional cytotoxicity mechanism of oxaliplatin

Alternative cytotoxicity mechanisms usually arise due to differential signaling pathways activation in various cell lines. It is already shown that cisplatin and oxaliplatin can activate different cell cycle-associated genes dependent on treatment settings [140]. Moreover, the activation of the p53-p21 pathway is believed to be a major determinant of sensitivity to oxaliplatin [141]. However, the exact mechanism of how p53 is involved in cell response to oxaliplatin in the absence of conventional DNA damage-

induced signals remains unclear. Furthermore, our previous findings revealed that the majority of oxaliplatin-sensitive cells undergo caspase-3 activation-independent cell death. In light of this data, we decided to check which type of cell death is more prevalent in the parental cell line after oxaliplatin treatment using inhibitors specific to various cell death-associated pathways. Executive caspase-3/7 inhibitor was used to inhibit intrinsic apoptosis, caspase-8 plays an important role in the extrinsic apoptosis pathway, the caspase-1 inhibitor was used to rule out pyroptosis and necrostatin-1 was used to inhibit necroptosis. The results of cell death assay showed that only pan-caspase, caspase-3/7, and caspase-8 inhibition were effective against oxaliplatin-caused cytotoxicity (Figure 37 A). Even though caspase-3/7 inhibition is quite effective against oxaliplatin-induced cell death, a substantial amount of cells dies in a caspase-3/7-independent manner. Furthermore, activation of the extrinsic apoptosis pathway via caspase-8 is also crucial for the cytotoxic effect of oxaliplatin.

Activation of extrinsic apoptosis pathway can cause cell death in several different ways: (I) caspase-8 can directly activate executor caspases, (II) caspase-8 can cause mitochondrial outer membrane permeabilization (MOMP) and formation of apoptosome with subsequent caspase-3 activation or (III) caspase-8 can cause MOMP and caspase-independent cell death [142]. As most of these pathways cause MOMP, we decided to check how BH3 mimetic will affect the oxaliplatin-sensitive cells. BH3 mimetic is a compound inhibiting Bcl-2 protein which protects cells from permeabilization of mitochondrial membrane [130]. Indeed, BH3 mimetic sensitized HCT-P cells to oxaliplatin treatment showing that MOMP is an inevitable and important process for oxaliplatin-induced cytotoxicity (Figure 37 A).

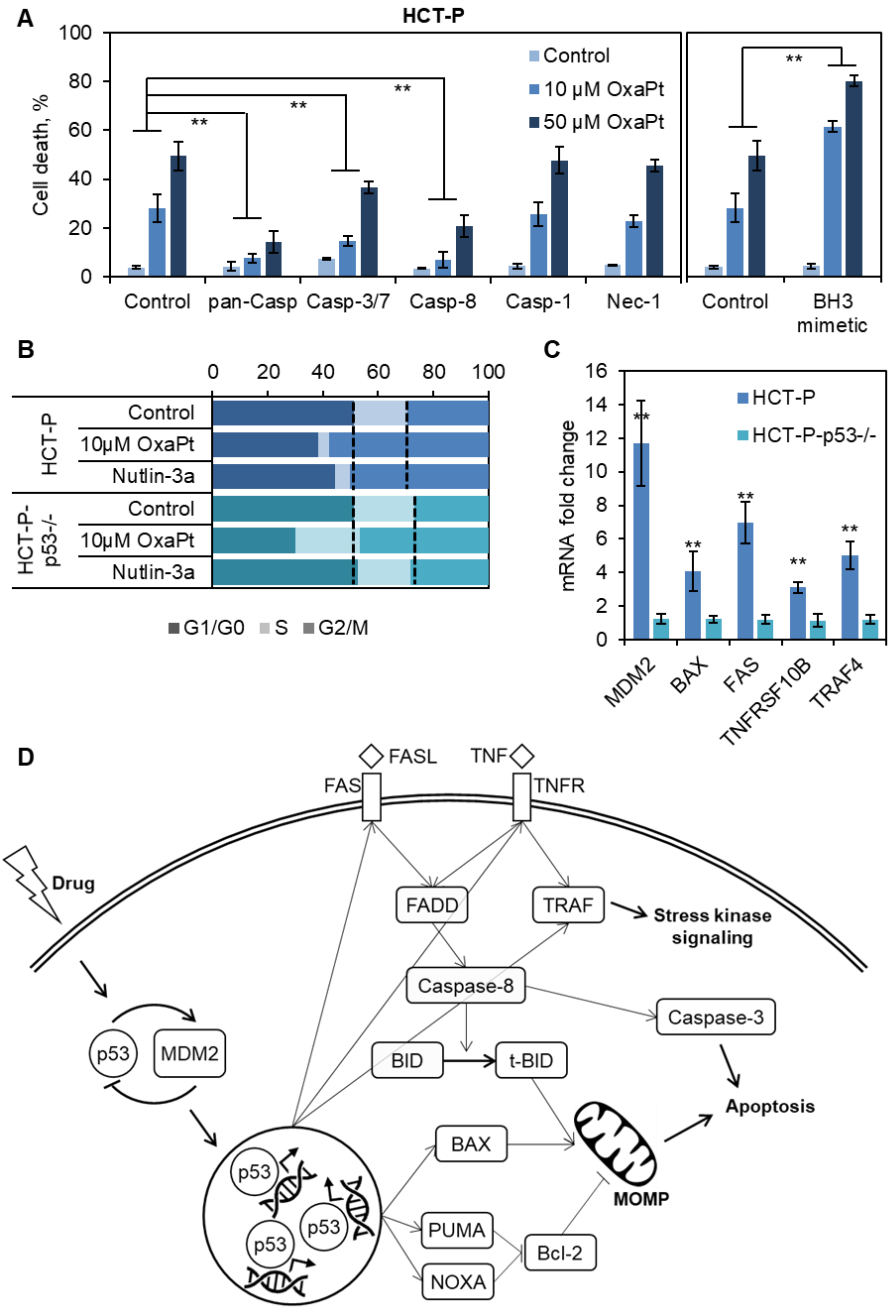

Figure 37. Oxaliplatin exerts its cytotoxic effect by activating the extrinsic apoptosis pathway via p53 transcriptional targets. **A.** Cell death analysis by propidium iodide staining assay after 10 µM or 50 µM treatment with oxaliplatin for 48h. Cells were pre-treated with inhibitors targeting various types of cell death for 1 h before drug treatment. Bars are ± SD, significant differences are marked by asterisks: * $p < 0.05$, ** $p < 0.01$, ANOVA, n = 3. **B.** Cell cycle evaluation after 10 µM oxaliplatin or p53-MDM2 interaction inhibitor Nutlin-3a

of parental and p53 knockout cell lines. **C.** Change of expression of p53 transcriptional targets measured by RT-qPCR in HCT-P and HCT-P-p53$^{-/-}$ cells after 10 μM oxaliplatin treatment for 24 h. Bars are ± SD, significant differences are marked by asterisks: * $p < 0.05$, ** $p < 0.01$, ANOVA, n = 3. **D.** Schematic representation of probable p53 involvement in the activation of extrinsic apoptosis pathway activation.

The next step was to examine what role p53 plays in oxaliplatin-mediated signaling pathways leading to cell death. First, we examined if cell cycle changes after oxaliplatin treatment are p53 activation-dependent. Nutlin-3a was used to artificially increase p53 quantity in cells by inhibiting MDM2 and p53 interaction and, thus, preventing p53 from degradation. Cell cycle changes of the parental cell line after Nutlin-3a treatment closely resembled cell cycle changes after oxaliplatin treatment (Figure 37 B). On the other hand, p53-deficient cells accumulated in the G2/M cell cycle phase after oxaliplatin treatment but treatment with Nutlin-3a didn't have any effect on cell cycle distribution. Second, we investigated the increase of p53-regulated genes involved in apoptosis induction after oxaliplatin treatment in parental and p53 knockout cell lines. The results showed an increase in both intrinsic cell apoptosis regulating proteins, such as BAX, and extrinsic apoptosis regulating proteins, such as FAS receptor, death receptor 5 (encoded by *TNFRSF10B* gene) and TNF receptor-associated factor 4 (encoded by *TRAF4* gene) (Figure 37 C).

As extrinsic apoptosis pathway-associated proteins are involved in the activation of stress kinase signaling pathways, we decided to check for kinases involved in the stress-activated MAPK pathway. For this purpose, we performed multiplexed kinase inhibitor bead (MIB) analysis to examine differences in active kinases in parental and oxaliplatin-resistant cells. Kinases were isolated from cell lysates using MIB enrichment, which captures a broad range of active protein kinases by five different inhibitors covalently coupled to beads [64].

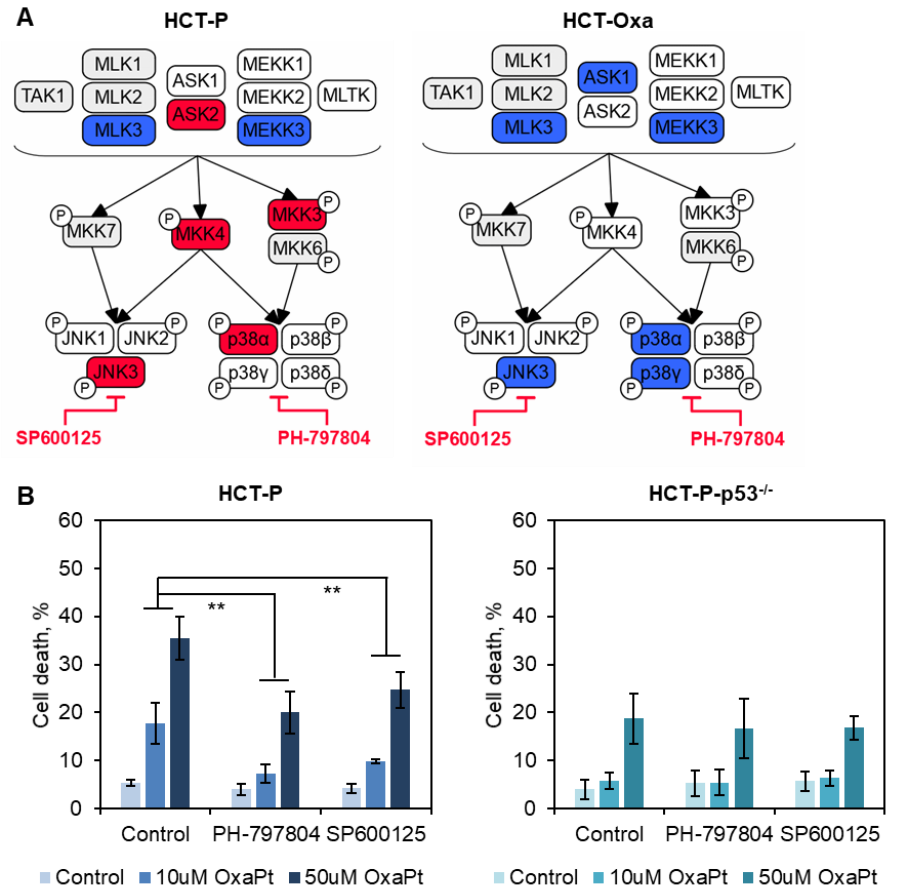

Figure 38. Stress-activated MAPK pathway activation plays an important role in the oxaliplatin-induced cytotoxicity. **A.** Stress-activated MAPK pathways were analyzed in the MIB dataset comparing cells that were untreated or treated with 10 μM oxaliplatin for 24h. Red node color indicates increased activity of MIB dataset kinases, blue – decreased. Nodes without color indicate proteins that belong to the pathway but their quantity did not change in the MIB dataset and grey nodes were not identified. Inhibitors used to inhibit these pathways are designated in red. **B.** Cell death analysis by propidium iodide staining assay after 10 μM or 50 μM treatment with oxaliplatin for 48h. Cells were pre-treated with inhibitors targeting stress-activated MAPK pathways for 1 h before drug treatment. Bars are ± SD, significant differences are marked by asterisks: * $p < 0.05$, ** $p < 0.01$, ANOVA, n = 3.

Stress-activated MAPK were chosen for analysis due to an important role in the regulation of apoptosis, cell cycle arrest, growth inhibition, differentiation, and, most importantly, in the differential response to chemotherapy drugs that could involve unconventional cell death mechanisms [143]. The analysis of the MIB dataset revealed an increase in active kinases involved in JNK and p38 stress kinase pathways in the parental but not oxaliplatin-resistant cell line (Figure 38 A). Moreover,

inhibition of both JNK and p38 pathways with specific inhibitors resulted in increased resistance of HCT-P cells to oxaliplatin treatment (Figure 38 B). Interestingly, this effect was revoked by p53 knockout suggesting the interplay between stress-activated MAPK and p53 pathways.

Altogether, these results suggest that activation of extrinsic apoptosis and stress-activated MAPKs, JNK and p38, pathways can be crucial for oxaliplatin cytotoxicity in the HCT116 cell line. Moreover, wild-type p53 activation in this cell line seems to play a major role in oxaliplatin-induced extrinsic apoptosis pathway (Figure 37 D) as well as stress kinase activation.

FINAL REMARKS

The purpose of this thesis was to show possible applications of differential global proteomic, kinomic and phosphoproteomic analysis as well as confocal microscopy for the elucidation of cancer cell resistance mechanisms. Cancer cell resistance is a diverse process and can vary in every case observed, therefore, individualization of cancer patient's treatment is inevitable. Proteomic and microscopy approaches can be useful for the identification of various predictive markers that could ease the selection of more effective therapy or foreseeing the possible resistance mechanisms and, thus, suggest the complex therapy to avoid its development.

In this research, we investigated two different cancer tumor types and different types of drugs. In the first case, we tried to predict the resistance mechanism of TNBC cell line MDA-MB-231 to RH1 drug which together with its analogs is in clinical trials. RH1 is converted to its active form in tumor cells by specific reductases which are elevated in cancerous cells. In MDA-MB-231 cells the activity levels of these reductases are undetectable, moreover, the RH1-resistant cell line doesn't show any increase in the oxidation-reduction potential even though it is the most common mechanism of resistance to this type of drugs. However, MDA-MB-231 cells are still sensitive to the drug and develop resistance to it after prolonged treatment.

With all this data in mind, we tried to elucidate the resistance mechanism of the MDA-MB-231 cell line using a combination of kinomic and phosphoproteomic analyses. The data showed changes in cell cycle-related processes, the JNK signaling pathway, and activation of the c-KIT-AKT-mTOR axis. These findings were validated by other methods and as cell cycle changes are inevitable in the resistance development and importance of JNK pathway activation was already shown, we concentrated on the significance of the c-KIT-AKT-mTOR axis. Further analysis revealed that the RH1-resistant cell line is enriched with cancer stem cells which are more aggressive, invasive and often associated with resistance and cancer renewal. Our data suggest that inhibition of the c-KIT receptor along with RH1 can prevent the enrichment of the CSC population and, therefore, diminish the chances of TNBC cell resistance to RH1 treatment.

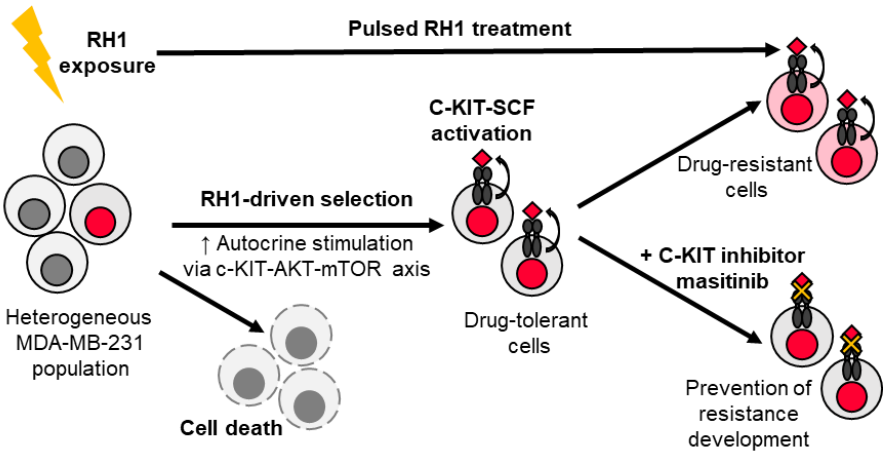

Figure 39. Schematic representation of mechanism of MDA-MB-231 acquired resistance to RH1.

In the second case, we used already widely used chemotherapy drugs, 5-fluorouracil and oxaliplatin, and colorectal carcinoma cell line HCT116. The resistant cells were developed by continuous treatment with the drug and complex high-throughput differential proteomic and miRNomic analyses were performed. In the case of the 5-fluorouracil-resistant cell line global proteomic analysis showed changes in proteins involved in 5-fluorouracil metabolism. This data was further supported by the lack of DNA-damage response pathways activation after the treatment of drug-resistant cells. Thus, the potential application of global differential proteomic analysis for the search of already known resistance markers was demonstrated.

The elucidation of oxaliplatin resistance mechanisms was more complex as the exact mechanisms of oxaliplatin-induced cytotoxicity aren't fully understood and can vary in different cell lines. First of all, we combined high-throughput proteomic and miRNomic approached to expose changes in the epithelial-mesenchymal state of these cells. Our data showed changes in EMT-regulating miRNAs and proteins in the resistant cell line. Moreover, experiments with cells deficient in one of the resistance-associated and EMT-linked miRNA miR-23b highlighted the importance of partial EMT phenotype for the CRC cells' resistance to oxaliplatin. Furthermore, increased expression of EMT-inducing transcription factor SNAI2 appears to be important for the resistance development as well as for the maintenance of the intermediate epithelial-mesenchymal state.

Second, proteomic analysis together with sequencing data revealed differential regulation and mutations in one of the major genome stability ensuring protein p53. The changes in the capability of p53 protein to activate

its transcriptional targets as well as the importance of this activation for oxaliplatin-induced cytotoxicity was examined by other methods involving manipulation of p53 quantity using shRNA, inducible vector and CRISPR/Cas9 knockout techniques. This data confirmed the importance of wild-type p53 transcriptional targets activation for the response to oxaliplatin and proved p53 mutations as one of the resistance-assuring factors in the oxaliplatin-resistant cell line. Moreover, the experiments with p53 protein in parental HCT116 cell line uncovered the unconventional mechanism of oxaliplatin cytotoxicity involving activation of extrinsic apoptosis pathways as well as MAPK stress kinases p38 and JNK. All this data with the oxaliplatin-resistant cell line once more emphasized the importance of cancer cell plasticity for resistance development as well as the importance of mutational analysis of tumor suppressor genes and oncogenes before the selection of treatment.

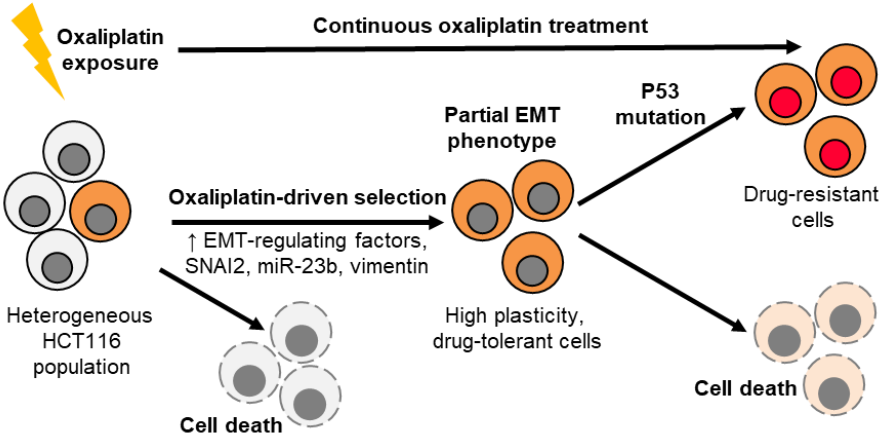

Figure 40. Schematic representation of mechanism of HCT116 acquired resistance to oxaliplatin.

CONCLUSIONS

1.The analysis of RH1-resistant triple-negative breast cancer MDA-MB-231 cell line reveals changes in cell cycle regulation, activation of the JNK signaling pathway and the c-KIT-AKT-mTOR axis as possible mechanisms of resistance.

2. The selection of MDA-MB-231 cells resistant to RH1 causes the enrichment in $CD44^{high}$ population exhibiting stem cell-like properties that can be reverted by the combination treatment with a c-KIT inhibitor.

3. The analysis of the 5-fluorouracil-resistant colorectal carcinoma HCT116 cell line shows changes in nucleotide metabolism genes resulting in diminished DNA damage response.

4. EMT-associated miRNA miR-23b and EMT-inducing transcription factor SNAI2 maintain epithelial-mesenchymal status in HCT116 cells and are involved in the development of resistance to oxaliplatin.

5. Transcriptional target activation by wild-type p53 protein is essential for the cytotoxic effect of oxaliplatin in the HCT116 cell line.

PUBLICATIONS AND SCIENTIFIC PARTICIPATION

Publications:

Gasiulė, S.; **Dreize, N**.; Kaupinis, A.; Ražanskas, R.; Čiupas, L.; Stankevičius, V.; Kapustina, Ž.; Laurinavičius, A.; Valius, M.; Vilkaitis, G. Molecular Insights into miRNA-Driven Resistance to 5-Fluorouracil and Oxaliplatin Chemotherapy: miR-23b Modulates the Epithelial-Mesenchymal Transition of Colorectal Cancer Cells. J. Clin. Med. 2019, 8, 2115. **Impact Factor: 5.58.**

Kuciauskas, D.; **Dreize, N.**; Ger, M.; Kaupinis, A.; Zemaitis, K.; Stankevicius, V.; Suziedelis, K.; Cicenas, J.; Graves, L.M.; Valius, M. Proteomic Analysis of Breast Cancer Resistance to the Anticancer Drug RH1 Reveals the Importance of Cancer Stem Cells. Cancers 2019, 11, 972. **Impact Factor: 6.16.**

Oral presentations:

Dreize, N.; Kuciauskas, D.; Ger, M.; Kaupinis, A.; Zemaitis, K.; Stankevicius, V.; Suziedelis, K.; Cicenas, J.; Graves, L.M.; Valius, M. Proteomic Analysis of Breast Cancer Resistance to the Anticancer Drug RH1 Reveals the Importance of Cancer Stem Cells. 5th International Conference of Lithuanian Association of Stem Cells Researchers, 2019, Vilnius, Lithuania.

Poster presentations:

Iesmantaite, M.; **Dreize, N.**; Valius M. P53 Knockout by CRISPR-Cas9 System in HCT116 Cell Line Highlighted Importance of P53 Activation to Chemotherapy Drug Response. International Conference The COINS 2020, Vilnius, Lithuania.

Iesmantaite, M.; **Dreize, N.**; Valius M. P53 Knockout in HCT116 Cell Line Revealed Clonal Heterogeneity. 4th International Life Sciences Conference “Vita Scientia”, 2020, Vilnius Lithuania.

Urnikytė, S.; **Dreižė, N.**; Valius M. EMT-inducing Transcription Factor SNAI2 Modulates Colorectal Cancer Cell Resistance to Oxaliplatin. 4th

International Life Sciences Conference “Vita Scientia”, 2020, Vilnius Lithuania.

Dreize, N.; Kaupinis, A.; Ger, M.; Cicenas, J.; Laurinavicius, A.; Valius M. Proteomic Analysis of Colorectal Cancer Cell Resistance to 5-Fluorouracil and Oxaliplatin Reveals New Mechanisms, Prognostics Markers, and Options for Novel Second Line Therapy. 2018 NCRI Cancer Conference, Glasgow, UK.

Dreize, N.; Kaupinis, A.; Ger, M.; Cicenas, J.; Laurinavicius, A.; Valius M. Proteomic Analysis of Colorectal Cancer Cell Resistance to 5-Fluorouracil and Oxaliplatin Reveals New Mechanisms, Prognostics Markers, and Options for Novel Second Line Therapy. Life Sciences Baltics 2018, Vilnius, Lithuania.

Dreize, N.; Kuciauskas, D.; Ger, M.; Kaupinis, A.; Zemaitis, K.; Stankevicius, V.; Suziedelis, K.; Cicenas, J.; Graves, L.M.; Valius, M. Proteomic Analysis of Breast Cancer Resistance to the Anticancer Drug RH1 Reveals the Importance of Cancer Stem Cells. International Conference The COINS 2018, Vilnius, Lithuania.

Butkytė, S.; **Dreižė, N.;** Čiupas, L.; Maželis, I.; Kukcinavičiūtė, E.; Valius, M.; Vilkaitis, G. MiRNA-mediated Chemoresistance to 5-Fluorouracil and Oxaliplatin in Colorectal Cells. EMBO/EMBL Symposium “Non-coding genome”, 2017, Germany.

Butkytė, S.; **Šumilova, N.**; Ger, M.; Ražanskas, R.; Čiupas, L.; Jonušienė, V.; Valius, M.; Vilkaitis, G. MiRNA-mediated Chemoresistance to 5-Fluorouracil and Oxaliplatin in 3D Colorectal Cell Culture. EMBO/EMBL Symposium “Organoids, Modelling Organ Development and Disease in 3D Culture”, 2016, Germany.

REFERENCES

[1] C. Holohan, S. Van Schaeybroeck, D. B. Longley, and P. G. Johnston, "Cancer drug resistance: an evolving paradigm," *Nat. Rev. Cancer*, vol. 13, no. 10, pp. 714–726, Oct. 2013.

[2] M. Dean, T. Fojo, and S. Bates, "Tumour stem cells and drug resistance," *Nat. Rev. Cancer*, vol. 5, no. 4, pp. 275–284, Apr. 2005.

[3] P. Dalerba, R. W. Cho, and M. F. Clarke, "Cancer Stem Cells: Models and Concepts," *Annu. Rev. Med.*, vol. 58, no. 1, pp. 267–284, Feb. 2007.

[4] L. T. H. Phi *et al.*, "Cancer Stem Cells (CSCs) in Drug Resistance and their Therapeutic Implications in Cancer Treatment," *Stem Cells Int.*, vol. 2018, pp. 1–16, 2018.

[5] B. Beck and C. Blanpain, "Unravelling cancer stem cell potential," *Nat. Rev. Cancer*, vol. 13, no. 10, pp. 727–738, Oct. 2013.

[6] B. P. Sorrentino, "Gene therapy to protect haematopoietic cells from cytotoxic cancer drugs," *Nat. Rev. Cancer*, vol. 2, no. 6, pp. 431–441, Jun. 2002.

[7] L. Kelland, "The resurgence of platinum-based cancer chemotherapy," *Nat. Rev. Cancer*, vol. 7, no. 8, pp. 573–584, Aug. 2007.

[8] D. B. Longley, D. P. Harkin, and P. G. Johnston, "5-Fluorouracil: mechanisms of action and clinical strategies," *Nat. Rev. Cancer*, vol. 3, no. 5, pp. 330–338, May 2003.

[9] C. Gorrini, I. S. Harris, and T. W. Mak, "Modulation of oxidative stress as an anticancer strategy," *Nat. Rev. Drug Discov.*, vol. 12, no. 12, pp. 931–947, Dec. 2013.

[10] H. Zahreddine and K. L. B. Borden, "Mechanisms and insights into drug resistance in cancer," *Front. Pharmacol.*, vol. 4, p. 28, Mar. 2013.

[11] P. Bouwman and J. Jonkers, "The effects of deregulated DNA damage signalling on cancer chemotherapy response and resistance," *Nat. Rev. Cancer*, vol. 12, no. 9, pp. 587–598, Sep. 2012.

[12] M. A. Shah and G. K. Schwartz, "Cell cycle-mediated drug resistance: an emerging concept in cancer therapy.," *Clin. cancer Res.*, vol. 7, no. 8, pp. 2168–81, Aug. 2001.

[13] G. Deep and R. Agarwal, "New Combination Therapies with Cell Cycle Agents," *Curr. Opin. Investig. drugs*, vol. 9, no. 6, p. 591, 2008.

[14] K. T. Bieging, S. S. Mello, and L. D. Attardi, "Unravelling mechanisms of p53-mediated tumour suppression," *Nat. Rev. Cancer*, vol. 14, no. 5, pp. 359–370, May 2014.

[15] V. J. N. Bykov, S. E. Eriksson, J. Bianchi, and K. G. Wiman, "Targeting mutant p53 for efficient cancer therapy," *Nat. Rev.*

Cancer, vol. 18, no. 2, pp. 89–102, Feb. 2018.
[16] E. R. Kastenhuber and S. W. Lowe, "Putting p53 in Context," *Cell*, vol. 170, no. 6, pp. 1062–1078, Sep. 2017.
[17] P. A. J. Muller and K. H. Vousden, "p53 mutations in cancer," *Nat. Cell Biol.*, vol. 15, no. 1, pp. 2–8, Jan. 2013.
[18] M. Oren and V. Rotter, "Mutant p53 Gain-of-Function in Cancer," *Cold Spring Harb. Perspect. Biol.*, vol. 2, no. 2, Feb. 2010.
[19] M. P. Kim and G. Lozano, "Mutant p53 partners in crime," *Cell Death Differ.*, vol. 25, no. 1, pp. 161–168, Jan. 2018.
[20] K. H. Vousden and C. Prives, "Blinded by the Light: The Growing Complexity of p53," *Cell*, vol. 137, no. 3, pp. 413–431, May 2009.
[21] A. L. Paek, J. C. Liu, A. Loewer, W. C. Forrester, and G. Lahav, "Cell-to-Cell Variation in p53 Dynamics Leads to Fractional Killing," *Cell*, vol. 165, no. 3, pp. 631–642, Apr. 2016.
[22] E. Batchelor, A. Loewer, and G. Lahav, "The ups and downs of p53: understanding protein dynamics in single cells," *Nat. Rev. Cancer*, vol. 9, no. 5, pp. 371–377, May 2009.
[23] C. J. Lord and A. Ashworth, "The DNA damage response and cancer therapy," *Nature*, vol. 481, no. 7381, pp. 287–294, Jan. 2012.
[24] W. G. Kaelin, "The Concept of Synthetic Lethality in the Context of Anticancer Therapy," *Nat. Rev. Cancer*, vol. 5, no. 9, pp. 689–698, Sep. 2005.
[25] A. Sonnenblick, E. de Azambuja, H. A. Azim, and M. Piccart, "An update on PARP inhibitors—moving to the adjuvant setting," *Nat. Rev. Clin. Oncol.*, vol. 12, no. 1, pp. 27–41, Jan. 2015.
[26] A. Gschwind, O. M. Fischer, and A. Ullrich, "The discovery of receptor tyrosine kinases: targets for cancer therapy," *Nat. Rev. Cancer*, vol. 4, no. 5, pp. 361–370, May 2004.
[27] M. J. Lee *et al.*, "Sequential Application of Anticancer Drugs Enhances Cell Death by Rewiring Apoptotic Signaling Networks," *Cell*, vol. 149, no. 4, pp. 780–794, May 2012.
[28] J. B. Casaletto and A. I. McClatchey, "Spatial regulation of receptor tyrosine kinases in development and cancer," *Nat. Rev. Cancer*, vol. 12, no. 6, pp. 387–400, Jun. 2012.
[29] F. de Sousa e Melo and L. Vermeulen, "Wnt Signaling in Cancer Stem Cell Biology," *Cancers (Basel).*, vol. 8, no. 7, p. 60, Jun. 2016.
[30] J. Lennartsson and L. Rönnstrand, "Stem Cell Factor Receptor/c-Kit: From Basic Science to Clinical Implications," *Physiol. Rev.*, vol. 92, no. 4, pp. 1619–1649, Oct. 2012.
[31] B. Foster, D. Zaidi, T. Young, M. Mobley, and B. Kerr, "CD117/c-kit in Cancer Stem Cell-Mediated Progression and Therapeutic Resistance," *Biomedicines*, vol. 6, no. 1, p. 31, Mar. 2018.
[32] J. A. Engelman *et al.*, "MET Amplification Leads to Gefitinib Resistance in Lung Cancer by Activating ERBB3 Signaling," *Science (80-.).*, vol. 316, no. 5827, pp. 1039–1043, May 2007.

[33] J. A. Engelman, “Targeting PI3K signalling in cancer: opportunities, challenges and limitations,” *Nat. Rev. Cancer*, vol. 9, no. 8, pp. 550–562, Aug. 2009.
[34] F. Janku, T. A. Yap, and F. Meric-Bernstam, “Targeting the PI3K pathway in cancer: are we making headway?,” *Nat. Rev. Clin. Oncol.*, vol. 15, no. 5, pp. 273–291, May 2018.
[35] K. E. O’Reilly *et al.*, “mTOR Inhibition Induces Upstream Receptor Tyrosine Kinase Signaling and Activates Akt,” *Cancer Res.*, vol. 66, no. 3, pp. 1500–1508, Feb. 2006.
[36] E. F. Wagner and Á. R. Nebreda, “Signal integration by JNK and p38 MAPK pathways in cancer development,” *Nat. Rev. Cancer*, vol. 9, no. 8, pp. 537–549, Aug. 2009.
[37] D. N. Dhanasekaran and E. P. Reddy, “JNK signaling in apoptosis,” *Oncogene*, vol. 27, no. 48, pp. 6245–6251, Oct. 2008.
[38] A. Cuenda and S. Rousseau, “p38 MAP-Kinases pathway regulation, function and role in human diseases,” *Biochim. Biophys. Acta - Mol. Cell Res.*, vol. 1773, no. 8, pp. 1358–1375, Aug. 2007.
[39] S. Fulda, “Tumor resistance to apoptosis,” *Int. J. Cancer*, vol. 124, no. 3, pp. 511–515, Feb. 2009.
[40] I. Dagogo-Jack and A. T. Shaw, “Tumour heterogeneity and resistance to cancer therapies,” *Nat. Rev. Clin. Oncol.*, vol. 15, no. 2, pp. 81–94, Feb. 2018.
[41] S. Boumahdi and F. J. de Sauvage, “The great escape: tumour cell plasticity in resistance to targeted therapy,” *Nat. Rev. Drug Discov.*, vol. 19, no. 1, pp. 39–56, Jan. 2020.
[42] N. McGranahan and C. Swanton, “Biological and Therapeutic Impact of Intratumor Heterogeneity in Cancer Evolution,” *Cancer Cell*, vol. 27, no. 1, pp. 15–26, Jan. 2015.
[43] S. Negrini, V. G. Gorgoulis, and T. D. Halazonetis, “Genomic instability — an evolving hallmark of cancer,” *Nat. Rev. Mol. Cell Biol.*, vol. 11, no. 3, pp. 220–228, Mar. 2010.
[44] R. Brown, E. Curry, L. Magnani, C. S. Wilhelm-Benartzi, and J. Borley, “Poised epigenetic states and acquired drug resistance in cancer,” *Nat. Rev. Cancer*, vol. 14, no. 11, pp. 747–753, Nov. 2014.
[45] J. E. Ohm *et al.*, “A stem cell–like chromatin pattern may predispose tumor suppressor genes to DNA hypermethylation and heritable silencing,” *Nat. Genet.*, vol. 39, no. 2, pp. 237–242, Feb. 2007.
[46] S. V. Sharma *et al.*, “A Chromatin-Mediated Reversible Drug-Tolerant State in Cancer Cell Subpopulations,” *Cell*, vol. 141, no. 1, pp. 69–80, Apr. 2010.
[47] A. Dongre and R. A. Weinberg, “New insights into the mechanisms of epithelial–mesenchymal transition and implications for cancer,” *Nat. Rev. Mol. Cell Biol.*, vol. 20, no. 2, pp. 69–84, Feb. 2019.
[48] T. Shibue and R. A. Weinberg, “EMT, CSCs, and drug resistance: the mechanistic link and clinical implications,” *Nat. Rev. Clin. Oncol.*,

vol. 14, no. 10, pp. 611–629, Oct. 2017.
[49] X. Ye and R. A. Weinberg, “Epithelial–Mesenchymal Plasticity: A Central Regulator of Cancer Progression,” *Trends Cell Biol.*, vol. 25, no. 11, pp. 675–686, Nov. 2015.
[50] J. van Staalduinen, D. Baker, P. ten Dijke, and H. van Dam, “Epithelial–mesenchymal-transition-inducing transcription factors: new targets for tackling chemoresistance in cancer?,” *Oncogene*, vol. 37, no. 48, pp. 6195–6211, Nov. 2018.
[51] S. J. Danson *et al.*, “Phase I pharmacokinetic and pharmacodynamic study of the bioreductive drug RH1,” *Ann. Oncol.*, vol. 22, no. 7, pp. 1653–1660, Jul. 2011.
[52] S. Sharif, M. J. O’Connell, G. Yothers, S. Lopa, and N. Wolmark, “FOLFOX and FLOX Regimens for the Adjuvant Treatment of Resected Stage II and III Colon Cancer,” *Cancer Invest.*, vol. 26, no. 9, pp. 956–963, Jan. 2008.
[53] K. J. Livak and T. D. Schmittgen, “Analysis of Relative Gene Expression Data Using Real-Time Quantitative PCR and the 2−ΔΔCT Method,” *Methods*, vol. 25, no. 4, pp. 402–408, Dec. 2001.
[54] J. R. Wiśniewski, A. Zougman, N. Nagaraj, and M. Mann, “Universal sample preparation method for proteome analysis,” *Nat. Methods*, vol. 6, no. 5, pp. 359–362, May 2009.
[55] P. Shannon, “Cytoscape: A Software Environment for Integrated Models of Biomolecular Interaction Networks,” *Genome Res.*, vol. 13, no. 11, pp. 2498–2504, Nov. 2003.
[56] G. Bindea *et al.*, “ClueGO: a Cytoscape plug-in to decipher functionally grouped gene ontology and pathway annotation networks,” *Bioinformatics*, vol. 25, no. 8, pp. 1091–1093, Apr. 2009.
[57] G. Bindea, J. Galon, and B. Mlecnik, “CluePedia Cytoscape plugin: pathway insights using integrated experimental and in silico data,” *Bioinformatics*, vol. 29, no. 5, pp. 661–663, Mar. 2013.
[58] R. L. Siegel, K. D. Miller, and A. Jemal, “Cancer statistics, 2019,” *CA. Cancer J. Clin.*, vol. 69, no. 1, pp. 7–34, Jan. 2019.
[59] R. Dent *et al.*, “Triple-Negative Breast Cancer: Clinical Features and Patterns of Recurrence,” *Clin. Cancer Res.*, vol. 13, no. 15, pp. 4429–4434, Aug. 2007.
[60] C. Yan, J. K. Kepa, D. Siegel, I. J. Stratford, and D. Ross, “Dissecting the Role of Multiple Reductases in Bioactivation and Cytotoxicity of the Antitumor Agent 2,5-Diaziridinyl-3-(hydroxymethyl)-6-methyl-1,4-benzoquinone (RH1),” *Mol. Pharmacol.*, vol. 74, no. 6, pp. 1657–1665, Dec. 2008.
[61] G. Tudor *et al.*, “Cytotoxicity of RH1: NAD(P)H:quinone acceptor oxidoreductase (NQO1)-independent oxidative stress and apoptosis induction,” *Anticancer. Drugs*, vol. 16, no. 4, pp. 381–391, Apr. 2005.
[62] L. Lombardi *et al.*, “Adjuvant colon cancer chemotherapy: where we

are and where we'll go," *Cancer Treat. Rev.*, vol. 36, no. SUPPL. 3, pp. S34–S41, Nov. 2010.
[63] T. André *et al.*, "Improved Overall Survival With Oxaliplatin, Fluorouracil, and Leucovorin As Adjuvant Treatment in Stage II or III Colon Cancer in the MOSAIC Trial," *J. Clin. Oncol.*, vol. 27, no. 19, pp. 3109–3116, Jul. 2009.
[64] M. J. Cooper *et al.*, "Application of Multiplexed Kinase Inhibitor Beads to Study Kinome Adaptations in Drug-Resistant Leukemia," *PLoS One*, vol. 8, no. 6, p. e66755, Jun. 2013.
[65] P. V Hornbeck, B. Zhang, B. Murray, J. M. Kornhauser, V. Latham, and E. Skrzypek, "PhosphoSitePlus, 2014: mutations, PTMs and recalibrations," *Nucleic Acids Res.*, vol. 43, no. D1, pp. D512–D520, Jan. 2015.
[66] D. D. Sarbassov, S. M. Ali, and D. M. Sabatini, "Growing roles for the mTOR pathway," *Curr. Opin. Cell Biol.*, vol. 17, no. 6, pp. 596–603, Dec. 2005.
[67] G. L. Johnson and K. Nakamura, "The c-jun kinase/stress-activated pathway: Regulation, function and role in human disease," *Biochim. Biophys. Acta - Mol. Cell Res.*, vol. 1773, no. 8, pp. 1341–1348, Aug. 2007.
[68] D. E. Levy and J. E. Darnell, "STATs: transcriptional control and biological impact," *Nat. Rev. Mol. Cell Biol.*, vol. 3, no. 9, pp. 651–662, Sep. 2002.
[69] J. Liu and A. Lin, "Role of JNK activation in apoptosis: A double-edged sword," *Cell Res.*, vol. 15, no. 1, pp. 36–42, Jan. 2005.
[70] M.-T. Park *et al.*, "The anti-tumour compound, RH1, causes mitochondria-mediated apoptosis by activating c-Jun N-terminal kinase," *Br. J. Pharmacol.*, vol. 163, no. 3, pp. 567–585, Jun. 2011.
[71] D. C. Fingar, C. J. Richardson, A. R. Tee, L. Cheatham, C. Tsou, and J. Blenis, "mTOR Controls Cell Cycle Progression through Its Cell Growth Effectors S6K1 and 4E-BP1/Eukaryotic Translation Initiation Factor 4E," *Mol. Cell. Biol.*, vol. 24, no. 1, pp. 200–216, Jan. 2004.
[72] M. Deng *et al.*, "Identification and Functional Analysis of a Novel Cyclin E/Cdk2 Substrate Ankrd17," *J. Biol. Chem.*, vol. 284, no. 12, pp. 7875–7888, Mar. 2009.
[73] J. Zhou *et al.*, "Activation of the PTEN/mTOR/STAT3 pathway in breast cancer stem-like cells is required for viability and maintenance," *Proc. Natl. Acad. Sci.*, vol. 104, no. 41, pp. 16158–16163, Oct. 2007.
[74] K. Bačević, G. Lossaint, T. N. Achour, V. Georget, D. Fisher, and V. Dulić, "Cdk2 strengthens the intra-S checkpoint and counteracts cell cycle exit induced by DNA damage," *Sci. Rep.*, vol. 7, no. 1, p. 13429, Dec. 2017.
[75] D. Fang *et al.*, "Phosphorylation of β-Catenin by AKT Promotes β-Catenin Transcriptional Activity," *J. Biol. Chem.*, vol. 282, no. 15,

pp. 11221–11229, Apr. 2007.
[76] T. Valenta, G. Hausmann, and K. Basler, “The many faces and functions of β-catenin,” *EMBO J.*, vol. 31, no. 12, pp. 2714–2736, Jun. 2012.
[77] Y. Huang *et al.*, “IRS-1 regulates proliferation, invasion and metastasis of pancreatic cancer cells through MAPK and PI3K signaling pathways,” 2018.
[78] C. G. Concannon, A. M. Gorman, and A. Samali, “On the role of Hsp27 in regulating apoptosis,” *Apoptosis*, vol. 8, no. 1, pp. 61–70, 2003.
[79] A. Sawicka and C. Seiser, “Histone H3 phosphorylation – A versatile chromatin modification for different occasions,” *Biochimie*, vol. 94, no. 11, pp. 2193–2201, Nov. 2012.
[80] S. Maddika, S. R. Ande, E. Wiechec, L. L. Hansen, S. Wesselborg, and M. Los, “Akt-mediated phosphorylation of CDK2 regulates its dual role in cell cycle progression and apoptosis,” *J. Cell Sci.*, vol. 121, no. 7, pp. 979–988, Apr. 2008.
[81] C. Giacinti and A. Giordano, “RB and cell cycle progression,” *Oncogene*, vol. 25, no. 38, pp. 5220–5227, Aug. 2006.
[82] J. R. Biggs, L. F. Peterson, Y. Zhang, A. S. Kraft, and D.-E. Zhang, “AML1/RUNX1 Phosphorylation by Cyclin-Dependent Kinases Regulates the Degradation of AML1/RUNX1 by the Anaphase-Promoting Complex,” *Mol. Cell. Biol.*, vol. 26, no. 20, pp. 7420–7429, Oct. 2006.
[83] A. Marais, Z. Ji, E. S. Child, E. Krause, D. J. Mann, and A. D. Sharrocks, “Cell Cycle-dependent Regulation of the Forkhead Transcription Factor FOXK2 by CDK·Cyclin Complexes,” *J. Biol. Chem.*, vol. 285, no. 46, pp. 35728–35739, Nov. 2010.
[84] M. Qiao, P. Shapiro, M. Fosbrink, H. Rus, R. Kumar, and A. Passaniti, “Cell Cycle-dependent Phosphorylation of the RUNX2 Transcription Factor by cdc2 Regulates Endothelial Cell Proliferation,” *J. Biol. Chem.*, vol. 281, no. 11, pp. 7118–7128, Mar. 2006.
[85] J. S. Myers, R. Zhao, X. Xu, A.-J. L. Ham, and D. Cortez, “Cyclin-Dependent Kinase 2–Dependent Phosphorylation of ATRIP Regulates the G 2 -M Checkpoint Response to DNA Damage,” *Cancer Res.*, vol. 67, no. 14, pp. 6685–6690, Jul. 2007.
[86] A. Kreso and J. E. Dick, “Evolution of the Cancer Stem Cell Model,” *Cell Stem Cell*, vol. 14, no. 3, pp. 275–291, Mar. 2014.
[87] M. Al-Hajj, M. S. Wicha, A. Benito-Hernandez, S. J. Morrison, and M. F. Clarke, “Prospective identification of tumorigenic breast cancer cells,” *Proc. Natl. Acad. Sci.*, vol. 100, no. 7, pp. 3983–3988, Apr. 2003.
[88] E. Olsson *et al.*, “CD44 isoforms are heterogeneously expressed in breast cancer and correlate with tumor subtypes and cancer stem cell

markers," *BMC Cancer*, vol. 11, no. 1, p. 418, Dec. 2011.
[89] J. H. Lin and M. Yamazaki, "Role of P-Glycoprotein in Pharmacokinetics," *Clin. Pharmacokinet.*, vol. 42, no. 1, pp. 59–98, Oct. 2003.
[90] F. Russel, J. Koenderink, and R. Masereeuw, "Multidrug resistance protein 4 (MRP4/ABCC4): a versatile efflux transporter for drugs and signalling molecules," *Trends Pharmacol. Sci.*, vol. 29, no. 4, pp. 200–207, Apr. 2008.
[91] D. Ponti *et al.*, "Isolation and In vitro Propagation of Tumorigenic Breast Cancer Cells with Stem/Progenitor Cell Properties," *Cancer Res.*, vol. 65, no. 13, pp. 5506–5511, Jul. 2005.
[92] J. Loughery, M. Cox, L. M. Smith, and D. W. Meek, "Critical role for p53-serine 15 phosphorylation in stimulating transactivation at p53-responsive promoters," *Nucleic Acids Res.*, vol. 42, no. 12, pp. 7666–7680, Jul. 2014.
[93] C. Zeng *et al.*, "Evaluation of 5-ethynyl-2′-deoxyuridine staining as a sensitive and reliable method for studying cell proliferation in the adult nervous system," *Brain Res.*, vol. 1319, pp. 21–32, Mar. 2010.
[94] T. Scholzen and J. Gerdes, "The Ki-67 protein: From the known and the unknown," *J. Cell. Physiol.*, vol. 182, no. 3, pp. 311–322, Mar. 2000.
[95] X. Sun, A. Bizhanova, T. D. Matheson, J. Yu, L. J. Zhu, and P. D. Kaufman, "Ki-67 Contributes to Normal Cell Cycle Progression and Inactive X Heterochromatin in p21 Checkpoint-Proficient Human Cells," *Mol. Cell. Biol.*, vol. 37, no. 17, pp. 1–27, Sep. 2017.
[96] X. Yu, Z. Li, J. Yu, M. T. V. Chan, and W. K. K. Wu, "MicroRNAs predict and modulate responses to chemotherapy in colorectal cancer," *Cell Prolif.*, vol. 48, no. 5, pp. 503–510, Oct. 2015.
[97] M. Gabriel *et al.*, "Role of the splicing factor SRSF4 in cisplatin-induced modifications of pre-mRNA splicing and apoptosis," *BMC Cancer*, vol. 15, no. 1, p. 227, Dec. 2015.
[98] C. Urfali-Mamatoglu, H. H. Kazan, and U. Gündüz, "Dual function of programmed cell death 10 (PDCD10) in drug resistance," *Biomed. Pharmacother.*, vol. 101, pp. 129–136, May 2018.
[99] B. Sun, Y. Fang, Z. Li, Z. Chen, and J. Xiang, "Role of cellular cytoskeleton in epithelial-mesenchymal transition process during cancer progression," *Biomed. Reports*, vol. 3, no. 5, pp. 603–610, Sep. 2015.
[100] S. Lamouille, J. Xu, and R. Derynck, "Molecular mechanisms of epithelial–mesenchymal transition," *Nat. Rev. Mol. Cell Biol.*, vol. 15, no. 3, pp. 178–196, Mar. 2014.
[101] J. Shankar and I. R. Nabi, "Actin Cytoskeleton Regulation of Epithelial Mesenchymal Transition in Metastatic Cancer Cells," *PLoS One*, vol. 10, no. 3, p. e0119954, Mar. 2015.
[102] P. Friedl and D. Gilmour, "Collective cell migration in

morphogenesis, regeneration and cancer," *Nat. Rev. Mol. Cell Biol.*, vol. 10, no. 7, pp. 445–457, Jul. 2009.
[103] H. Acloque, M. S. Adams, K. Fishwick, M. Bronner-Fraser, and M. A. Nieto, "Epithelial-mesenchymal transitions: the importance of changing cell state in development and disease," *J. Clin. Invest.*, vol. 119, no. 6, pp. 1438–1449, Jun. 2009.
[104] L. Kerosuo and M. Bronner-Fraser, "What is bad in cancer is good in the embryo: Importance of EMT in neural crest development," *Semin. Cell Dev. Biol.*, vol. 23, no. 3, pp. 320–332, May 2012.
[105] I. M. Shapiro *et al.*, "An EMT–Driven Alternative Splicing Program Occurs in Human Breast Cancer and Modulates Cellular Phenotype," *PLoS Genet.*, vol. 7, no. 8, p. e1002218, Aug. 2011.
[106] C. C. Warzecha and R. P. Carstens, "Complex changes in alternative pre-mRNA splicing play a central role in the epithelial-to-mesenchymal transition (EMT)," *Semin. Cancer Biol.*, vol. 22, no. 5–6, pp. 417–427, Oct. 2012.
[107] A. J. Ridley, "Cell Migration: Integrating Signals from Front to Back," *Science (80-.).*, vol. 302, no. 5651, pp. 1704–1709, Dec. 2003.
[108] D. M. Gonzalez and D. Medici, "Signaling mechanisms of the epithelial-mesenchymal transition," *Sci. Signal.*, vol. 7, no. 344, pp. re8–re8, Sep. 2014.
[109] J. Heuberger and W. Birchmeier, "Interplay of Cadherin-Mediated Cell Adhesion and Canonical Wnt Signaling," *Cold Spring Harb. Perspect. Biol.*, vol. 2, no. 2, pp. a002915–a002915, Feb. 2010.
[110] G. F. Le Bras, K. J. Taubenslag, and C. D. Andl, "The regulation of cell-cell adhesion during epithelial-mesenchymal transition, motility and tumor progression," *Cell Adh. Migr.*, vol. 6, no. 4, pp. 365–373, Jul. 2012.
[111] M. A. Huber *et al.*, "NF-κB is essential for epithelial-mesenchymal transition and metastasis in a model of breast cancer progression," *J. Clin. Invest.*, vol. 114, no. 4, pp. 569–581, Aug. 2004.
[112] J.-P. Hong, X.-M. Li, M.-X. Li, and F.-L. Zheng, "VEGF suppresses epithelial-mesenchymal transition by inhibiting the expression of Smad3 and miR-192, a Smad3-dependent microRNA," *Int. J. Mol. Med.*, vol. 31, no. 6, pp. 1436–1442, Jun. 2013.
[113] M. G. Mendez, S.-I. Kojima, and R. D. Goldman, "Vimentin induces changes in cell shape, motility, and adhesion during the epithelial to mesenchymal transition," *FASEB J.*, vol. 24, no. 6, pp. 1838–1851, Jun. 2010.
[114] K. Vuoriluoto *et al.*, "Vimentin regulates EMT induction by Slug and oncogenic H-Ras and migration by governing Axl expression in breast cancer," *Oncogene*, vol. 30, no. 12, pp. 1436–1448, Mar. 2011.
[115] A. Jeanes, C. J. Gottardi, and A. S. Yap, "Cadherins and cancer: how does cadherin dysfunction promote tumor progression?," *Oncogene*,

vol. 27, no. 55, pp. 6920–6929, Nov. 2008.
[116] V. Sundararajan, M. Tan, T. Z. Tan, J. Ye, J. P. Thiery, and R. Y.-J. Huang, “SNAI1 recruits HDAC1 to suppress SNAI2 transcription during epithelial to mesenchymal transition,” *Sci. Rep.*, vol. 9, no. 1, p. 8295, Dec. 2019.
[117] I. Gourdier *et al.*, “Drug specific resistance to oxaliplatin is associated with apoptosis defect in a cellular model of colon carcinoma,” *FEBS Lett.*, vol. 529, no. 2–3, pp. 232–236, Oct. 2002.
[118] J. Fallica *et al.*, “Macrophage Migration Inhibitory Factor Is a Novel Determinant of Cigarette Smoke–Induced Lung Damage,” *Am. J. Respir. Cell Mol. Biol.*, vol. 51, no. 1, pp. 94–103, Jul. 2014.
[119] W.-R. Park and Y. Nakamura, “p53CSV , a Novel p53-Inducible Gene Involved in the p53-Dependent Cell-Survival Pathway,” *Cancer Res.*, vol. 65, no. 4, pp. 1197–1206, Feb. 2005.
[120] S. E. Brock, B. E. Rendon, D. Xin, K. Yaddanapudi, and R. A. Mitchell, “MIF Family Members Cooperatively Inhibit p53 Expression and Activity,” *PLoS One*, vol. 9, no. 6, p. e99795, Jun. 2014.
[121] M. V. Kuleshov *et al.*, “Enrichr: a comprehensive gene set enrichment analysis web server 2016 update,” *Nucleic Acids Res.*, vol. 44, no. W1, pp. W90–W97, Jul. 2016.
[122] J. Kantelinen *et al.*, “Mismatch repair analysis of inherited MSH2 and/or MSH6 variation pairs found in cancer patients,” *Hum. Mutat.*, vol. 33, no. 8, pp. 1294–1301, Aug. 2012.
[123] O. Cazzalini, A. I. Scovassi, M. Savio, L. A. Stivala, and E. Prosperi, “Multiple roles of the cell cycle inhibitor p21CDKN1A in the DNA damage response,” *Mutat. Res. Mutat. Res.*, vol. 704, no. 1–3, pp. 12–20, Apr. 2010.
[124] L. Liu *et al.*, “CUL4A Abrogation Augments DNA Damage Response and Protection against Skin Carcinogenesis,” *Mol. Cell*, vol. 34, no. 4, pp. 451–460, May 2009.
[125] R. Chhabra, R. Dubey, and N. Saini, “Cooperative and individualistic functions of the microRNAs in the miR-23a~27a~24-2 cluster and its implication in human diseases,” *Mol. Cancer*, vol. 9, no. 1, p. 232, Sep. 2010.
[126] R. Maqbool, S. N. Lone, and M. Ul Hussain, “Post-transcriptional regulation of the tumor suppressor p53 by a novel miR-27a, with implications during hypoxia and tumorigenesis,” *Biochem. J.*, vol. 473, no. 20, pp. 3597–3610, Oct. 2016.
[127] N. Srivastava *et al.*, “miR-24-2 controls H2AFX expression regardless of gene copy number alteration and induces apoptosis by targeting antiapoptotic gene BCL-2: a potential for therapeutic intervention,” *Breast Cancer Res.*, vol. 13, no. 2, p. R39, Apr. 2011.
[128] J. Yu and L. Zhang, “The transcriptional targets of p53 in apoptosis control,” *Biochem. Biophys. Res. Commun.*, vol. 331, no. 3, pp. 851–

858, Jun. 2005.
[129] J. Pawlowski and A. S. Kraft, “Bax-induced apoptotic cell death,” *Proc. Natl. Acad. Sci.*, vol. 97, no. 2, pp. 529–531, Jan. 2000.
[130] P. Bouillet and A. Strasser, “BH3-only proteins - evolutionarily conserved proapoptotic Bcl-2 family members essential for initiating programmed cell death.,” *J. Cell Sci.*, vol. 115, pp. 1567–74, Apr. 2002.
[131] B. Leroy *et al.*, “The TP53 website: an integrative resource centre for the TP53 mutation database and TP53 mutant analysis,” *Nucleic Acids Res.*, vol. 41, no. D1, pp. D962–D969, Jan. 2013.
[132] R. L. Weinberg, D. B. Veprintsev, M. Bycroft, and A. R. Fersht, “Comparative Binding of p53 to its Promoter and DNA Recognition Elements,” *J. Mol. Biol.*, vol. 348, no. 3, pp. 589–596, May 2005.
[133] X. Lin and S. B. Howell, “DNA mismatch repair and p53 function are major determinants of the rate of development of cisplatin resistance,” *Mol. Cancer Ther.*, vol. 5, no. 5, pp. 1239–1247, May 2006.
[134] S. Geisler *et al.*, “TP53 gene mutations predict the response to neoadjuvant treatment with 5-fluorouracil and mitomycin in locally advanced breast cancer.,” *Clin. Cancer Res.*, vol. 9, no. 15, pp. 5582–8, Nov. 2003.
[135] K. H. Vousden, “Outcomes of p53 activation - spoilt for choice,” *J. Cell Sci.*, vol. 119, no. 24, pp. 5015–5020, Dec. 2006.
[136] D. Menendez, A. Inga, and M. A. Resnick, “The Biological Impact of the Human Master Regulator p53 Can Be Altered by Mutations That Change the Spectrum and Expression of Its Target Genes,” *Mol. Cell. Biol.*, vol. 26, no. 6, pp. 2297–2308, Mar. 2006.
[137] Z. H. Siddik, “Cisplatin: mode of cytotoxic action and molecular basis of resistance,” *Oncogene*, vol. 22, no. 47, pp. 7265–7279, Oct. 2003.
[138] Y. L. Lyu *et al.*, “Topoisomerase II Mediated DNA Double-Strand Breaks: Implications in Doxorubicin Cardiotoxicity and Prevention by Dexrazoxane,” *Cancer Res.*, vol. 67, no. 18, pp. 8839–8846, Sep. 2007.
[139] M. Podhorecka, A. Skladanowski, and P. Bozko, “H2AX Phosphorylation: Its Role in DNA Damage Response and Cancer Therapy,” *J. Nucleic Acids*, vol. 2010, pp. 1–9, 2010.
[140] C. Voland, “Repression of cell cycle-related proteins by oxaliplatin but not cisplatin in human colon cancer cells,” *Mol. Cancer Ther.*, vol. 5, no. 9, pp. 2149–2157, Sep. 2006.
[141] F. Toscano *et al.*, “p53 dependent and independent sensitivity to oxaliplatin of colon cancer cells,” *Biochem. Pharmacol.*, vol. 74, no. 3, pp. 392–406, Aug. 2007.
[142] G. Kroemer and S. J. Martin, “Caspase-independent cell death,” *Nat. Med.*, vol. 11, no. 7, pp. 725–730, Jul. 2005.

[143] X. Sui *et al.*, “p38 and JNK MAPK pathways control the balance of apoptosis and autophagy in response to chemotherapeutic agents,” *Cancer Lett.*, vol. 344, no. 2, pp. 174–179, Mar. 2014.

ACKNOWLEDGEMENTS

I would like to express my deepest appreciation to my supervisor Dr. Mindaugas Valius for all the support, guidance and encouragement. All the scientific disscussions and arguements were extremely valuable and meaningful in the developement of my scientific knowledge and shaping my scientific standpoints.

I am also very grateful to all the people who have helped and motivated me throughout my Ph.D. studies:

Dr. Marija Ger for all the methodical counseling and guidance, extremely in the early stages of my scientific development. Dr. Marija Ger, Dr. Algirdas Kaupinis and Dalius Kučiauskas for all the help with proteomic data acquisition and analysis, all the advice and tutoring that made this process a lot less complicated than it could have been.

Silvija Urnikytė for personal support, friendship, and all the coffee breaks. All present and former colleagues and students for helping me grow and accomplish the research tasks.

Dr. Giedrius Vilkaitis and Stasė Gasiulė for help with miRNA-related subjects. Dr. Violeta Jonušienė for the development of resistant cell lines. Dr. Kęstutis Sužiedėlis and Dr. Vaidotas Stankevičius for methodical counseling and collaboration in the RH1 resistance project. Prof. Dr. Lee M. Graves for MIB technology and supply.

And, most importantly, my precious family for unconditional love, support, and tolerance that made it all possible.

Vilniaus universiteto leidykla
Saulėtekio al. 9, III rūmai, LT-10222 Vilnius
El. p. info@leidykla.vu.lt, www.leidykla.vu.lt
Tiražas 12 egz.